

Dipl.-Ing. Detlev Gross

**Acquisition and location
of partial discharge - esp.
in transformers**

DISSERTATION

zur Erlangung des akademischen Grades

Doktor der technischen Wissenschaften

eingereicht an der

Technischen Universität Graz

Betreuer

Em. Univ.-Prof. Dipl.-Ing. Dr. techn. Dr. h.c. Michael Muhr

Institut für

Hochspannungstechnik und Systemmanagement

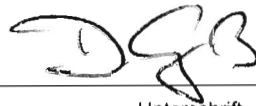
Zweiter Begutachter: Prof. Dr.-Ing. Rainer Haller
University of West Bohemia, Pilsen

EIDESSTATTLICHE ERKLÄRUNG

Ich erkläre an Eides statt, dass ich die vorliegende Arbeit selbstständig verfasst, andere als die angegebenen Quellen/Hilfsmittel nicht benutzt, und die den benutzten Quellen wörtlich und inhaltlich entnommenen Stellen als solche kenntlich gemacht habe. Das in TUGRAZonline hochgeladene Textdokument ist mit der vorliegenden Dissertation identisch.

4.11.2016

Datum



Unterschrift

Preface

Partial discharge is a quite exotic field in electrical engineering. For me it started in 1979, being a student then, with an internship with the development department of the Cable Company Felten & Guilleaume in Cologne. At that time they switched from double extruded to triple extruded polyethylene cable and had to change their partial discharge testing completely. I was happy to become involved. Without this internship I'd surely do something else now. In 1980 I started also working as student assistant at the high voltage institute of RWTH Aachen. Here, I designed custom electronics for partial discharge testing. Both positions I kept until finishing my diploma in 1986, after which I started immediately my company initially as engineering office. Since then I did spend most of my professional life with partial discharge.

While I was assisting with a partial discharge testing task at TU Graz in 2010, Prof. Michael Muhr kindly offered me his support for a thesis on partial discharge diagnosis. 2011, after some hesitation, I became student again. Having this work completed by now, I am very grateful that Prof. Muhr offered me this opportunity. Moreover, I am thankful for him insisting and reminding me to continue. Likewise, I am grateful that Prof. Rainer Haller agreed to take responsibility as second reviewer.

Additionally, I wish to express my sincere thanks for the support and warm welcome that I have received generally at the Institute for High Voltage Technique and System Management. Especially, I have to mention the discussions at the "Hochspannungszeichensaal", which further encouraged me to start with this adventure.

Graz, November 2016

Detlev Gross

Content

1.	Introduction	1
2.	Partial discharge in electrical insulation systems	4
2.1	Partial discharges.....	6
2.2	Partial discharge measurements.....	9
3.	Partial discharge signal properties	12
3.1	Electron avalanche.....	13
3.2	Signal transmission	33
3.3	Calibration	41
4.	Coupling methods and circuits	49
4.1	Capacitive coupling	49
4.2	Inductive coupling.....	54
4.3	Antennas (electromagnetic)	58
4.4	Acoustic detection	61
4.5	Optical detection.....	65
5.	Bandwidth and processing circuits	66
5.1	IEC60270	66
5.2	Acoustic.....	76
5.3	HF, VHF, and UHF	78
6.	Visualization and interpretation	85
6.1	Analysis in time domain.....	87
6.2	Analysis in phase domain.....	94
6.3	Analysis in frequency domain.....	99

7.	Finding partial discharge in power transformers	103
7.1	Factory acceptance testing	104
7.1.1	Narrowing the location of the source	115
7.1.2	Identifying and separating different sources	117
7.1.3	Using a two-dimensional φ - q -trigger matrix	119
7.1.4	Acoustic location	121
7.2	Onsite testing	131
7.3	Online monitoring	139
8.	Résumé	142
9.	Summary	146
10.	Appendix	148
10.1	Grid transformer with cable box	148
10.2	Grid autotransformer	151
10.3	Large shell-type autotransformer	153
10.4	Large grid autotransformer	156
10.5	Partial discharge pattern examples	158
11.	Literature	166

1 Introduction

Partial discharge activity as a threat for insulation lifetime is as old as the technical application of high voltage insulation systems. The early steps of electrification covered mostly lighting of single buildings, such as hotels or theaters and, hence, local power generation was needed. However, when changing to more remote power generation, quickly the change to high voltage insulation systems had to be taken to reduce transmission costs and losses. Thus, high voltage insulation systems, such as rubber-insulated or mass-impregnated cables were in use since the late 1890s.

Noticing, understanding, and avoiding "corona" was firstly only based on using the senses of seeing, hearing, and getting the smell of ozone. However, quickly the transition to measurements was made with loss angle measurements in the beginning and disturbance receivers from on the 1930s.

Modern partial discharge testing began about fifty years ago with Kreuger's introduction of the charge-based measurement in the 1960s, which made it quickly into an international IEC standard, the publication 270 in 1968 [270₁].

With progress in microelectronics and the availability of notebook computers, the phase-resolved partial discharge measurement with the φ - q - n pattern became common practice [Fru93]. Research on the properties of the φ - q - n pattern enhanced the understanding of the deterioration processes [Nie95]. Moreover, the new instruments offered then firstly a true portability and the new technique was increasingly applied under field conditions.

However, leaving the shielded test room makes dealing with the onsite difficulties and ambiguities a demanding task. Over the years, the basic partial discharge measurement technique was enhanced with strategies, circuits, and accessories to cope with the onsite conditions. Here, the task is dealing with high frequency interference, noise signals, spurious antenna effects of coupling circuits, and acoustic noise interference, to mention only few.

Partial discharge measurements are a proven tool for acceptance testing of power transformers in a factory environment and increasingly on-site in a field environment. The increasing use of polymeric material in power transformers and transformer bushings, increasingly optimized insulation systems, and a growing awareness of the risks of ongoing partial discharge in power transformers led to lower partial discharge acceptance magnitudes. A decade ago, an acceptance level of 500pC was common sense, while nowadays utilities increasingly demand significantly lower acceptance levels.

Measuring such low magnitudes is a demanding task in light of the typical motor generator set and especially the more recently introduced inverter based sources as used for transformer acceptance testing. Moreover, identifying and separating different partial discharge sources that occur simultaneously in a transformer requires adequate measurement as well as filtering techniques.

There are several electrical and acoustical location methods. However, standard acoustic triangulation techniques based on solving the sphere functions have limited application in real-life transformers, as two required conditions – the tank is a thin membrane, and the interior is homogeneously filled – are not given for a liquid filled power transformer. Here, the special transmission properties of transformer isolation and structural materials have to be taken into account. Moreover, with current technology, acoustic location of multiple internal partial discharge sources is not possible under the presence of noise and external discharge.

Therefore, as adequate tools are presently not available, the research tasks of this thesis are:

- To develop strategies to locate partial discharge sources in transformers under the non-ideal conditions of real-life transformers,
- To identify, interpret, and separate partial discharge activities that occur simultaneously, and
- To find methods to reliably separate and acoustically locate partial discharge sources that occur simultaneously.

In order to create an understanding for the non-linear development of partial discharge testing, this thesis begins with an historic overview of partial discharge testing and the development steps over the decades as well as the changing industrial requirements.

Further, the different partial discharge processes and their impact as well as the impact of electrode configurations on φ - q - n pattern is presented. This is followed by an introduction in the high frequency signal transmission of partial discharge signals in power engineering equipment and a section covering calibration of the measurements.

Subsequently, the different circuits that can be used as coupling device for partial discharge measurements as well as applicable bandwidth and achievable sensitivity are discussed.

This is followed by a discussion concerning the different frequency bands and the applicable detection circuits according to the standards as well as outside of the standards. Additionally, the different ways of visualization of measurement results and their interpretation are presented.

The previously described techniques can be applied to any high voltage insulation system. The main part of the thesis outlines then the application of these techniques on power transformers as an example. Here, the difficulties of applying simple triangulation techniques, the strategies to identify and locate partial discharge, and how to apply this under field conditions are discussed. Further, a new trigger technique based on the φ - q - n pattern is presented and its application explained.

After résumé and summary an appendix is found, which contains few cases of partial discharge location in large power transformers. Finally, there is a small catalog of φ - q - n partial discharge pattern including the ones spread over the thesis. Besides transformer partial discharge pattern, it covers also more generic partial discharge pattern.

This thesis is written in American English and, hence, punctuation includes the serial comma. Citations are given in an alphanumeric format with the first three letters of the principal author followed by two digits of the publication year.

2 Partial discharge in electrical insulation systems

Concerning electricity, besides lightning, especially discharge of static electricity early amazed mankind and attracted researcher. Here, St. Elmo's fire is a good example (Fig.2.1, a), as it led Benjamin Franklin to develop a lightning rod [Jer28], as part of his research (Fig. 2.1,b) and as firstly described in 1749.



Fig. 2.1 St. Elmo's fire (a), Franklin's work on static electricity¹ (b), and an "electrophorus" (c)

Generally, during the 18th century and especially during its second half, many of the basic principles of electricity and magnetism were firstly subject to in depth research. In 1762, Johan Carl Wilcke, a Swedish Professor, invented a capacitive generator that produces electrostatic charge (Fig. 2.1, c). Later, Alessandro Volta named this manually operated machine "electrophorus". With this electrostatic generator, the lower dielectric plate was charged using triboelectric principles by rubbing it with a cat fur. The upper metallic plate with a handle made of insulating material was then used to (partially) transfer charge electrostatically. However, this caused also charge transfer inside the dielectric plate.

¹ Franklin and Electricity, vignette engraved by Alfred Jones, for the Bureau of Engraving and Printing, Public Domain.

Based on Wilcke's work, likewise, in the second half of the 18th century, Georg Christoph Lichtenberg built a large version of the electrophorus and found on the dielectric plate figures formed by initially accidentally applied dielectric dust. Lacking any photographic possibilities at that time (1777), Lichtenberg transferred the dust figures using sticky black paper (Fig. 2.2).

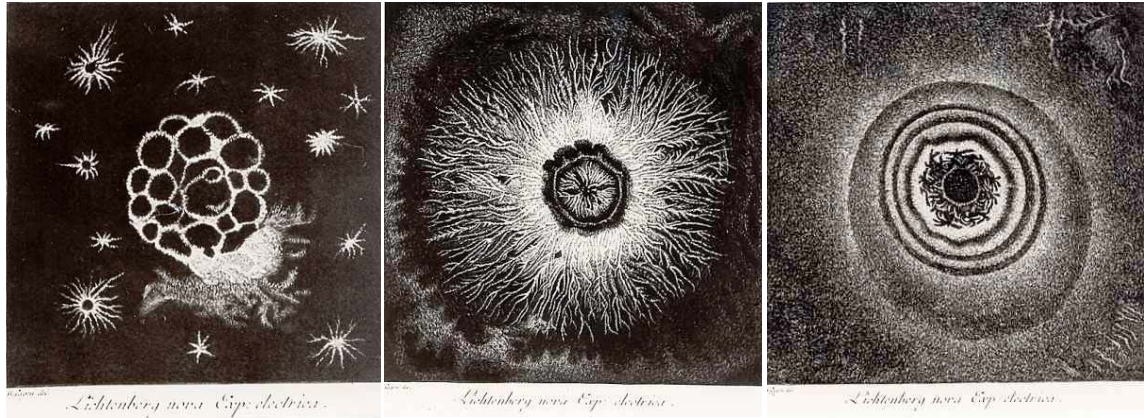


Fig. 2.2 Lichtenberg figures – transferred from the dielectric plate using sticky black paper

Lichtenberg's electrophorus was very large with a diameter of 2m. It is reported that this electrophorus supported arcs of up to 40cm, which corresponds to about 200kV. Lichtenberg noted already differences between the traces of positive and negative discharges. Fig. 2.3 shows a smaller electrophorus (a, with the cat fur) and an example of Lichtenberg's sketches of his experiments (b).

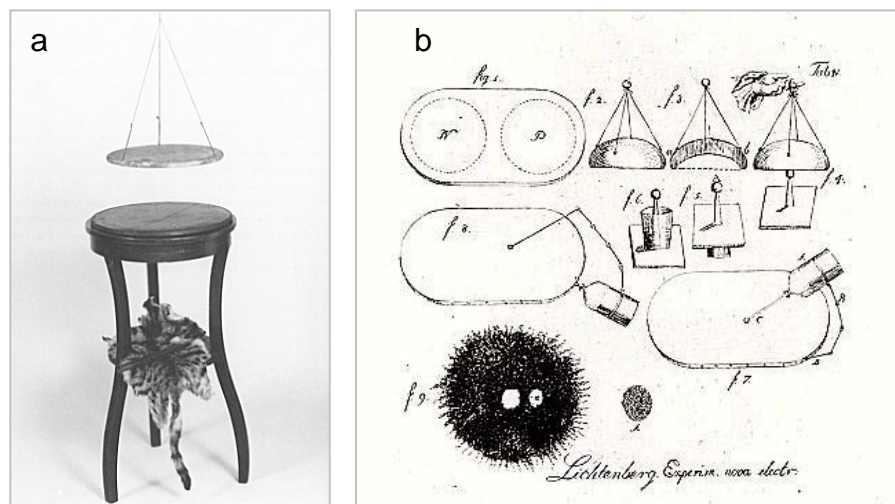


Fig. 2.3 Electrophorus (a) and an example of Lichtenberg's notes of his experiments (b)

Shortly after the beginning of the electrification, transmission of electric energy was needed. However, as the transmission losses at lower voltage force using large and costly conductors, the operating voltages of cables quickly increased. At the Niagara Falls Power Generation, in 1897, firstly 11kV rubber-insulated cables were used. Mass-impregnated paper cables were in use at about the same time, which is, by the way, the time (1897), when John Sealy Townsend started his work on the basic partial discharge mechanism – the electron avalanche, which later became part of his book "Electricity in Gases" [Tow15].

2.1 Partial discharges

It did not take long that the impact of partial discharge – then called corona in general – caught the interest of researchers and engineers, as those processes have the tendency to reduce the lifetime of an insulation system.

Just a decade after the very first application of high voltage insulation systems, a broad understanding of the occurrence, the discharge mechanism, the caused deterioration, and methods to avoid corona can be found in textbooks [Pee15]. Here, partial discharge effects in cables, bushings, high voltage rotating machines and transformers are already well described. Likewise, strategies to reduce the electric field by grading or stacking insulation material, to avoid air-filled pockets are well described (Fig. 2.4).

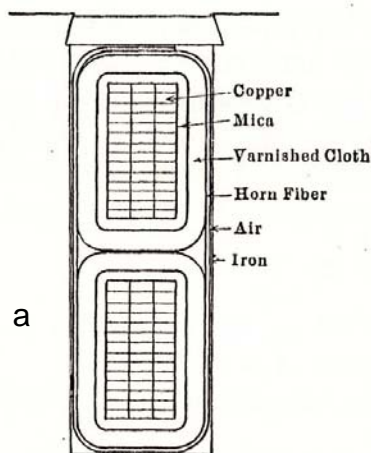


FIG. 176.—Corona on generator coils.

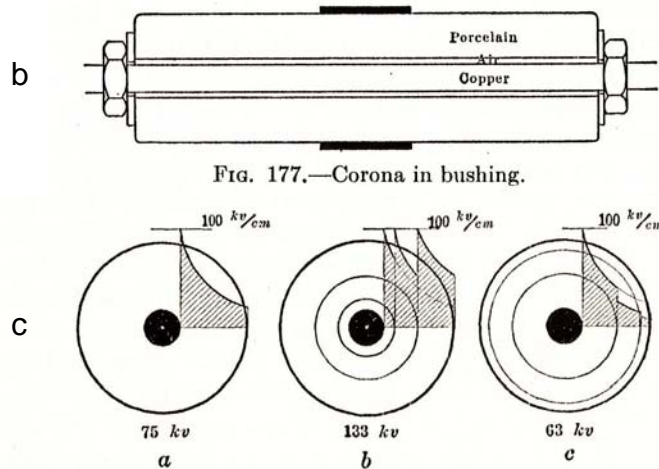


FIG. 177.—Corona in bushing.

FIG. 178.—Graded cable.

(a) Not graded. (b) Insulations properly arranged. (c) Insulations improperly arranged. Noted break-down voltage in each case.

Fig. 2.4 "Corona" in generator (a) and bushing (b) – stacking of cable insulation (c) [Pee15]

The stacking of insulation material, i.e., having material of higher relative permittivity and/or higher breakdown strength closer to the conductor, where the electric field is higher, can be found frequently at that time. In Fig. 2.4 this is shown for stacked cable insulation (c), which at that time was wrapped and, hence, allowed changing materials. Likewise, although not expressively mentioned, this is also found with Fig. 2.4, a, where the inner insulation is made of mica tapes, before the insulation changes to varnished cloth. Notably, the design of the generator bar shown, although being advertised as 13.2kV, does not have any "slot corona protection", i.e., a semiconductive taping, as it is commonly used nowadays. In this paragraph F. W. Peek states 1915:

"Since the disruptive strength of air is 31 kv./cm., it will break down, forming corona. Experience has shown that in time the corona eats away the insulation by mechanical bombardment, local heating, and chemical action, and ultimately a short circuit results." [Pee15, pp. 216-217]

Thus, at that time, rotating machine insulation systems were heavily over-designed in order to avoid having partial discharge occurring in the air pockets of the slot section. Fig. 2.5 shows an example of a 5.9kV generator (a) as built 1905 for the Heimbach hydro power plant (b), which was at the time of commissioning Europe's largest hydro power plant with in total 12MW. Initially, the plant served the administrative district of Aachen via a 35kV overhead line. The insulation was about 30mm for 5.9kV, then. The machines were 70 years in service, when the plant was modernized in 1975, installing two new machines. The power house from 1905, then built in the style of the "art nouveaux", serves as museum since and additionally as a place for concerts today.

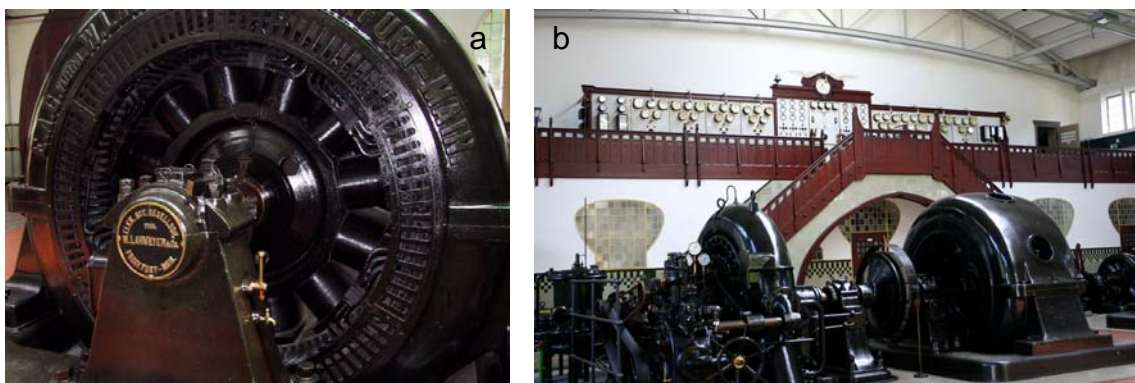


Fig. 2.5 5.9kV generator built 1905 (a) for the Heimbach hydro power plant (b)

Besides the already early gained awareness concerning the deterioration of insulation systems by partial discharge, further interest in partial discharge activity was gained, when in the 1920s commercial radio broadcasting began and quickly became very popular. The then used amplitude modulation is very prone to impulse-like disturbance by remote lightning, but, of course, also "corona" of any improperly designed overhead high voltage system.

The next step in awareness of partial discharge and its deterioration processes took place, when the use of polymeric insulation systems began. Here, especially, in the 1970s the introduction of polyethylene as cable insulation marked the change. In the beginning, polyethylene wasn't cross-linked during the production process and the early design was only double extruded, while applying graphite powder provided the outer protection against partial discharge. The later introduced triple-extruded production process, however, is less prone to partial discharge problems, as the outer semiconductive layer is solidly bonded.

Another, further increase in awareness of the importance of partial discharge occurred with the deregulation of the energy market in the Western Hemisphere starting in 1992 in the U.S. with the "Energy Policy Act" and a couple of years later in Western Europe.

Before the deregulation of the energy markets, the utilities had their protected market areas and their focus was primarily on availability of power and durability of the equipment, while the mere cost of the equipment was considered being of lower priority. When viewed primarily from an economic standpoint, this policy of the regulation period led to "over engineering". In other words, deregulation led to an "optimization" of the designs, among others, of high voltage insulation systems and the power engineering equipment in general. Thus, the headroom provided by larger safety margins in high voltage design was gone and needed to be replaced with more care during production and testing.

Moreover, deregulation led also to more service-aged substation equipment, as reinvestment decisions, as well as maintenance strategies were seen under economic parameters, primarily. In consequence, utilities closed their own maintenance departments to save cost, but lost in the same moment their long-term knowledge concerning their assets.

2.2 Partial discharge measurements

The application and evolution of partial discharge measurements follows in principle the changing needs over time, as outlined in the previous chapter. Of course, additionally, progress in engineering in general, availability of new techniques and their naturally somewhat delayed use on niche applications influenced the progress of partial discharge measuring techniques.

Likewise, standardization follows emerging techniques, whenever a certain stability of a technique has been reached. Thus, whenever a technique is changing rapidly, standards are either adapting after some time and reached stability or are eventually being dropped.

Initially, with the first high voltage insulation systems, understanding and avoiding "corona" effects was mostly a visual task, while emphasis was put primarily on insulation resistance and breakdown voltage. Additionally, the smell of ozone helped identifying discharge activity. The initial approach to assess "corona" by measurement was to measure the "corona losses". Fig. 2.6 shows the circuit to measure such losses for a rotating machine [Pee15].

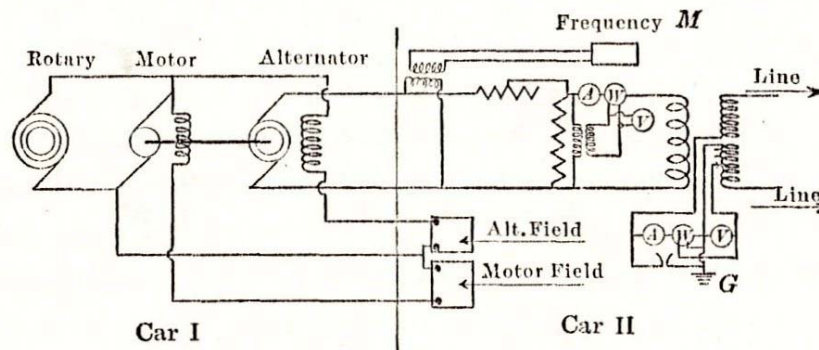


FIG. 114.—Circuit connections in corona loss measurements.

Fig. 2.6 Early circuit description for the measurement of partial discharge [Pee15]

Shortly after, the Schering Bridge for loss measurements found a wide application [Sch20]. However, with the integral measurement of the resistive component of the otherwise capacitive current, several effects are covered, such as insulation resistance, polarization losses, and finally partial discharge.

Abb. 169. Prinzipschaltbild der Verlustfaktormeßbrücke nach SCHERING. *FS* Schutzfunkenstrecken, C_1 verlustbehaftetes Meßobjekt, C_2 verlustfreie Vergleichskapazität (Normalkondensator). Weitere Erläuterungen siehe Text.

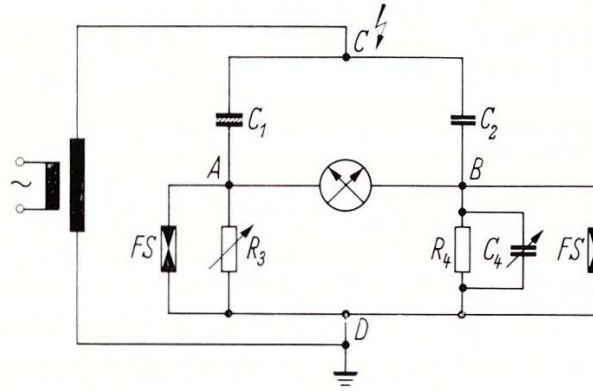


Fig. 2.7 Basic circuit of the Schering Bridge for loss measurements [Sch69]

Fig. 2.7 shows the basic circuit of a Schering Bridge for an ungrounded test object. I.e., the bridge is connected to the ground leads of test object C_1 and reference capacitor C_2 . The lower bridge elements R_3 , R_4 and C_4 are protected with spark gaps *FS*. The bridge is adjusted by bringing the reading of the central null indicator to zero. Partly, the different effects could be separated by measuring the $\tan \delta$ versus voltage and, for instance, detect partial discharge inception by observing a sudden increase of the $\tan \delta$ [Sch69].

The rapid development of commercial radio broadcasting as well as the availability of electron valves gave partial discharge testing a new momentum. As any broadband sparking signal poses disturbance signal for the then used amplitude modulation, all overhead insulation systems became subject for "radio influence voltage" measurements (RIV). Here, newly developed measurement receivers from communication engineering were used. The technique evolved in the late 1930s, whereas the Radio Manufacturers Association pushed the NEMA standardization in 1940 [107₁] (firstly revised in 1964 [107₂]). Also in other parts of the world disturbance receivers were used to detect "corona".

The next larger step was initiated, when F. H. Kreuger proposed a charge impulse based method to measure partial discharge in the 1960s [Kre64]. This proposal was vividly discussed and led to the development of different instruments and related accessories, such as "Enraf Nonius" (Delft, NL), or the ERA detector (UK), TEM77 (MWB), and many others. In parallel, the technique was standardized beginning with VDE 0434 [434] in 1966 and followed by the IEC publication 270 [270₁] in 1968.

Introduction of this then new measurement technique felt together with the introduction of polymeric insulation systems, as mentioned earlier. Here, especially the "non forgiving" polyethylene insulation system requires high sensitivity measurements, as any small partial discharge can be a starting treeing, which subsequently leads to breakdown. Thus, shielded rooms, adequate filtering of high voltage as well as power supply, efficient coupling, and sensitive instrumentation was needed.

Improvements based on experience gained with the then new technique as well as progress in electronic and computer technique initiated the next large step. By the early 1990s, the phase resolved partial discharge pattern firstly was applied in research and shortly after led to the development of lightweight, portable instruments, when additionally notebook computer came up and new software tools allowed designing virtual instruments.

The driving force for the next step in progress was initiated by the aforementioned deregulation of the energy sector. Arising economic constraints led to extending service age of substation equipment and "cost optimized" insulation systems of new equipment. This led to the need to increasingly apply the techniques being used in shielded rooms to now being applied under field conditions, or even use it as monitoring device.

Such online, onsite use of partial discharge measurement systems forces the application of noise cancellation, filter, and gating techniques. Additionally, this leads to the use of frequency bands not covered by the standards that were written for lab application. Likewise, bringing test voltage sources on site is a demanding task.

Progress in this area continues up to today. However, the current momentum is still driven by economical concerns, but now increasingly by political motivation, as for instance the change to "renewable energy", influence the focus of the energy sector, which finally also adjusts the focus of measurement and monitoring techniques.

3 Partial discharge signal properties

As said before, partial discharge is a local and partial breakdown of an overall insulation system. Partial discharge mostly concerns discharges in gases, whereas discharges in solid or liquid insulation material quickly change into gas discharge due to gases produced by the ongoing discharge activity after the initial breakdown of the solid or liquid material. For instance, partial discharge in polyethylene forms a gas-filled tree-like structure, after the initial break-up of the material at a sharp point, which causes a highly enhanced electric field. Thus, only this initial break-up of the polyethylene concerns the breakdown field strength of the solid material, while the ongoing discharge activity is then a gas discharge process within the gas-filled tree structure (Fig. 3.1). Here, only the further propagation of the tree and the carbonization of the "older" parts of the tree are still related to the properties of the solid material.



Fig. 3.1 Treeing in polymeric material – here caused by space charges in PMMA²

² The propagation of such treeing structure follows the local electric field under the impact of all neighboring tree branches. Further, local orientation of the partially crystallized polymeric material causes the "natural" growth. However, this example is not caused by slowly propagating partial discharge, but by a rapid discharge of a layer type space charge formation caused by an electron beam irradiation, whereas the electrons have a penetration depth according to their acceleration.

Likewise, a discharge under oil along a fiber bridge, for instance, causes gases that do not dissolve quickly enough after the first partial discharge event and, hence, supports then ongoing gas discharge, especially, if the gas is trapped between insulation layers.

Thus, with this chapter, mostly the effects of partial discharge as gas discharge are discussed. Moreover, emphasis is put on such effects and properties that influence rise time and signal bandwidth, as well as the phase-resolved appearance of partial discharge activity including their impact on acquisition, identification, and interpretation of partial discharge activity.

3.1 Electron avalanche

In a gaseous insulation, occurrence of partial discharge simply requires that the critical electric inception field is surpassed and that there is a free (ionized) electron that can be accelerated in this electric field [Tow15, Nie95]. Here, the meaning of critical inception field is that this accelerated electron reaches such a high speed and, hence, kinetic energy within its average free travel path that it causes secondary electrons, when it hits another gas molecule. Moreover, the secondary electron generation efficiency must be larger than 1 within a certain area in case of non-homogeneous field. Thus, the initial accelerated electron causes an electron avalanche.

This initial discharge mechanism, having only the collision ionization and no space charges involved, is called Townsend discharge [Riz14]. In practical life, the plain Townsend mechanism concerns the so-called Trichel discharge, as it occurs initially at sharp points on high voltage in the negative half cycle. Also, the initial stage of surface discharge at a rotating machine's slot exit follows the Townsend principle. Another example is partial discharge in small spherical gas inclusions in solid or liquid material. Generally, the Townsend discharge principle applies to small discharge magnitudes up to approximately 10pC, only [Sr16]. As soon as the magnitude increases and space charges are involved, additionally, photo ionization due to the then stronger radiation of recombination processes cause additional nearby electron avalanches and the discharge process changes into the streamer discharge [Nie89, Sr16].

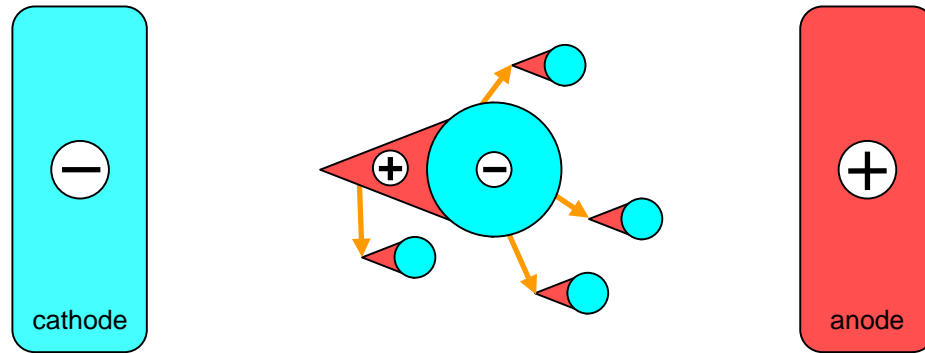


Fig. 3.2 Streamer mechanism – nearby photo ionization due to stronger recombination

Fig. 3.2 illustrates the generation of the additional discharge avalanches due to photo ionization. The radiation as emitted under the recombination in the main avalanche (photo) ionizes nearby gas molecules and causes additional avalanches, which are quickly forming a conductive channel – called streamer [Riz14, Srz16].

The next escalation in the gas discharge process is adding thermal ionization. In case the temperature in the discharge channel gets high enough to cause also thermal ionization, the number of free electrons increases rapidly and the current in the comparably narrow channel increases strongly. The leader discharge is the strongest partial discharge mode before breakdown. In air, leader discharge can only be maintained in case of a strongly inhomogeneous electric field and comparable large distances.

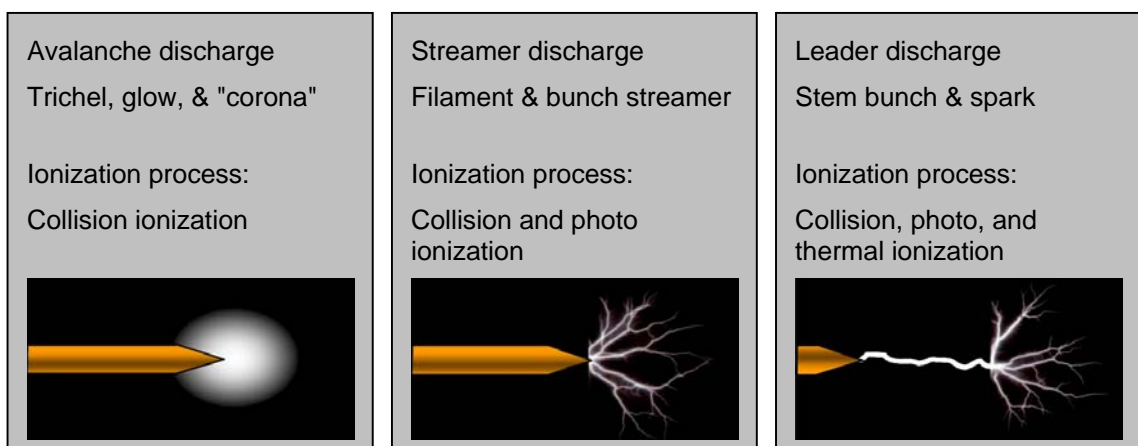


Fig. 3.3 Appearance of partial discharge – avalanche (a), streamer (b), and leader (c) [Srz16]

Fig. 3.3 illustrates the basic three types of partial discharge processes due to their different ionization processes involved [Sr16]. The initial avalanche discharge based only on collision ionization includes Trichel, glow and the so-called corona discharge. With increased recombination radiation, photo ionization incepts as well and the discharge changes into the streamer discharge including filamentary and bunch-type discharge. Finally, with a certain current density in the discharge channel, additionally thermal ionization contributes to the generation of free electrons and the discharge changes into the leader discharge covering stem bunch and spark-like discharge.

Depending on the insulation system, the different partial discharge processes have different relevance. For assessing the condition of insulation systems that are designed to withstand partial discharge temporarily or permanently, such as the epoxy-mica insulation of rotating machines, diagnostic relevance have mostly streamer and partially even leader discharge activities. Assessing the insulation condition on the other extreme with non-forgiving insulation systems, such as polyethylene of high voltage cables, emphasis is mostly on the inception of partial discharge and, hence, the processes of the basic avalanche discharge are relevant. Here, only for ongoing discharge and external surface discharge streamer processes are relevant.

In order to understand the root cause of a partial discharge activity, the impact of the statistics to derive the initial electron and the electrons to support the ongoing discharge is of predominant interest. Here, especially, the ionization processes, space charge effects, and de-trapping effects including their statistical delay have a central importance.

Again, having the critical electric field to support an electron avalanche, it needs a free electron to be accelerated in the electric field. Fresh polymeric surfaces, such as a gas inclusion in a freshly cured epoxy resin, or freshly extruded polyethylene, have literally no free electron. Here, the electron needed is ionized by the natural radioactivity (γ radiation), which includes cosmic photons, natural radioactivity of the soil, radiation due to the radioactive noble gas radon (^{86}Rn), having several isotopes that decay under γ radiation between 2.9 and 6.4 MeV, and the remains of atmospheric nuclear tests. Such atmospheric tests were conducted until 1980 and still contribute to the exposition.

Having now such a gas inclusion within fresh polymeric material (Fig. 3.4), initially, nothing will happen, when the electric field is raised above the critical inception field, as the first free electron is missing. Depending on the location, different densities of the γ radiation to ionize a gas molecule are given, whereas the values reach from $2 \times 10^6 \text{ kg}^{-1} \text{ s}^{-1}$ [Nie95] to "some hundreds to even thousands per second" [Riz14]. Tests with small bubbles in fresh polymeric material [Gro95] tend more to support the lower number as given with [Nie95]. Based on this figure, a spherical void of 1mm diameter having no own free electrons shows an average statistical delay of 10^3 s to be hit by the first photon. Thus, it takes in average about 16min until the partial discharge activity of such 1mm void starts. Obviously, this sheds an interesting light on standard testing times of a minute, for instance.

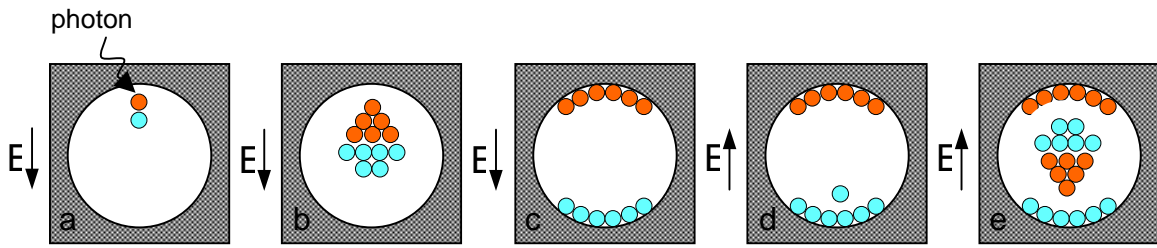


Fig. 3.4 Initial electron and de-trapping of surface charge

Fig. 3.4 shows the initial sequence in such spherical void in polymeric material. Firstly, as described, there is the statistical time lag until the first energetic photon hits the cavity and provides the first ionization (Fig. 3.4, a), whereas the first discharge avalanche occurs immediately (b). Some of the ions and the electrons will recombine, while others will make it to the adjacent surface according to their drift velocity (c). This surface charge cause an electric field that is superimposed to the external field and, from now on, the internal electric field shows an offset, which changes with every discharge event. Upon reversal of the external field, an electron attached to the surface may be de-trapped (d). In case, an electron avalanche occurs in the opposite polarity (Fig. 3.4, e). However, this de-trapping process has its own material related time constant. Moreover, there is statistical variation, since the thermal movement of the trapped electron superimposes the bond energy, i.e. modulates the energy needed for de-trapping.

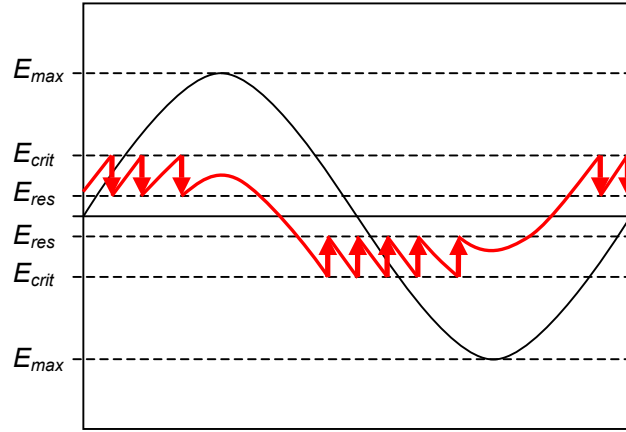


Fig. 3.5 Consecutive row of partial discharge pulses for a high availability of initial electrons

If assuming now a high availability of the aforementioned initial electron, there would be always an electron available, once the critical electric field is reached (Fig. 3.5). In case, there would be a partial discharge pulse whenever E_{crit} is reached, the internal field breaks down to the residual field E_{res} and the internal field would again increase up to the critical field. This causes a consecutive row of pulses of even amplitude and, as charging into the opposite polarity starts already after the maximum, does cause the typical phase shift for internal discharge to be occurring predominately in the first and third quarter.

Similar graphs are still frequently published as a general example for cavity discharge, although it is very uncommon to have such high availability of the initial electron and, hence, such stable magnitude. However, when this was firstly published [Gem32₂], it described the discharge of a spark gap with pre-capacitor³. Later, the used capacitive model was applied for cavity discharge in general and persisted over the decades. In fact, only applying strong irradiation by X-ray, or UV light having sufficient energy can achieve such regular discharge magnitude for fresh cavities in polymeric material [Gro98₁, Teh13].

³ The research of Gemant and Philoppoff on a "spark-gap with pre-capacitor" was conducted to gain understanding of an observation of Gemant published earlier the same year in the same periodical [Gem32₁]. This earlier publication covered research on $\tan \delta$ measurements on insulators with air-filled gaps. It was observed that the $\tan \delta$ value increased at some voltage with the ionization, but sometimes dropped again at higher voltage. This effect can be explained with the changes in phase shift of the average discharge current, which can, depending on the configuration, get a higher capacitive component at higher voltages. This effect is well described by the capacitive model [Gem32₂], but the model lacks the influence of the increasing discharge magnitude due to the time lag of the initial electrons.

In case there is no such external irradiation, only ionization processes of the natural radioactivity as well as the described de-trapping mechanism provide the free electrons needed to start the electron avalanche of the partial discharge event. As the internal surface conductivity of such fresh voids in polymers is in the range of 10^{-14} to 10^{-16} S, surface charges can survive several tens of milliseconds and remain available for de-trapping [Nie95].

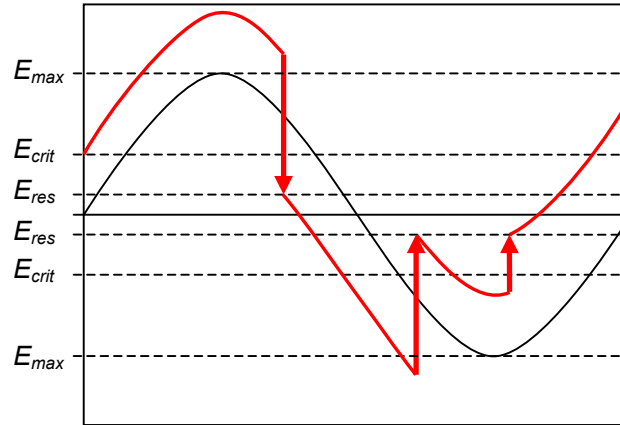


Fig. 3.6 Time lag of de-trapping causes higher internal field and non-regular PD activity

Hence, in case such small fresh void has seen the initial electron avalanche due to natural radioactivity, the number of free electrons derived by de-trapping of surface charge left over of previous activity is much higher than the number of electrons derived from natural radioactivity. Thus, such partial discharge activity is just "switched on" and then maintains its activity. Due to the comparable long lifetime of the charge carriers, such void discharge can also be intermittent.

Fig. 3.6 illustrates the situation in case of a low availability of free electrons to start the electron avalanche. Here, the time lag of the electrons derived from natural radioactivity or de-trapping is high enough that the internal electric field can become much larger than the critical electric field E_{crit} for partial discharge inception. The average time lag for electrons due to de-trapping was found in the range of milliseconds and depends on material properties. This time lag gets shorter with an incepting degradation of the polymeric internal surface of the cavity due to partial discharge, as the discharge activity creates defects that additionally allow electrons to attach and, hence, the overall number of electrons being available for de-trapping increases.

Fig. 3.7 shows the activity of a spherical, Nitrogen filled void in a glass bead, which has been embedded in clear epoxy resin between two bolts (Fig. 3.8). In order to provide a high number of initial electron to have the discharge incepting right after reaching the critical electric field, the specimen is exposed to direct sun light, which spectrum is covering ultraviolet light up to about a wave length of 300nm, which corresponds to an energy of about 4eV. The activity is shown as PRPD (phase resolved partial discharge) pattern or ϕ - q - n pattern, where the acquired pulses are shown as dots in the in the ϕ - q plane and the number n (frequency of occurrence) is coded in color.

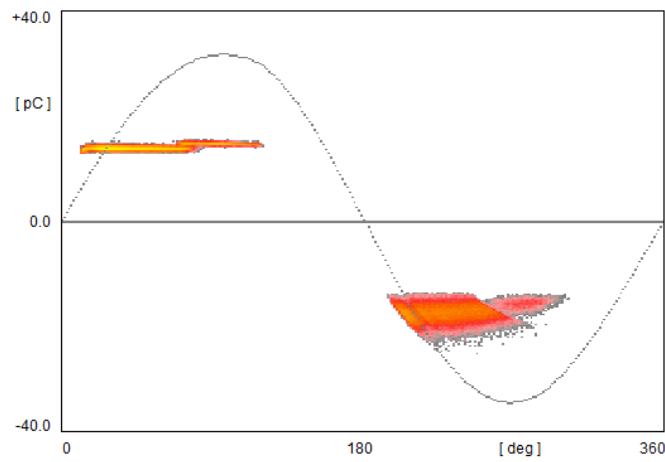


Fig. 3.7 Partial discharge in a glass bead with void under UV light – $E \approx 1.2 E_{crit}$

The irradiation hits the specimen from top and, hence, the lower side, facing the ground side of the specimen is exposed mostly, which predominately provides the starting electrons for the positive half cycle, where the recorded pulses show no variation in amplitude.

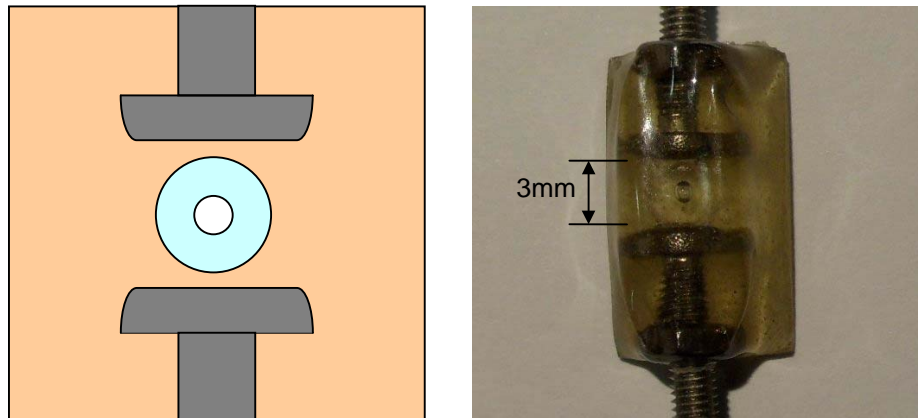


Fig. 3.8 Glass bead with spherical nitrogen-filled void – principle (left) and specimen (right)

The alternating component of the internal electric field of such cavity is proportional to the applied external voltage, whereas every discharge activity causes a direct electric field offset. Thus, every discharge pulse and the caused offset change the start conditions of the next discharge depending on its phase position of occurrence.

This offset causes another phenomenon of the cavity discharge, which is the hysteresis factor k as ratio of inception U_{inc} ⁴ and extinction voltage U_{ext} ⁴ (3.1) and which is equivalent to the ratio of critical field E_{crit} and minimum field E_{min} . If at the inception voltage U_{inc} and, hence, at the inception field E_{crit} the first discharge pulse occurs (Fig. 3.9) in the maximum of the positive half cycle, the internal electric field breaks down to the residual field E_{res} , which causes an offset ΔE of $E_{crit} - E_{res}$.

If the voltage stays stable, the internal field in the void would reach in the negative half cycle twice the critical field minus the residual field E_{res} . Thus, immediately after inception with only little increase of the applied voltage, the typical cavity discharge shows already two pulses per half cycle, as shown with Fig. 3.7 for approximately $1.2 U_{inc}$.

$$k = \frac{U_{inc}}{U_{ext}} = \frac{E_{crit}}{E_{min}} \geq 1 \quad (3.1)$$

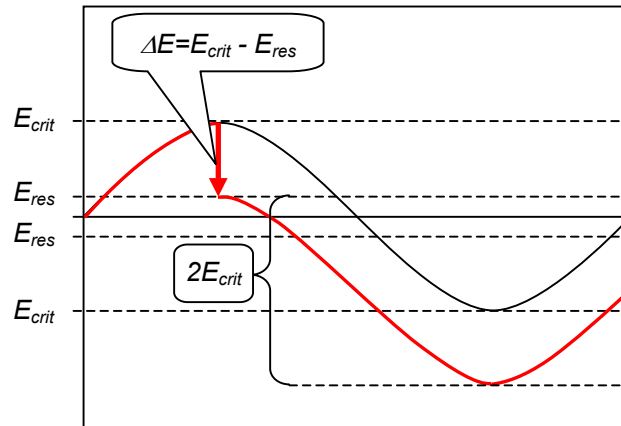


Fig. 3.9 Partial discharge in a spherical void at inception voltage

⁴ The inception voltage U_{inc} is the applied voltage at which partial discharge activity starts, while the extinction voltage U_{ext} is the applied voltage where the activity stops. The ratio between U_{inc} and U_{ext} is one of the typical indicators for the discharge type. For a floating potential with metal electrodes, the inception voltage equals the extinction voltage, for instance.

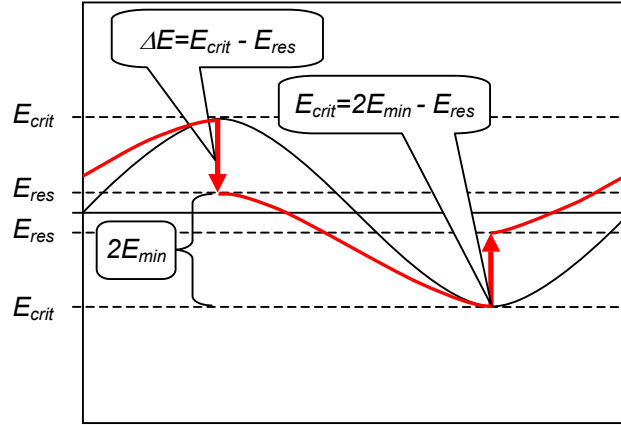


Fig. 3.10 Partial discharge in a spherical void at extinction voltage

If after inception the voltage is reduced, the extinction voltage U_{ext} is reached (Fig. 3.10), if $2 E_{min} - E_{res}$ equals the critical field E_{crit} in the negative half cycle (3.2). In case, the already mentioned offset $\Delta E = E_{crit} - E_{res}$ causes that the critical field of the opposite polarity is reached.

Thus, replacing E_{min} in formula 3.2 with E_{crit}/k (3.1) results in formula 3.3. Rearranging this formula (3.3) gives for the hysteresis factor k formula 3.4.

$$2E_{min} - E_{res} = E_{crit} \quad (3.2)$$

$$\frac{2E_{crit}}{k} - E_{res} = E_{crit} \quad (3.3)$$

$$k = \frac{U_{inc}}{U_{ext}} = \frac{2E_{crit}}{E_{crit} + E_{res}} \quad (3.4)$$

Thus, once incepted, ideal cavity discharge shows a hysteresis factor k of almost two (3.1). I.e., the extinction voltage U_{ext} is slightly above 50% of the inception voltage U_{inc} .

For cavity discharge with high availability of charge carriers (Fig. 3.5), the hysteresis factor k can be easily determined. However, in case of low availability (Fig. 3.6) this is more difficult, as the inception is delayed due to the initial discharge caused by photo ionization.

Fig. 3.11 shows the activity of the same specimen at the identical voltage as Fig. 3.7, but without the UV irradiation. Hence, the availability of free electrons is dropping drastically and, thus, the partial discharge activity changes its shape and properties, as illustrated with Fig. 3.5 versus 3.6. Instead of incepting at E_{crit} , the internal field gets much higher and the outer shape of the pulse distribution in the φ - q plane is controlled by the possible maximum value of the electrical field and the minimum field E_{crit} at which discharge may occur.

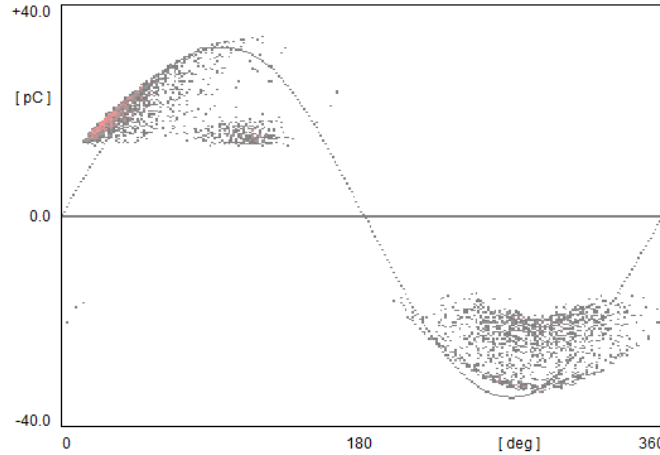


Fig. 3.11 Partial discharge in a glass bead with void as Fig. 3.7 – no irradiation

Besides the two examples given, a full set of files covering 24 hours was taken showing the impact of UV irradiation over day and night – it was taken on a day with bright sunlight and in a laboratory having roof-light domes allowing the UV components of the sun to enter the test setup.

Thus, with this experiment every parameter that controls the discharge process was kept stable and only the number of free electrons was modulated by the presence of the sunlight and the resulting ionization due to the surface photo effect. This makes it a good candidate for both simulation and numerical assess to derive basic parameters controlling the discharge process.

Research on such numerical analysis show that the appearance of such pattern mostly rely on the rate of charge carrier generation per second c due to the different effects and the decay time constant τ of the void's internal electric field [Alt02]. This decay time constant τ is mostly related to the internal surface conductivity of the void and is found in the range of several seconds for fresh voids in polymeric material or glass. Thus, in case, this decay time has only little impact on processes occurring within a 10ms half cycle of the applied test voltage.

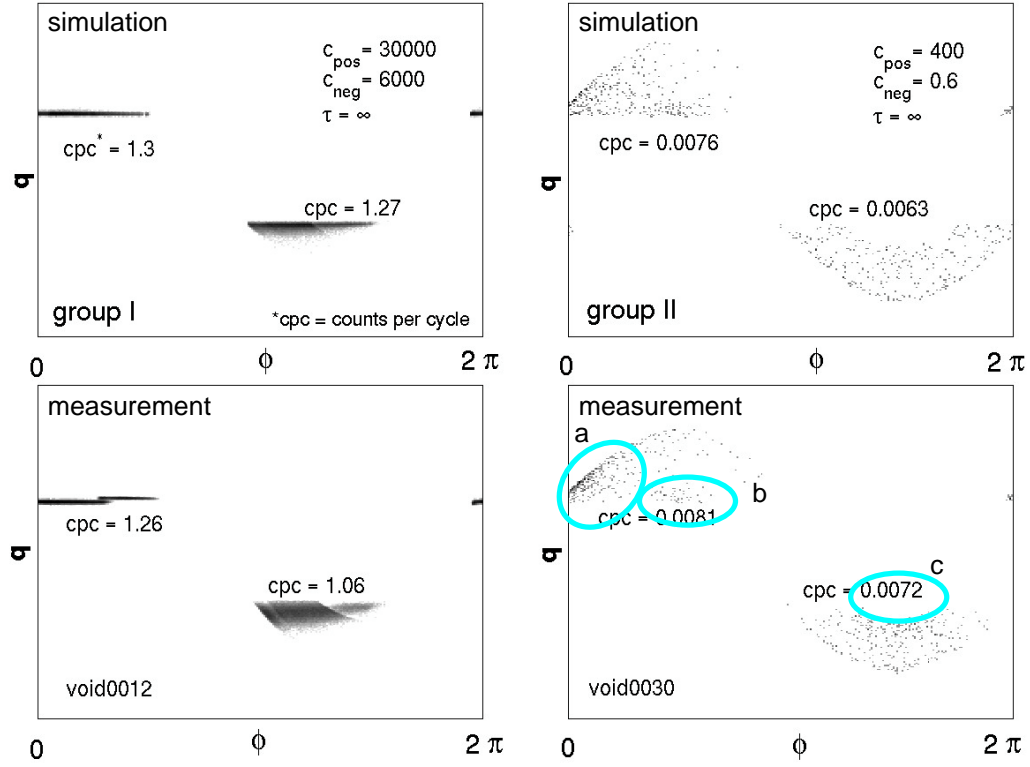


Fig. 3.12 Measured versus simulated partial discharge pattern

Fig. 3.12 shows simulation and measurement of such discharge activity, whereas the lower left pattern is identical to the pattern shown with Fig. 3.7 and the lower right pattern with Fig. 3.9, respectively. In this work [Alt02], parameter sets have been numerically extracted from the measurements and then applied for the simulation, as shown in the upper row of Fig. 3.12.

Here, for the positive half cycle under UV irradiation, a charge carrier rate of 30000s^{-1} was estimated, while for the negative half cycle only 6000s^{-1} charge carriers were estimated. This would be in line with the UV exposure on the lower surface being responsible for the discharges in the positive half cycle.

However, during dark, also an asymmetric carrier generation was estimated and subsequently used for the simulation. Here, the positive rate c_{pos} was estimated to be 400s^{-1} , while the negative rate c_{neg} was found to be 0.6s^{-1} , only. Here, it can be seen that the much higher availability of free electrons for discharges starting at the lower surface (pos. half cycle) cause a higher count rate at the lower phase angles, while the low availability in the negative half cycles causes an even distribution.

The count rate per cycle *cpc*, however, is with 0.0081 versus 0.0073 almost identical. It shall be also noted that the simulation (Fig. 3.12, lower left graph) results in the same behavior to have a second pulse (b) following the first pulse (a) for the positive half cycle, while this second pulse does not occur in the negative half cycle (c). The reason for this is the significantly lower charge carrier generation of 0.6s^{-1} , which makes it very unlikely that a second discharge takes place only few milliseconds later.

Apparently, the internal surface of the cavity has significant differences in its ability to provide free electrons. The tools used to manufacture the glass bead and to inject the nitrogen bubble may have caused these differences. The decay time constant was determined to be in the range of few seconds and, hence, has been set to infinite for the simulation.

This example shows that understanding the stochastic nature of charge carrier generation⁵ gives a much better insight into the appearance of φ - q - n partial discharge pattern than the approach to apply macroscopic models, such as the capacitive model with spark gap, as introduced by Gemant and Philippoff [Gem32₂]. However, such simplified models are easier to apply and, hence, are still widely applied.

Depending on the aforementioned parameters to describe the stochastic properties of the charge carrier generation, as well as the internal surface properties of the cavity and the surrounding material, different typical appearance of partial discharge pattern of voids can be observed.

Fig. 3.13 shows the partial discharge pulses of a single void in epoxy resin (injected air before curing). The pattern shows clearly a higher count rate at the leading edge of the area occupied with pulses, as seen already with Fig. 3.9, positive half cycle. This indicates a higher availability of the electrons to start the avalanche. The count rate per cycle *cpc* is here relatively high with 0.68.

⁵ Lutz Niemeyer and his colleagues at ABB's Swiss corporate research lab firstly applied this stochastic approach [Fru92, Nie95, Gut95, Hei99]. However, this approach remained like an exotic side-line of partial discharge research, while a statistical approach, for instance, became much more "main stream". In fact, understanding "what the electrons are doing" helps best to understand, separate, and classify discharge activities.

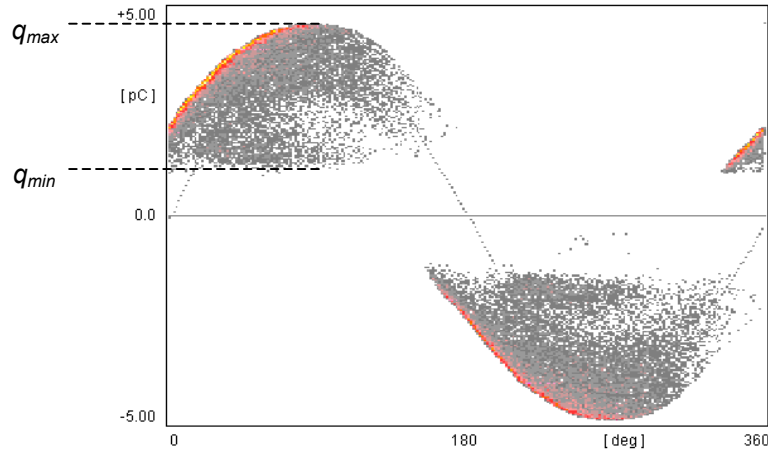


Fig. 3.13 Single void (air-filled bubble) in epoxy resin

With a decay time constant τ of the internal electric field of few seconds, it can be set to infinite at this count rate. I.e., after a discharge, the superimposed external field adds to the residual field as shown with Fig. 3.6 without decay.

There is a distinct area in the void partial discharge pattern of Fig. 3.13, which can be characterized with q_{max} and q_{min} . Their ratio is a function of the minimum discharge possible, as illustrated in Fig. 3.9, which is related to $E_{crit} - E_{res}$, while the maximum charge is related to $2(E_{max} - E_{res})$, as illustrated with Fig. 3.14.

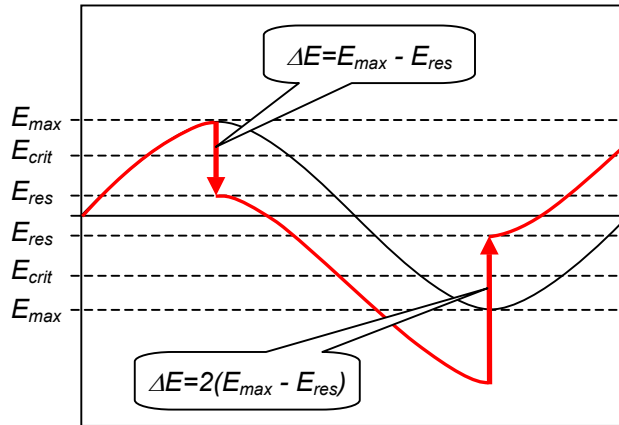


Fig. 3.14 Step function response of the basic RLC coupling circuit

Thus, the ratio of q_{max} and q_{min} can be calculated based on the related electric field $2(E_{max} - E_{res})$ versus $(E_{crit} - E_{res})$ (3.4), whereas E_{max} is the maximum electric field in the void without discharge occurrence.

$$\frac{q_{max}}{q_{min}} = 2 \frac{E_{max} - E_{res}}{E_{crit} - E_{res}} \quad (3.4)$$

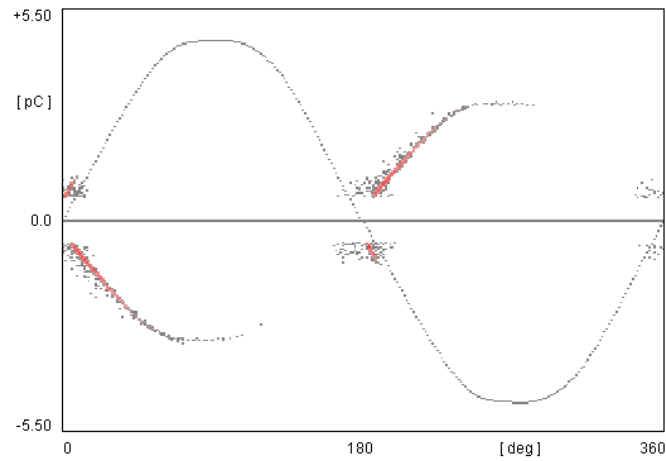


Fig. 3.15 Discharge pattern of an air-filled void in polymeric material

Fig. 3.15 shows as well discharge of a spherical gas inclusion in polymeric material. The count rate per cycle cpc is with approx. 0.7 about the same as with Fig. 3.13. However, the number of available charge carriers is much smaller and, hence, there is not a filled pattern but the distinct line-type pattern.

Another example of such line-type pattern can be found in chapter 7 (Fig. 7.16). Other than with the previous examples, we do have multiple voids. The count rate per cycle cpc per void is with approx. 0.25 not much smaller than with Figs. 3.13 and 3.15. Again, the low availability of electrons makes the difference.

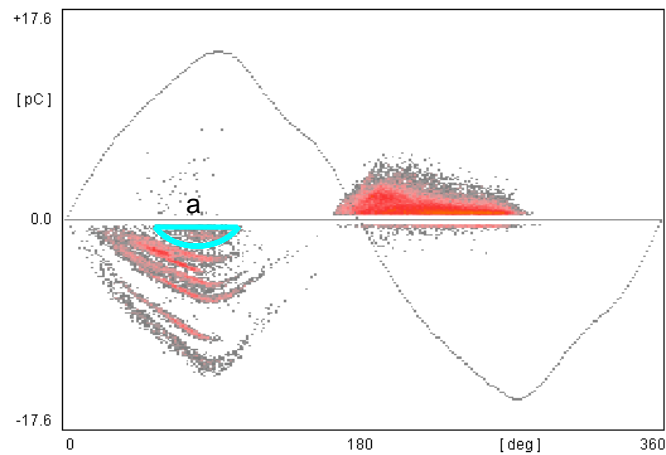


Fig. 3.16 Asymmetrical partial discharge pattern of void discharge

Fig. 3.16 shows another example of multiple voids. Here, we do have up to ten gas inclusions, which can be visually separated in the positive half cycle (partially overlapped). However, in the negative half cycle, the partial discharge pattern shows a higher count rate, while the magnitude is substantially lower.

The count rate per cycle cpc is about 11 for the positive half cycle and, if assuming ten defects, then 1.1 per void. Thus, in the center part in the positive half cycle (Fig. 3.16, a), few second pulses of some of the activity accumulate (as with Fig. 3.12, b). For the negative half cycle, cpc is in the range of 2.6 per void, if again assuming ten individual defects. Here, the pattern changes into the typical triangular-shaped pattern of multiple voids with high availability of electrons, while the individual defects can no longer be distinguished.

Fig. 3.16 shows another important property of discharge of spherical voids with low charge carrier availability. The applied high voltage has a high content of the 3rd harmonic and, hence, causes an almost triangular shape of the voltage. Discharges of spherical voids under a low rate of charge carrier generation directly reflect the electric field and, hence, show the wave shape and its distortions one-to-one. Thus, here, the triangular voltage due to the 3rd harmonic causes triangular partial discharge pattern.

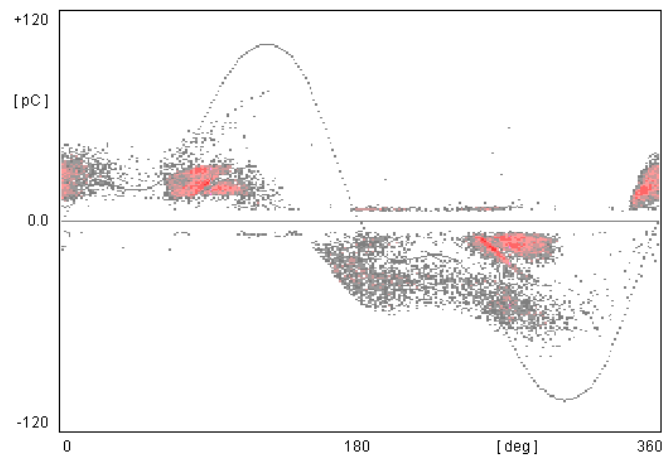


Fig. 3.17 Distorted void discharge pattern due to core saturation

Likewise, Fig. 3.17 shows a distorted shape of the high voltage with a dominant content of the 2nd harmonic due to core saturation⁶ and the related distortion of the cavity discharge pattern. Here, interestingly, the larger, scattered pattern in the negative half cycle (indicating low electron availability) directly shows the distortion, while the discharge in the positive half cycle with a higher availability of electrons is split into two pattern [Gro98₂].

⁶ This was a measurement on site, where a voltage transformer of a GIS was used as high voltage source with a big variac. At some voltage during the test the VT's core saturated.

If the gas inclusion is not spherical, but a flat delamination, such as an air-filled pocket between layers of insulating material, the process to derive the starting electron and to bridge the gap is identical as for voids. Such embedded air pockets are the consequence of various degradation processes of technical insulation systems, such as delamination within mica layers, gas-filled pockets between paper layers of transformers, or delamination in cable accessories.

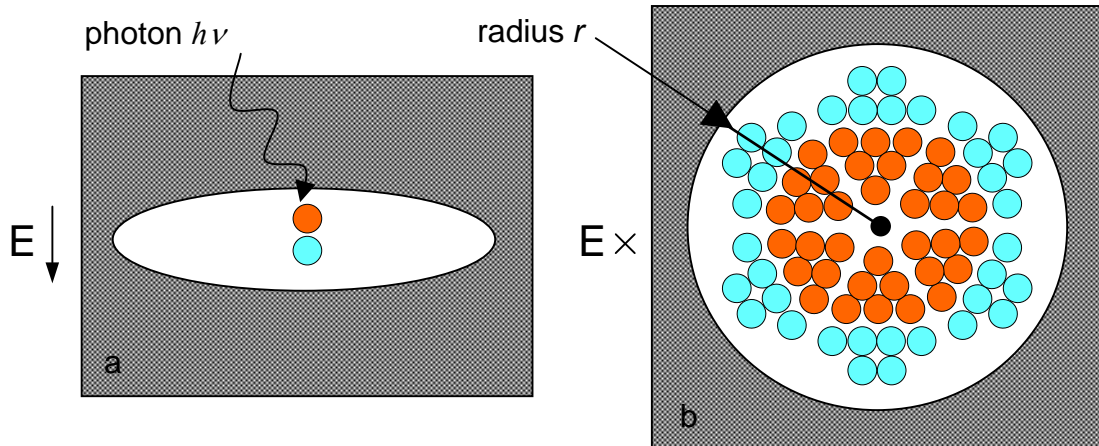


Fig. 3.18 Partial discharge mechanism in a flat gas-filled pocket or delamination

Fig. 3.18 shows on the left such delamination in a side view (a) and in a top view at the right hand side (b). Once the electron avalanche was started due to the first ionization by a photon having sufficient energy, the discharge bridges the gap. However, this discharge causes a surface discharge on the "landing" surface (b). The radius of the area covered by this so-called Lichtenberg figure on a dielectric surface is proportional to the local electric field at the start of the electron avalanche [Lee27]. Fig. 3.19 shows examples of such Lichtenberg figures as well as their calibration to the applied high voltage⁷. Already Lichtenberg (1742-1799) found during his experiments strong differences concerning the surface discharge of positive and negative polarity.

⁷ Interestingly, this contribution to the General Electric Review in the year 1927 used size, appearance, and the differences concerning the polarity as a measurement and recording device to study surges on transmission lines, as adequate instrumentation for onsite application wasn't available then. The instrument contained a brass rod electrode on a photographic film on top of homogeneous insulating material with a plane electrode on the opposite side. Their setup used two anti-parallel connected circuits of the configuration as described above to be able reading both surge polarities using the larger positive Lichtenberg figure.

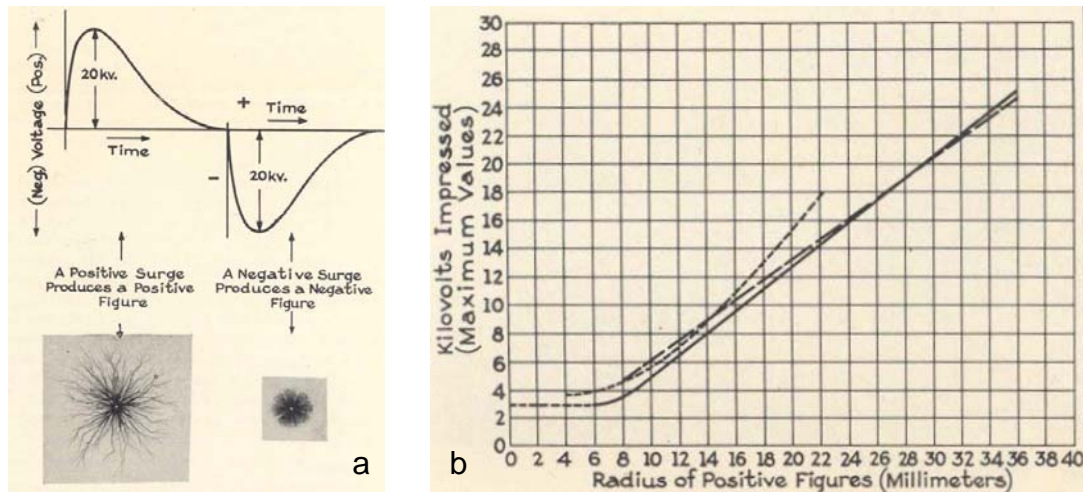


Fig. 3.19 Size of Lichtenberg figures as a measurement of surge amplitude [Lee27]

As found with the void discharge process already, the time lag to get the starting electron results in a correlation with the local electric field. Moreover, based on the found linear relation between the electric field and the radius of the resulting surface discharge, the area covered by this surface discharge is correlated to the square of the electric field. Thus, the envelope of the partial discharge pattern of an ideal flat delamination is correlated to the power of three to the local electric field at the time the discharge starts [Fru95₂, Gro98₂].

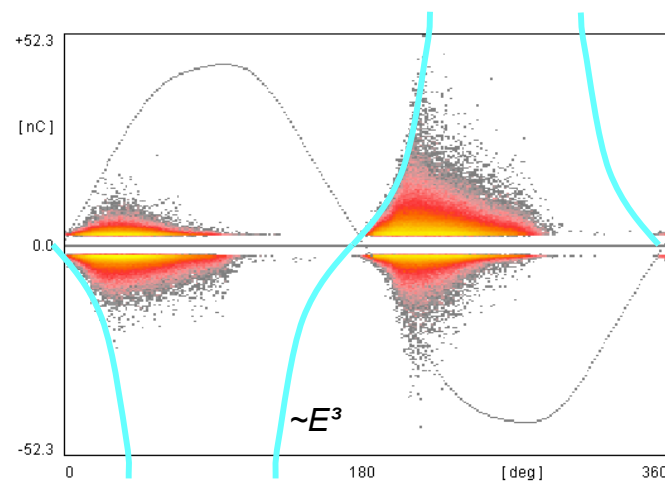


Fig. 3.20 Discharge of a flat delamination – pattern envelope correlated to E^3

Fig. 3.20 shows such delamination (surface) discharge and a superimposed curve according to sine to the power of three. As with the void discharge and depending on the generation of charge carriers, the surface conductivity and, hence, the decay time of the internal electric field, among other influences, not the entire possible area is filled with partial discharge events.

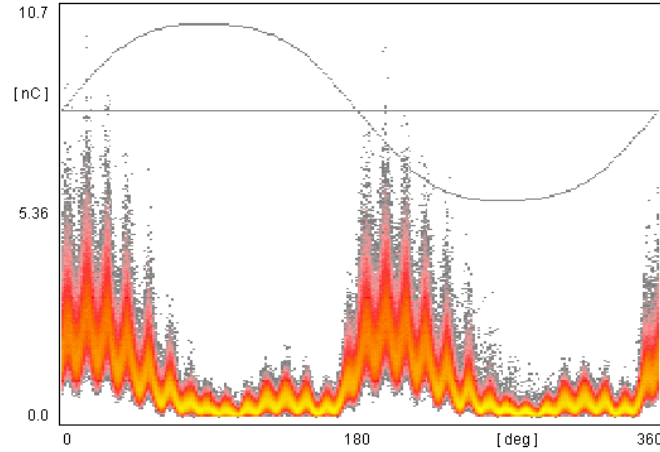


Fig. 3.21 Hydro generator in island operation – modulation by 29th power frequency harmonic

Due to this correlation to E^3 , such delamination discharge shows a much stronger influence of test voltage harmonics (off-line) or power frequency harmonics (online). Fig. 3.21 shows a partial discharge pattern as measured on a generator in a hydraulic pump storage plant. The generator was running in island operation and, hence, the grid does not attenuate the harmonics. Here, the basic pattern shows the typical shape of a service-aged epoxy-mica insulation system including the cross coupling of the neighbor phase. However, the partial discharge pattern is modulated by the 29th harmonic of the power frequency (1450Hz) [Bin00]. Although the amplitude of this dominant harmonic component is below 1% of the fundamental, it modulates the partial discharge pattern by almost 50%. Thus, especially with partial discharge of flat gas-pockets, the strong impact of harmonics shall be considered.

Other partial discharge activity is more controlled by the strong asymmetry of the electric field. Especially point plane discharge is a candidate with strong differences to the processes of discharge in spherical voids. In case of a sharp metallic tip, literally unlimited starting electrons are available. Thus, due to the strongly enhanced electric field at the tip, the critical electric field E_{crit} is firstly reached at the tip in negative polarity. The occurring Trichel pulses show even amplitude and the repetition rate is only controlled by the drift velocity of the charge carriers. The positive space charge cloud in front of the tip shields the tip, but increases the field directly at the tip. With the tip under positive polarity, the electron avalanche starts in the gas in front of the tip, which reduces the field strength directly at the tip, but increases the field in the vicinity.

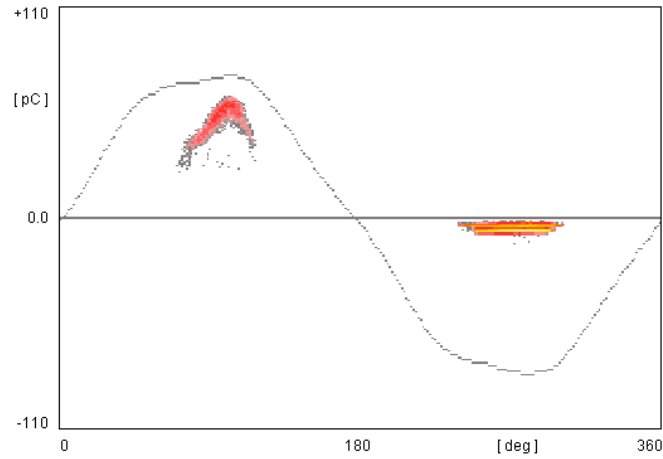


Fig. 3.22 Point-plane discharge – Trichel pulses in neg. and streamer pulses in pos. polarity

Thus, the streamer to leader transition at a sharp tip happens in the positive half cycle. Fig. 3.22 shows a partial discharge pattern of such (metallic) point-plane discharge after the inception of positive streamer. It can be seen that the positive streamer discharge is also prone to influence by power frequency harmonics and, hence, the transition into a leader discharge often happens abruptly.

Another discharge activity with metallic surfaces and, thus, having always immediately starting electrons available, is the discharge of a floating potential, as shown with Fig. 3.23. This is a metallic element in the electric field with typically a small gap to high voltage or ground potential. As soon as E_{crit} is reached, the electron avalanche can start and a row of pulses of even amplitude is generated. This setup produces discharge pulses, whenever the electric field is changing. Thus, the activity starts in zero-crossings, but leaves the 90° and 270° area unoccupied.

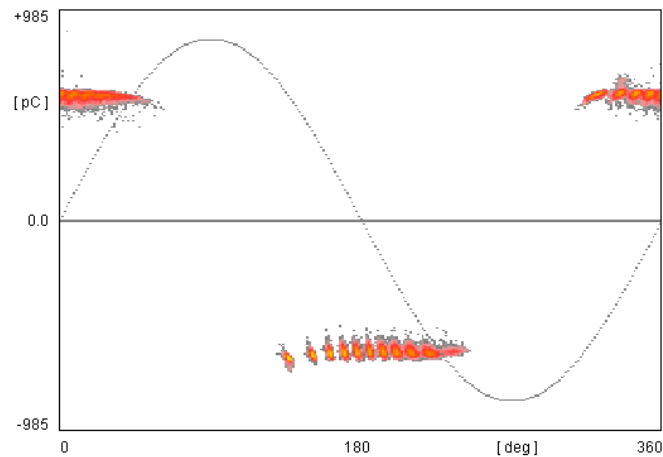


Fig. 3.23 Floating potential discharge with metallic surfaces – pulses of even amplitude

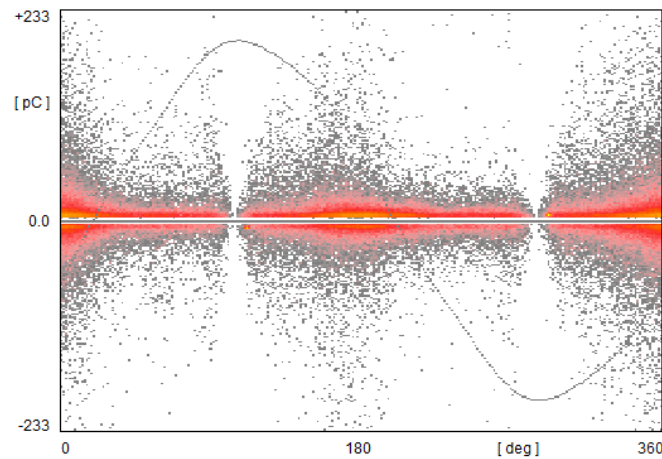


Fig. 3.24 Floating potential discharge with dielectric surfaces – pulse amplitude varies

If, however, the floating potential is covered or coated with insulating material, then, of course, aforementioned processes to derive electrons from polymeric surfaces apply here as well. Fig. 3.24 shows an example of such discharge, where the discharge magnitude varies due to the time lag of the charge carrier generation, while the small area of the test voltage maxima remain clear.

Another typical example is the so-called treeing discharge. Some materials, such as polyethylene, polypropylene, silicone rubber, epoxy resin, and many more are prone to a tree-like growth of a partial discharge channel, whereas always the enhanced field at the tree's tip forces the ongoing growth. As pointed out in the introduction of this chapter, due to ongoing carbonization of the "older" parts of the tree, the activity concerns mostly small gas-filled tubes in the utmost areas of the tree structure. Thus, the partial discharge pattern is mostly symmetrical. Fig. 3.25 shows a typical treeing pattern.

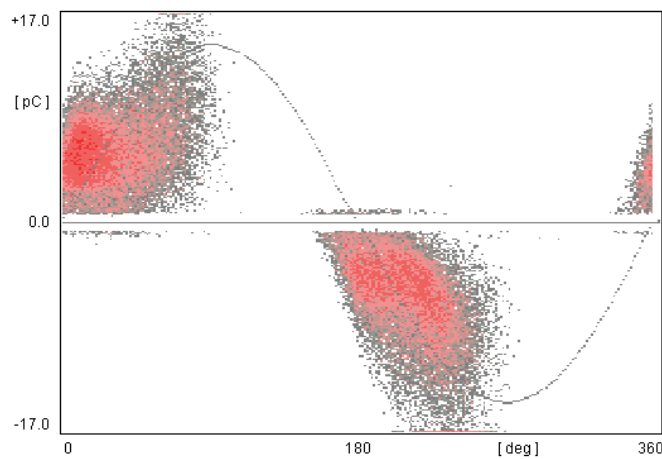


Fig. 3.25 Treeing in polyethylene – mostly symmetrical activity

Special discharge processes, such as discharge under SF_6 , for instance, have not been covered in this chapter. A catalogue of generic as well special partial discharge pattern including the examples of this chapter can be found with the appendix.

3.2 Signal transmission

Mostly, the transport of charge carriers due to partial discharge activity cannot be observed directly, but causes a displacement current at the terminals of the specimen, hence the use of the term "apparent charge". For physically small setups, the displacement current is an image of the underlying current due to moving charge carriers, which concerns mostly the faster moving electrons. At its origin, the resulting current due to an electron avalanche under dry air atmosphere has a rise time of about 1ns ⁸ [Hol91], which translates into a bandwidth of about 350MHz , if assuming an exponential transition and a 1st order decay. Under SF_6 , an electronegative gas, this rise time can be as short as 100ps ⁹ bringing the resulting bandwidth well above 2GHz [Tro10].

Whenever the test object gets physically large, the influence of the internal and external leads has to be considered. This concerns effects such as attenuation, dispersion, and reflection. Likewise, antenna effects – both concerning radiation as well as reception including cross coupling – have to be considered. Additionally, shielding or the lack of shielding and resonances have their influence.

However, already the fact that the said (displacement) current impulse is imposed on a conductor means that it changes into a voltage impulse scaled by the impedance of the conductor. Thus, already here, the general idea of a current impulse that makes it up to a partial discharge detectors measuring impedance is no longer true.

⁸ Measurements of the rise time under pure nitrogen atmosphere show a somewhat slower rise time of few nanoseconds, instead. Here, the impact of oxygen, being an electronegative gas as well, explains the difference [Hud93].

⁹ Such high-speed measurements in time domain are not easy to conduct, as already the required size of the test setup influences and potentially distorts the signal. However, applying spectrum analyzers on real-life gas-insulated switchgear along with antennas having a verified bandwidth, suggest that even pulses with a rise time below 100ps can be expected.

- Attenuation

Obviously, conductors and leads of high voltage equipment are designed to meet the power engineering requirements and are not designed to efficiently transmit high frequency signals. Thus, whenever high frequency (partial discharge) signal have to travel a certain length of power equipment conductor, the related imperfections have to be considered. For instance, such conductors are made of copper or aluminum and, hence, are prone to attenuation due to the skin effect, which cause that the conducting processes take place in an increasingly thin layer with the increase of the signal frequency. The skin effect is described with the skin depth or equivalent conducting layer, i.e., a tube instead of the solid conductor that has the same attenuation. For metallic conductors a simplified formula for the skin depth applies¹⁰ (3.6) [Zin00].

$$\delta = \sqrt{\frac{2\rho}{\omega\mu_0\mu_r}} \approx 503 \sqrt{\frac{\rho}{f\mu_r}} \quad (3.6)$$

Here, δ is the skin depth in meters, ρ the resistivity of the conductor, ω the angular frequency, f the frequency, μ_r the relative permeability¹¹ of the conductor, and μ_0 the permeability of the free space. For copper, as an example, the skin depth is already about 660 μm at a frequency of 10kHz and, hence, 66 μm at 1MHz. For frequencies above 100MHz the skin depth amount few micrometers, only. Thus, just based on the skin effect, a typical generator bar of a turbo generator with a length of 10m shows an attenuation of approx. 40dB at frequencies above 100MHz.

The same applies to the aluminum conductor of power cables, whereas the resistivity of aluminum is about 68% higher than the resistivity of copper, which increase the resistance linearly and increases the skin depth by about 30%.

¹⁰ The formula is more complex for poor conductors and semiconductors, as then also the dielectric constant has to be considered.

¹¹ Having the relative permeability in the denominator of the skin effect formula clearly shows why iron conductors are already poorly suited for 50 or 60Hz transmission. With a μ_r of about 2×10^5 for iron, the skin depth is in the range of 200 μm for 50Hz, only.

- Dispersion

Generally, the propagation speed v in cables depends on the dielectric properties of the insulation material used. The propagation speed in free space c_0 is reduced by the square root of the relative dielectric constant of the material ϵ_r . With the vacuum permeability μ_0 , the relative permeability μ_r and the dielectric constant ϵ_0 the propagation speed c is calculated (3.7).

$$v = \sqrt{\frac{1}{\epsilon\mu}} = \sqrt{\frac{1}{\epsilon_0\epsilon_r\mu_0\mu_r}} = c_0 \sqrt{\frac{1}{\mu_r\epsilon_r}} \quad (3.7)$$

However, due to polarization effects, the dielectric constant is frequency dependent. The complex permittivity ϵ^* , considering the relaxation of polarization with ϵ_{lo} as the permittivity for low frequencies, ϵ_{hi} for high frequencies, and τ as the relaxation time constant is (3.8) [Yad10]:

$$\epsilon^* = \epsilon_{lo} + \frac{\epsilon_{lo} - \epsilon_{hi}}{1 + i\omega\tau} \quad (3.8)$$

However, polymeric material shows a more complex behavior than the Debye theory as introduced for liquids, whereas the main differences are that the dipoles cannot move as freely as in liquids and that there is not a single polarization process and relaxation time constant [Yad10].

Another – technically more relevant – source of dispersion is caused by semi-conductive material being introduced in the insulation system to smoothen the electric field both on ground and on high voltage side. For polyethylene insulated cables, nowadays an inline triple extrusion process is used, where firstly a layer of semi-conductive copolymer is extruded, followed by the main polyethylene insulation, and finally another semi-conductive copolymer. Concerning dielectric properties and transmission properties this makes the insulation a stacked lossy insulation.

One can estimate the influence of this stacked lossy insulation in different ways. The theoretical approach would look at the Poynting vector (3.9), which is in the direction of the transmission for a loss-free cable, but which turns away from the

transmission direction into the semi-conductive layer, when approaching the conductors. This indicates the losses in the semi-conductive layer, as the electric field contains an axial component in the semi-conductive layer. Here, \vec{S} is the Poynting vector, \vec{E} the electric field, and \vec{H} the magnetic field [Kue13].

$$\vec{S} = \vec{E} \times \vec{H} \quad (3.9)$$

Another, more practical approach is using the aforementioned skin effect to calculate from on which frequency the semi-conductive layer cannot be any longer assigned to the conductor, as it is done at power frequencies.

If considering a resistivity of such carbon-loaded copolymer¹² in the range of 1-10Ωm, while using the simplified formula (3.3), the skin depth comes in the range of the typical thickness of such layers (~1mm) at a frequency of about 10MHz. Thus, above frequencies of few MHz, the influence of dispersion has to be considered for polymeric high voltage cables [Gro99, Gro03₂].

Likewise, the semi-conductive tapes as used in the production of generator bars have this effect to the signals traveling the coils. However, as those tape layers are usually thinner than the semi-conductive layers in extruded cables, the inception of the effect is higher in frequency and was found in the range of about 20MHz. At frequencies above 100MHz the impact of the dispersion dominates all other effects causing attenuation in stator coils [Hud01, Gro03₂]. Further, even internal paint layers in gas-insulated switchgear equipment can cause such effects, if they have intentionally some resistivity in the relevant order of magnitude to cope with surface charges, for instance. As this concerns only paint layer thickness, the effect incepts at much higher frequencies, but becomes relevant for UHF signals in GIS [Gro15₂].

In terms of high frequency signal integrity, the dispersion has two main effects. Firstly, the polarization effects in general and the impact of the aforementioned semi-conductive layers at its inception cause a different arrival time of different frequency components.

¹² The resistivity of such carbon-loaded copolymers is strongly temperature dependent and, hence, also the inception of the resulting attenuation is temperature dependent.

This effect distorts the shape of fast pulses and reduces the rise time, such if the found spectral components of a Fourier analysis would be recombined wrongly in time domain. For frequencies well above the inception of the influence as posed by the semi-conductive layers, the resulting dispersion just appears as attenuation.

- Reflection

With any conductor, a traveling wave undergoes a reflection, when the impedance changes. In power engineering this happens frequently, while it is strictly avoided in communication engineering. The impedance Z_L of a coaxial cable is defined by the outer diameter D , the inner diameter d , the permeability of the free space μ_0 , the permittivity of the free space ϵ_0 , and the relative permittivity of the insulation material ϵ_r (3.10) [Zin00].

$$Z_L = \frac{1}{2\pi} \sqrt{\frac{\mu_0}{\epsilon_0 \epsilon_r}} \ln \frac{D}{d} \approx \frac{60\Omega}{\sqrt{\epsilon_r}} \ln \frac{D}{d} \quad (3.10)$$

Thus, whenever there is a change of diameters, as it is very common in power engineering designs, there is an impedance change. For instance, cable joints are typically designed as shown in Fig. 3.26. Within the joint, the inner diameter is larger than the outer diameter of the cable to shield the crimping area, while the difference between the diameters $D-d$ approximately stays the same. With this example the impedance changes from $\sim 26\Omega$ ($D/d = 100\text{mm}/50\text{mm}$) for the cable to $\sim 13\Omega$ ($D/d = 170/120\text{mm}$) in the joint section [Gro99, Gro07₁].

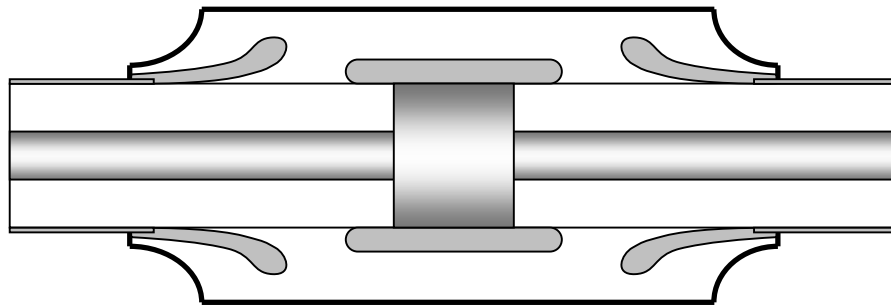


Fig. 3.26 Typical prefabricated cable joint of a polymeric high voltage cable

A reflection occurs at every change of the impedance. For a traveling impulse, this reflection can be positive or negative [Gro03₁, Gro04₁]. The reflection factor is calculated based on the impedances (3.11).

$$\Gamma = \frac{Z_1 - Z_2}{Z_1 + Z_2} \quad (3.11)$$

Whereas Γ is the reflection factor, Z_1 the impedance before, and Z_2 the impedance after the dimension change.

For the example given above, the reflection factor is -0.33, when the wave is entering the joint and +0.33, when the wave is exiting the joint. Thus, an impulse traveling the cable will cause a negative reflection that is immediately superimposed by a positive reflection. With help of this usually little s-type curve joints in cables can be identified, when doing the calibration with an impulse calibrator.

Likewise, for power engineering reasons, the internal diameter within gas-insulated equipment changes frequently. Fig. 3.27 shows a simplified cross section of a GIS load breaker chamber. Here, the numerous changes in impedance cause numerous reflections and make partial discharge signals bounce back and forth at each step. In the same way, the armature for insulator rods in gas-insulated lines both on high voltage and on ground potential cause such reflections. In GIS and GIL this has two main consequences. Firstly, the multiple reflections make the signal apparently ringing, as it can be seen with Fig. 6.15, for instance and, secondly, this appears as attenuation, as only a fraction of the signal makes it across the point of reflection. In GIL, this attenuation adds up for every insulator and, as there are plenty, easily accumulates to 20dB/100m.

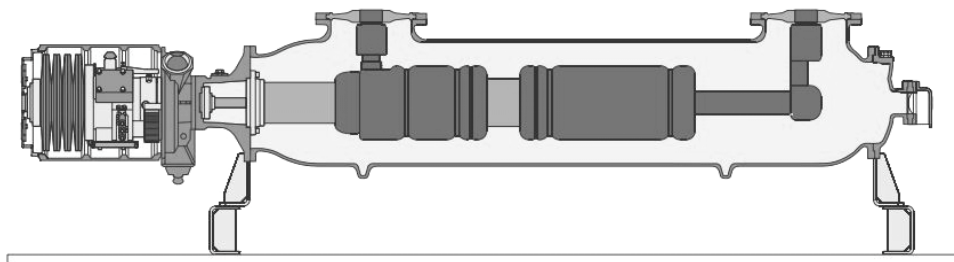


Fig. 3.27 GIS breaker chamber – diameter steps change the impedance and cause reflections

For the stator winding of rotating machines, the situation is even worse. In the slot section, the high frequency behavior is like a coaxial cable with comparably small impedance, as the insulation is relatively thin, while the cross section of the conductor is comparably large. Outside of the slot in the core, in the so-called overhang, the conductor acts like a bare conductor against remote ground. Thus, in the slot section, the impedance is in the range of $10\text{-}20\Omega$, while it is well above 100Ω in the overhang (Fig. 3.28). For typical winding designs with formula 3.11 this results in reflection factors of 80% and more. Thus, above a certain corner frequency, which is a function of the length of the bar, the high frequency components of an impulse-like signal are being trapped within the slot section of that specific bar, as the signal undergoes a positive reflection at each slot exit [Gro02₂, Gro03₁].

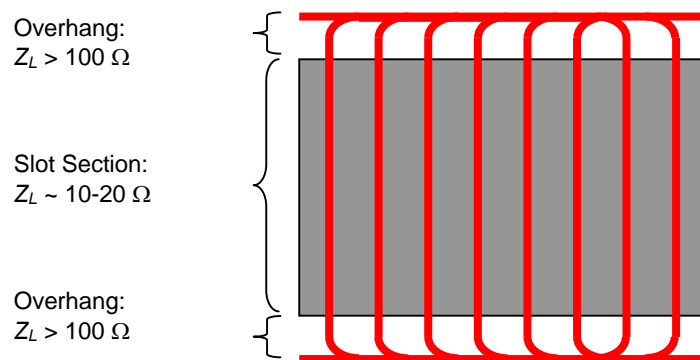


Fig. 3.28 Impedance of different sections of a stator coil

- Radiation and reception

Whenever the high frequency (partial discharge) signal travels an unshielded conductor, as for instance the overhang of a stator winding (Fig. 3.28), parts of the signal are radiated. Likewise, nearby overhang coils eventually receive parts of the radiated signal. Thus, this effect partially compensates the aforementioned effect to trap signals due the reflections. However, the efficiency of this process is almost unpredictable and assessment requires individual measurements on the device under test.

Likewise, in large power transformers many unshielded leads of different coils are being laid and meet at different places, which allow this radiation and receiving of usually higher frequency components, as the efficiency of those parasitic antennas increase with the frequency. Fig. 3.29 gives an idea of the numerous leads that are found in a transformer.

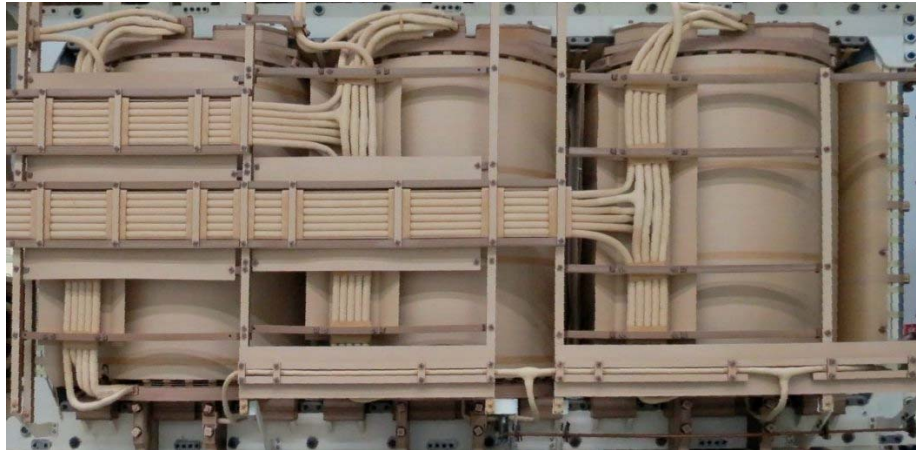


Fig. 3.29 Tap leads of an untanked autotransformer – possible signal coupling

Here, the tap leads, which are usually on common potential with an autotransformer, "travel" on the low voltage side from each coil to the tap-changer, which is left of the view shown. As further the high voltage coil is designed as a dual coil with the connection in the middle of the coil on the rear side, there are plenty of coupling possibilities involving radiation and receiving. Moreover, of course, those crossings are potential places for partial discharge activity, if, for instance, an air bubble was somewhere trapped in glue.

- Resonances

Power engineering requirements and high voltage design principles make the use of physically large components mandatory. With the size, the parasitic properties of inductors, capacitors, and leads increase. The inductance of a capacitor limits its usable frequency by causing a resonant behavior. Likewise, the winding (stray) capacitance of an inductor leads to resonances. For more complex systems, such as large power transformers, frequency response analysis (FRA) helps to understand the behavior in frequency domain.

Of course, partial discharge signal are in the same way influenced by such complex input impedances, when it comes to applying a calibration signal to a terminal of power equipment or, when a signal shows a surprising "gain" at certain frequencies. Here, parallel resonances are easier to detect than series resonances of input impedances, for example.

3.3 Calibration

Partial discharge measurements in terms of charge magnitudes are relative and not absolute measurements. I.e., the partial discharge detector is calibrated in the circuit with the device under test with an impulse charge source of known magnitude. The charge impulse q_0 is simply generated using a step voltage U_0 and an injection capacitor C_0 (3.12).

$$q_0 = U_0 C_0 \quad (3.12)$$

Fig. 3.30 shows how such charge impulse calibrator is connected across the test object to simulate an equivalent discharge in the test object [60270₁]. Of course, it shall be avoided to have a stray capacitance C_s bridging the injection capacitor C_0 and, in case, increase the injected charge. However, with commercially available charge calibrators, the injection capacitor C_0 typically is an integral internal part of the unit, while leads of the step voltage are shielded to avoid such influence.

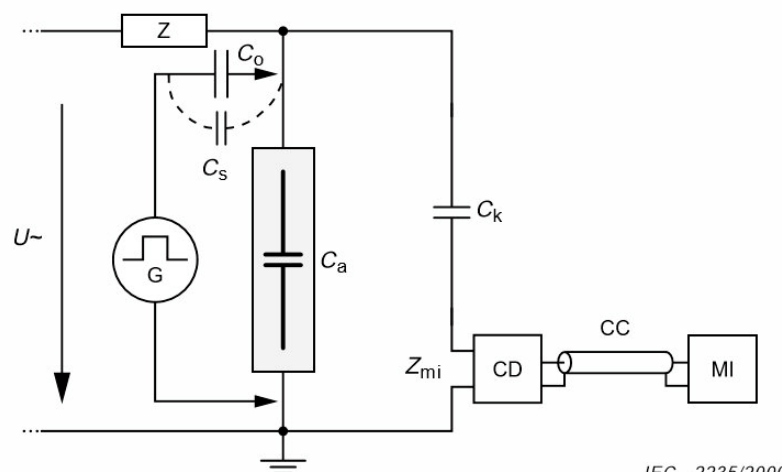


Fig. 3.30 Connecting an impulse calibrator to the test object

Looking at Fig. 3.30, it is obvious that C_0 shall be small against C_a , the test object, as otherwise the intended charge q_0 is lowered to q as a function of the said capacitances (3.13). The relevant standard [60270₂] sets the permissible limit to $C_0 < 0.1 \times C_a$. However, for calibration, the corrected charge value shall be used (3.13).

$$q = q_0 \frac{C_a}{C_a + C_0} \quad (3.13)$$

Further, it is essential that the rise time of the step voltage is short and, hence, the amplitude spectrum of the calibration pulse does well exceed the bandwidth of the detector used. Fig. 3.31 illustrates this requirement [60270₂].

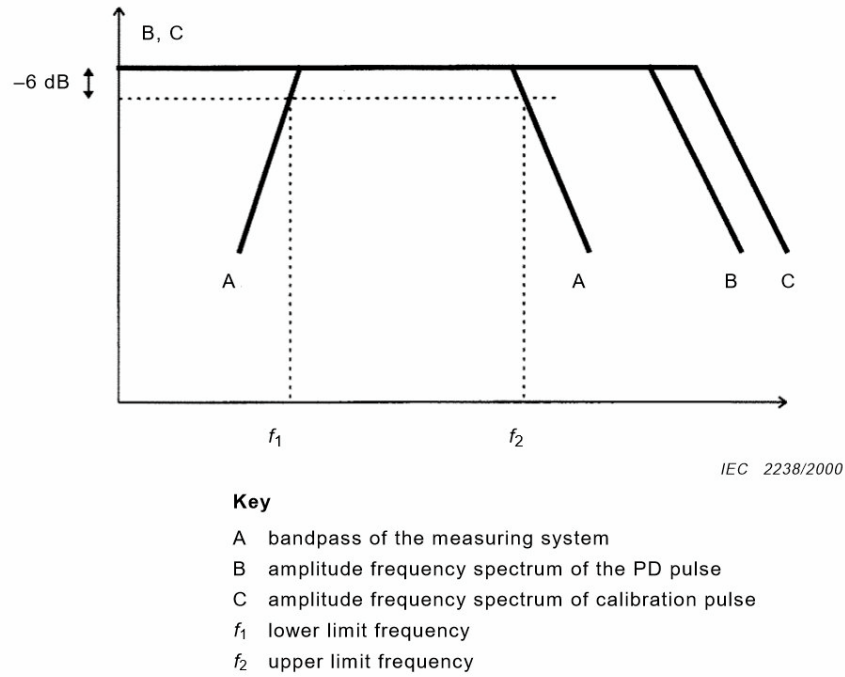
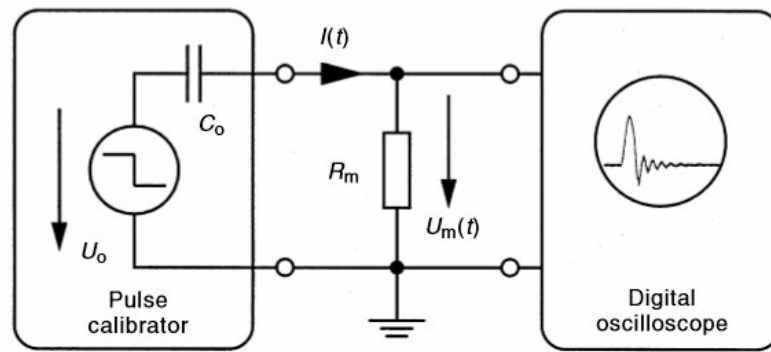


Fig. 3.31 Bandwidth relation of detector (A), partial discharge (B) and calibrator (C) signal

Of course, calibrators require calibration. With the 2000 revision of the IEC60270, an "alternative" calibration method was included with the normative appendix A.3 of the standard [60270₁]. This appendix describes the usage of a digital oscilloscope with numeric integration function to integrate the transient voltage drop u_m across a measuring resistor R_m of 50-200Ω (3.14).

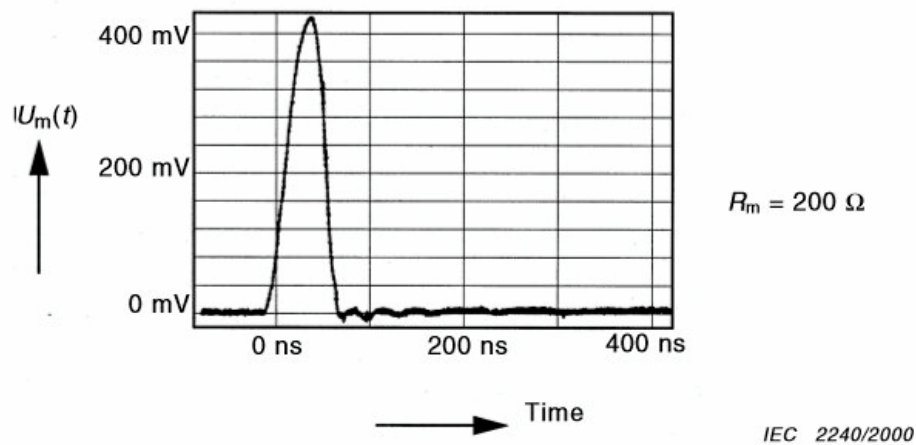
$$q = \int i(t) dt = \frac{1}{R_m} \int u_m(t) dt \quad (3.14)$$



IEC 2239/2000

Fig. 3.32 Circuit to calibrate a charge calibrator – alternative method A.3 [60270₁]

Fig. 3.32 shows the circuit proposed with A.3. The standard requires a minimum bandwidth of the digital oscilloscope of 50MHz. The resistor R_m shall be chosen to not produce ringing of the signal. In the same interest, the leads shall be kept short. Fig. 3.33 shows the voltage drop across R_m for a resistor of 200Ω.



IEC 2240/2000

Fig. 3.33 Voltage drop across R_m for a 100pC calibration impulse

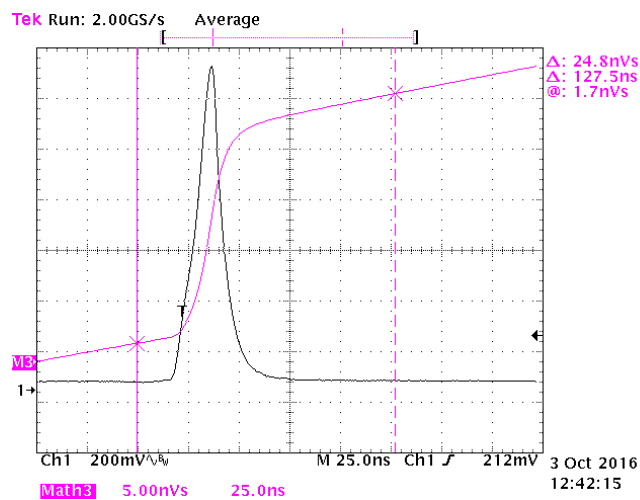


Fig. 3.34 Screenshot during calibration using a 4Gsample/s oscilloscope

Fig. 3.34 shows a screenshot during the calibration according to A.3 with a 100pC signal, an R_m of 200 Ω using an oscilloscope with a bandwidth of 1GHz and up to 4Gsample/s. The cursors are positioned to cover the signal starting before the impulse and well in the steady state. Before calibration, the offset of the numeric integration is taken and considered. Here, the integral of $u(t)$ between t_1 and t_2 is 24.8nVs, while the output of the integral without signal is -4.6nVs. Thus, the resulting charge value q is 20.2nVs/200 Ω = 101pC.

Of course, everybody can perform the calibration measurements as described. However, issuing a traceable calibration certificate requires an accreditation according the ISO/IEC17025. Besides determining the procedures, also estimating the uncertainty budget is part of the accreditation process. Using adequate equipment, the uncertainty budget for impulse charge calibration supports an expanded uncertainty U_q down to 2% (3.15) covering a range of 1pC to 50nC [Cal16].

$$U_q = 0.2pC + 0.02q \quad (3.15)$$

With the 2015 addendum to the IEC60270 [60270₂], an additional calibration method – "Step voltage response method" – was introduced and included under appendix A.4, which aim is to measure the step voltage across a know capacitor (Fig. 3.35).

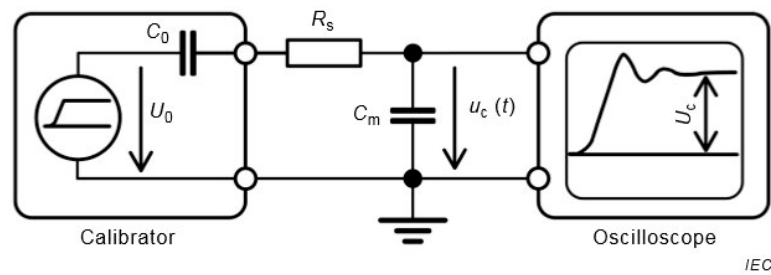


Fig. 3.35 Step voltage response method

As this method concerns only the initial step, it is obvious that this has to go along with very tight requirements for the step voltage of the calibrator, as every signal after the initial step would be ignored by this method, but would contribute to the integration result of the method described under A.3. Thus, a definition of the step voltage of the calibrator was added as well (Fig. 3.36).

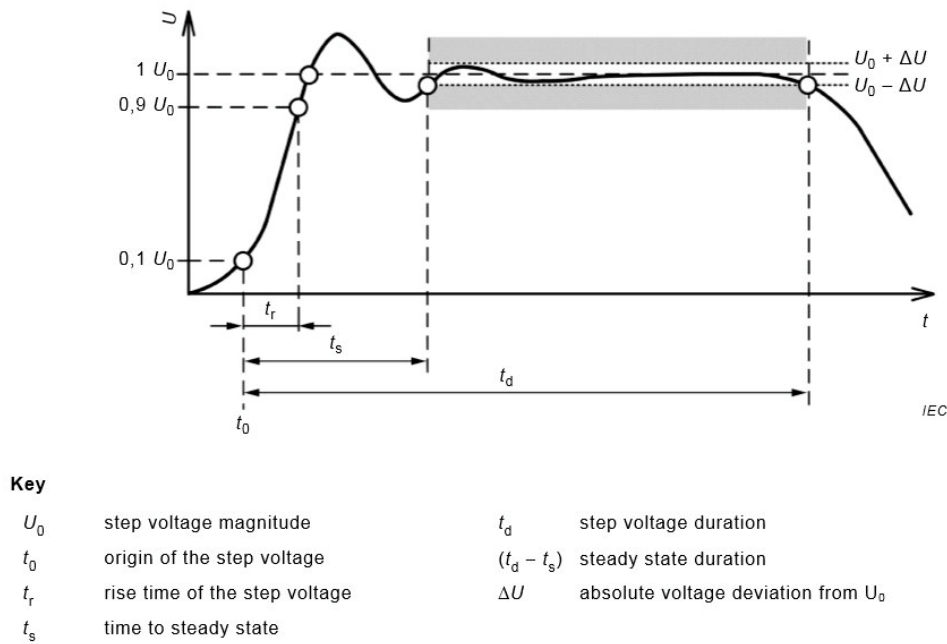


Fig. 3.36 Charge calibrator – definition of the step voltage properties [60270₂]

With the 2015 addendum, the rise time t_r was set to be not longer than 60ns, the time to steady state t_s not to be longer than 200ns, the stable step voltage duration t_d to be at least 5 μ s, and the deviation ΔU not be larger than 3% of U_0 . During the working group discussion, to support this method, it was requested to have ΔU limited to 0.5% of U_0 . However, this requirement did not survive the commenting and voting process. Moreover, meeting this requirement in terms of measurement in a calibration lab with a duly calculated uncertainty budget is more than demanding.

Thus, with ΔU agreed to be smaller than 3% and with respect to the graph defining the requirements (Fig. 3.36), the worst situation that can occur would be a signal being in the beginning at the upper limit, but staying most of the time at the lower limit or vice versa. Such unfavorable condition would cause the two methods according to A.3 and A.4 to deviate by almost 6%, which cannot be intended, as the accuracy of the partial discharge measurement shall be better than 5%, as stated in the standard as well.

Generally, the principle of quasi-integration can be used at higher frequencies as well. Here, the limitations as discussed in chapter 3.2 shall be considered. Thus, with an increasing size of the test object and increasing measurement frequencies used, the calibration turns more and more into a rough estimation of the sensitivity.

Moreover, when it comes to diagnostic partial discharge measurements, the main aim is to assess and understand the defect mechanism. When looking at the discharge magnitude in such cases, emphasis is put on comparison in a time line and not on absolute magnitudes. I.e., besides the pattern analysis, the trending information is the key to the analysis and, again, calibration is needed to have a rough idea of magnitude and sensitivity.

For gas-insulated equipment, this contradiction that charge-based measurements cannot be one-to-one transferred into very elevated frequencies is being solved with a verification of the sensitivity [Boe99, Neu00]. With this procedure, the result of the Cigré working group TF 15/33/03.05, in a first step, the gas-insulated switchgear is set up in a factory environment with a known partial discharge source of about 5pC, conventional partial discharge measurement equipment, UHF sensors to capture the high frequency partial discharge signals, and an UHF partial discharge measuring or monitoring system. The readings of IEC60270 and UHF measurements are compared and a steep pulse is injected with a calibrator having a rise time of 500ps or below (Fig. 3.37).



Fig. 3.37 UHF impulse calibrator – injecting step voltage signals with a rise time of <100ps

The magnitude of the step voltage signal that produces the same reading as the 5pC partial discharge signal is then determined. This is then valid for the combination of GIS, sensors, and instrumentation. In a second step, the found step voltage magnitude is then applied in a substation on the different sensors to determine, if partial discharge activity corresponding to the 5pC activity can be detected. However, even with this verification, the UHF monitoring instruments shall read rather dBm or dBμV referring to their input, as described in chapter 5.3 instead of using pC [Gro07₂, Tro10].

The rise time t_r of the step voltage impulse has a strong impact on the described sensitivity verification. For typical GIS, the dominant H_{10} ¹³ base mode is in the range of a couple of 100MHz and can be excited with a pulse of 500ps¹⁴ rise time. However, all higher modes that can also travel the GIS require a pulse rise time of 100ps or less, as it is found with partial discharge signals under SF₆.

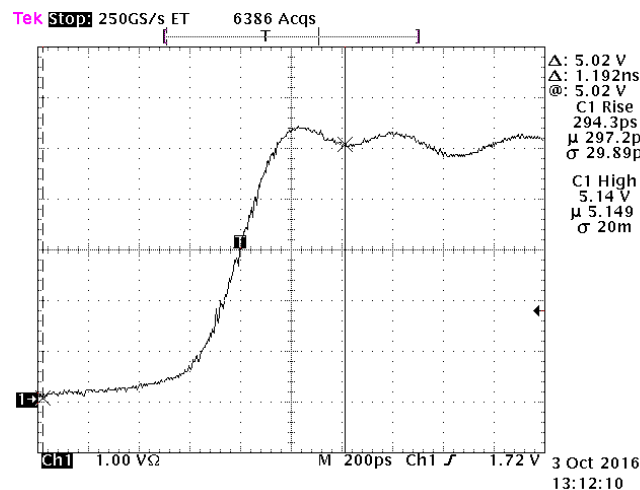


Fig. 3.38 Rise time of a CAL2B step voltage calibrator

Fig 3.38 shows the rise time of a CAL2B calibrator as measured on a fast oscilloscope Tektronix 784D. However, the oscilloscope's rise time is 210ps. Thus, in the first place, the oscilloscope's rise time is dominates measurement.

¹³ The H_{10} (or $TE_{1,0}$) mode offers the lowest frequency transmission in a rectangular waveguide. The first number denotes the multiple of $\lambda/2$ that fit the waveguide's long side.

¹⁴ The 500ps rise time is a critical limit of the so-called Dual-Use Regulation (Council Regulation (EC) No. 428/2009). Pulse generators having a rise time of 500ps or less, output amplitude of 6V or more into less than 55Ω are subject to export limitations. Thus, besides the CAL2B with a rise time of presumably below 100ps, there is also the model CAL2B/500 having a rise time slightly above the 500ps.

However, in light of the limitations for non-lumped components, as discussed with the previous chapter, the usage of the term calibration implies an accuracy that partial discharge measurements often cannot deliver.

Moreover, looking at common partial discharge testing periods of frequently a minute, which is surely understandable in terms of factory processes, it is obvious that applying such short testing times does not give justice to the generation processes of initial electrons for cavities in polymeric material.

Likewise, the use of the term guarantee level especially with non-forgiving insulation material such as polyethylene shall be seen critical. In such case, of course, it is needed to define a mandatory sensitivity or noise floor, but the goal should be rather "no visible partial discharge" at the required test voltage and not "just below the guarantee level" (Fig. 3.39).



Fig. 3.39 Guarantee level... (Lutz Niemeyer)

4 Coupling methods and circuits

As partial discharge testing requires applying high voltage to the test object, a safe method is needed to separate the high voltage potential and the high frequency partial discharge signal. Hence, such circuits are often called power separation filter.

Generally, different techniques are applicable and in use. They all have two main tasks in common to firstly reduce the remains of the power frequency to magnitudes that do not harm the user or subsequent equipment and, secondly, to efficiently de-couple the high frequency signals. In a typical 50Hz testing environment, power frequency and the lower cutoff frequency of the partial discharge measurement are just three decades apart, while it is only approximately two decades separation in case of the upper permissible power frequency of variable frequency resonant test sets. Thus, in general, high-pass filters of higher order are needed to achieve the desired attenuation.

4.1 Capacitive coupling

The capacitive coupling is the most efficient coupling technique. Here, a coupling capacitor is connected in parallel to the test object and, hence, provide the high frequency return path for the partial discharge impulses. A measuring impedance or quadrupole is fitted into this circuit. Concerning the high frequency behavior, it doesn't matter, whether the quadrupole Q is put into the ground lead of the coupling capacitor (Fig. 4.1, a) or into the ground lead of the test object (Fig. 4.1, b). However, as firstly the capacitance of the test object C_T is often larger than the capacitance of the coupling capacitor C_k , the quadrupole is usually put into the coupling branch to benefit from the smaller capacitive load current. Moreover, secondly, in the event of test object failure, the quadrupole would suffer from the short circuit current, if placed in the test object branch.

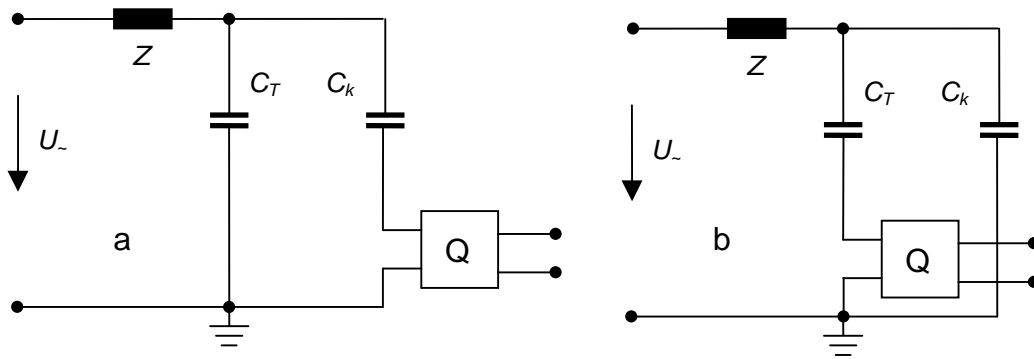


Fig. 4.1 Capacitive coupling - quadrupole underneath coupling capacitor (a) or test object (b)

A basic measuring impedance or quadrupole consists of an inductor and a damping resistor to form a second order high pass filter (Fig. 4.2). The corner frequency shall be below the lower cutoff of the partial discharge detectors. Thus, the inductance of the quadrupole must be matched to the coupling capacitor to match the detector's bandwidth, i.e., its lower cutoff frequency (4.1).

$$f = \frac{1}{2\pi} \sqrt{\frac{1}{LC}} \quad (4.1)$$

Additionally, a damping resistor is needed to avoid an oscillatory behavior of the circuit (Fig. 4.2). Typically, the damping of this second order filter (4.2) shall be aperiodic ($D = 0,707$). However, damping values between 0,3 and 1,0 produce suitable response. A stronger damping, i.e. a smaller resistor, reduces the overall sensitivity, while a weaker damping do cause oscillations, which at least reduce the pulse repetition rate¹⁴ that can be processed by the partial discharge detector.

$$D = \frac{1}{2R} \sqrt{\frac{L}{C}} \quad (4.2)$$

Whereas C , L , and R are the components as shown in Fig. 4.2.

¹⁴ The repetition rate that can be processed by a partial discharge detector is more prominently influenced by the reciprocal of the processing circuit's bandwidth. For 9kHz narrow band detection, for example, this rate will be few thousand pulses per second, only.

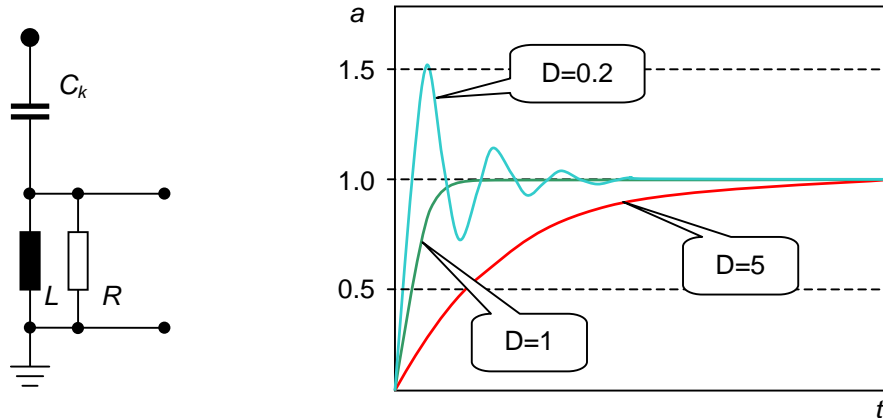


Fig. 4.2 Basic RLC coupling circuit and its step function response

The step function response of such a damped series resonance circuit is shown with Fig. 4.2 for different damping factors. For a typical 1nF coupling capacitor the inductance of the quadrupole shall be about 15mH to meet 40kHz, for instance. Hence, for this example, the damping resistor shall be about 2.7k Ω .

Obviously, such circuit would be inappropriately loaded, if connected to a detector using a cable of any style¹⁵. Using a cable with 50 Ω impedance (and termination) would cause a damping of >100 and shift the corner frequency to 3,18MHz with a first order decay of 20dB/dec. Thus, an impedance matching is needed directly at this point. This can be a matching transformer¹⁶, such as a balun¹⁷ or an active impedance converter, i.e. a voltage follower or amplifier as shown in Fig. 4.3.

¹⁵ However, although not very elegant, a coupling capacitor can be terminated with a 50 Ω (power) resistor. 11nF into 50 Ω creates a first order filter with a corner frequency of 290kHz.

¹⁶ Here, the critical property of such matching transformers is their winding and stray capacitance, which would introduce a self-resonance and a strong damping at higher frequencies. Thus, old-fashioned low-capacitance basket weave coils, as known from early radio sets offer lowest winding capacitance and a sufficiently high self-resonance frequency.

¹⁷ Balun stands for **balanced-unbalanced** and their main application is to match single-ended (unbalanced) lines, such as coaxial cables to parallel (balanced) lines such as twisted pair. In lower frequencies, baluns are commonly constructed using bifilar or trifilar isolated wires on ferrite ring cores, while in higher frequencies, short coaxial cable can cover the task. In case of quadrupoles, baluns serve to transform the impedance. For instance, a four-to-one balun transforms the impedance by a factor of 16 (4²). Hence, with such 4:1 balun, the 50 Ω of a conventional coaxial cable translates into 800 Ω .

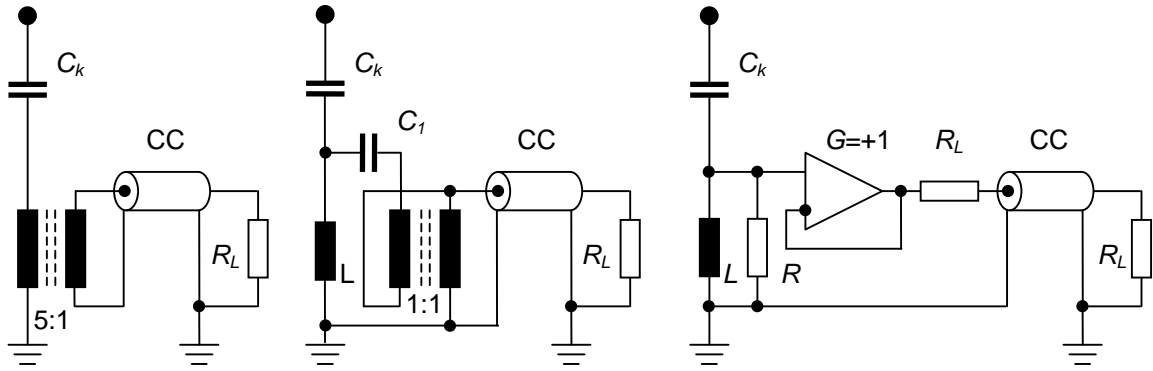


Fig. 4.3 Impedance matching: transformer, balun, and amplifier as voltage follower

As partial discharge signals are comparably faint, early amplification helps to reduce pickup of ambient noise on the signal path to the detector. Moreover, as the signal cable's sheath is preferably grounded on both sides, transient sheath currents can easily add to the faint signal. Here, clip-on ferrites¹⁸ act as sheath-current-transformers and reduce such effects.

If the capacitance C_1 of a transformer bushing is used instead of the afore discussed separate coupling capacitors, additionally the bushings stray capacitance C_2 to ground has to be taken into account (4.3).

$$f = \frac{1}{2\pi} \sqrt{\frac{1}{L(C_1 + C_2)}} \quad (4.3)$$

For composite bushings and bushings with the so-called test tap, this stray capacitance is in the same range as the main capacitance, while it can reach comparably high values for ANSI bushings with voltage tap¹⁹ and, hence, dominates the overall circuit.

¹⁸ Such clip-on-ferrites are commonly used to reach EMI requirements for commercial electronic equipment. The relevant EMI standards cover well the frequency bands needed for partial discharge testing (40-1000kHz).

¹⁹ The test tap is connected to the last layer of the stack of n capacitive layers that are separated with aluminum-coated paper. Thus, the capacitance $C_2 = n \times C_1$ can reach 20nF and above. Additionally, this high C_2 hampers the sensitivity of PD (and RIV) measurements.

Likewise, instead of a dedicated coupling capacitor, also a second (preferably identical) test object can provide the high frequency return path. Especially in a balanced circuit, i.e., with a balanced quadrupole, or a quadrupole in each branch, such configuration can greatly improve the circuit's noise immunity and overall sensitivity.

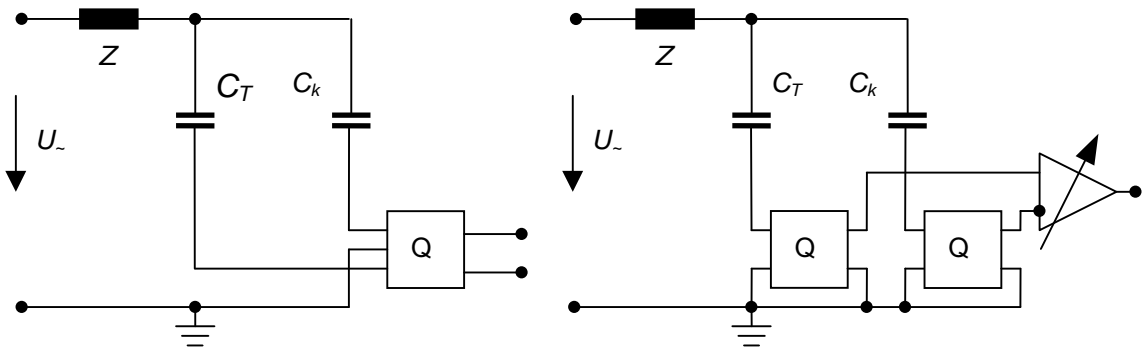


Fig. 4.4 Balanced circuit using a test object and a coupling capacitor or two test objects

With the balanced circuit²⁰ (Fig. 4.4), the common mode noise signal is in phase at the two quadrupoles, while the partial discharge signal is in antiphase. Thus, a differential amplifier cancels the noise signal, while it adds the two partial discharge signals. However, care must be taken to have identical corner frequencies and damping in order to reach an identical pulse decay and undershoot, as differences between the branch responses make the remains of noise signals survive the cancellation.

Besides the obvious capacitors, also stray capacitances of construction elements, such as internal shields of gas-insulated equipment, can be used for capacitive coupling, for example. Of course, the same rules for quadrupoles, as discussed before, apply.

²⁰ Traditional balanced circuits made use of a manually balanced bridge (Kreuger Bridge, [Kre64]), where the measurement impedances were inside the detector. The bridge was then adjusted for minimum noise, and subsequently calibrated. Nowadays, the differential amplification is done electronically, while the adjusting procedure remains the same, in principle.

4.2 Inductive coupling

The initial displacement current of the partial discharge cause transient currents in the overall configuration. Besides adding a coupling capacitor, those transient currents can also be captured inductively.

The most prominent inductive coupling is the RF (radio frequency) CT (current transformer). Usually, this is a ferrite core with two identical coils for compensation having a couple of turns (often 10) as shown in Fig. 4.5, left sketch.



Fig. 4.5 RF-CTs, principle and different technical examples (fixed aperture and clip-on)

Sharing the principle, there are different technical solutions adapted to the measurement task. For instance, there are fixed aperture CTs for permanent installation, clip-on type for installation on copper bars in cross-bonding boxes, or CTs with removable yoke (Fig. 4.5, from left to right). Seeing such CT terminated with a 50Ω cable as an electronic network, one can consider this as inserting a 0.5Ω resistor into the lead the CT is sitting on. Additionally, the core material has to be selected properly in order to avoid saturation²¹ due to power frequency currents.

²¹ Such power frequency currents are comparably moderate for surge capacitors on generators, while they can reach a couple of amps for cable cross-bonding leads, and may reach more than thousand amps in case of tapping a power cable at a transformers cable box.

On the other hand, the core material used has to offer an acceptable permeability over the frequencies of interest, which range from the IEC60270 band (40-1000kHz) up to frequencies of 100MHz. Depending on the power frequency currents of the given application, compromises may be needed.

Fig. 4.6 shows a larger clip-on CT for use on leads of up to 100mm diameter. Here, the impedance²² of the connected high voltage cable produces comparably high RF currents, which the CT picks up.



Fig. 4.6 Clip-on RF-CT tapping a 110kV cable to capture transformer PD

The braided copper underneath the RF CT is the termination of the shield of this 110kV cable. Thus, the CT "sees" the RF current coming from the transformer (and the cable), but superimposed by the 50Hz current of approximately 300A. Putting the CT instead on the braided ground lead would of course ease the problems of the 300A, but additionally pick up the transient RF signal on the cable shield, which are often more critical than coping with the PF currents.

²² The impedance of power cables is in the range of 20-30 Ω [Gro95] given by their dimensions. Thus, it is smaller for medium voltage high current cables and higher for EHV power cables.

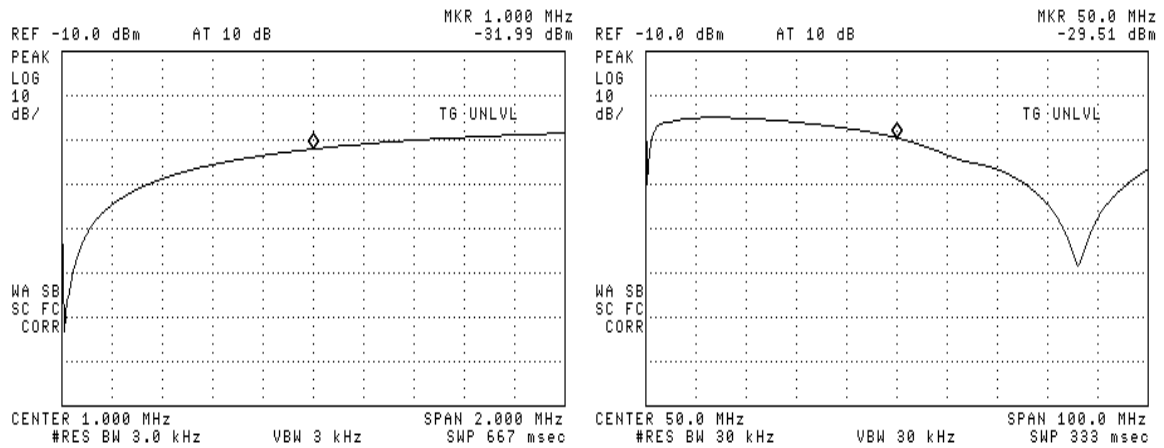


Fig. 4.7 Bandwidth of the clip-on RF-CT shown in Fig. 4.6 - Span: 2MHz (left), 100MHz (right)

The bandwidth of the clip-on RF-CT as shown in Fig. 4.6 reaches well into the range of 80MHz (Fig. 4.7). However, on the lower frequency end, the corner frequency is as high as 100kHz, which is the side effect of the tolerance against high power frequency currents of up to 800A.

Another inductive coupling method is given with the Rogowski coil. This is a coreless coil as shown in Fig 4.8. The common application of Rogowski coils is the measurement of low frequency (power frequency) currents. If used to capture high frequency impulse signals, a different design is needed, since the stray capacitance to the conductor under test adds a spurious capacitive coupling that jeopardizes the principle as such.

This can be avoided, if the Rogowski coil is shielded, however, this would increase the stray capacitance to ground dramatically and, as a consequence, lower the self-resonance frequency of the coil.

The aforementioned drawbacks can be avoided, if the Rogowski coil is made of (thin) coaxial cable. Fig. 4.8 shows the principle and the connection. Such coil has an excellent high frequency performance and noise immunity, but is in general several dB away from the sensitivity of a comparable RF-CT with ferrite core²³.

²³ Such questions of sensitivity and noise immunity cannot be answered in general, as besides the basic sensitivity in V/A, the local noise situation, the source impedance, as well as the following measuring chain do have a strong impact on the overall performance.



Fig. 4.8 Shielded high frequency Rogowski coil made of thin coaxial cable

Finally, inductive near-field probes can be used for capturing high frequency signals in close vicinity, such as surveying a cable joint for activity. As the signal decays quickly with the distance, such near-field probes can be used for amplitude-based location. Technically, wide-band inductive near-field probes can be designed as a coreless coaxial coil. Fig. 4.9 shows the principle of such coil (unbalanced version), which is identical with the above mentioned shielded Rogowski coil, and commercial examples. Additionally, especially for lower frequencies, standard RF bobbin core coils can be used for this task²⁴.



Fig. 4.9 Inductive near field probes (coaxial cable style – principle and examples)

²⁴ When using such standard components, it is essential to make sure that their self-resonance is well above the desired frequency, or frequency band. Using them close to the self-resonance increases of course the sensitivity, but reduces the counts per second that can be processed because of the ringing response. Such coils can be used up to few MHz, only.

4.3 Antennas (electromagnetic)

A wide range of antennas can be used for picking up electro-magnetic signals originating from partial discharge. This includes near-field probes, which have a certain overlap with capacitive couplers. Likewise, shields in GIS equipment, for instance behave in low frequency range as capacitive couplers (by their stray capacitance), but change to complex antennas, when it comes to UHF signals of higher modes [Gro04₂, Gro07₂].



Fig. 4.10 Wideband UHF antennas (left: spiral dipoles²⁵, right: log-periodic dipole array)

For mere UHF detection comparably small wideband antennas, such as wide-band dipoles or log-periodic dipole array antennas provide good sensitivity. However, integrating such circuits into high voltage equipment such as GIS or power transformers is in several aspects demanding.

Firstly, the presence of the electric field – both power frequency, as well as very fast transients (VFT) – force compromises that lead to less ideal high frequency properties. Generally, this must be seen in the light of the fact that substation equipment is not designed to nicely transmit high frequency signals, as discussed in chapter 3.1. Thus, the signal that arrives at the point of the antenna is already non-ideal, resonant, and shows reflections. Therefore, a less ideal behavior of such antennas is often tolerable and the subsequent signal processing must be able to cope with these non-ideal conditions.

²⁵ To allow tapping the dipoles this way, the second spiral arm is on the PCB's rear side.

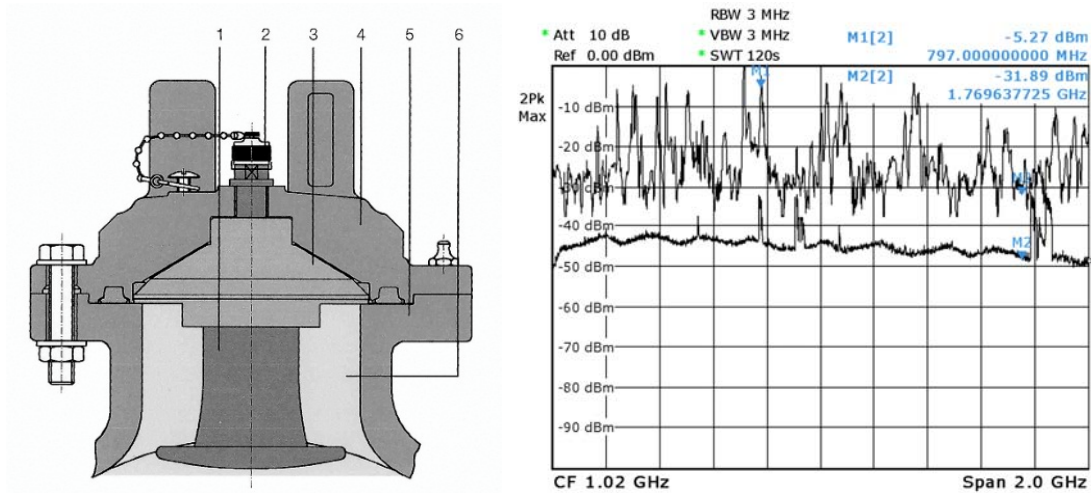


Fig. 4.11 Embedded UHF sensor (ABB) and its frequency response (nearby injection, 5V)

A typical example of an embedded GIS UHF sensor is shown with Fig. 4.11. Here, the cone of the inner part is matched to the outer shape to keep the 50Ω impedance of the subsequent cable and, hence, avoid any unnecessary reflection. Most important is that the whole construction is gas tight and does not enhance the internal electric field, which would introduce a weak point.

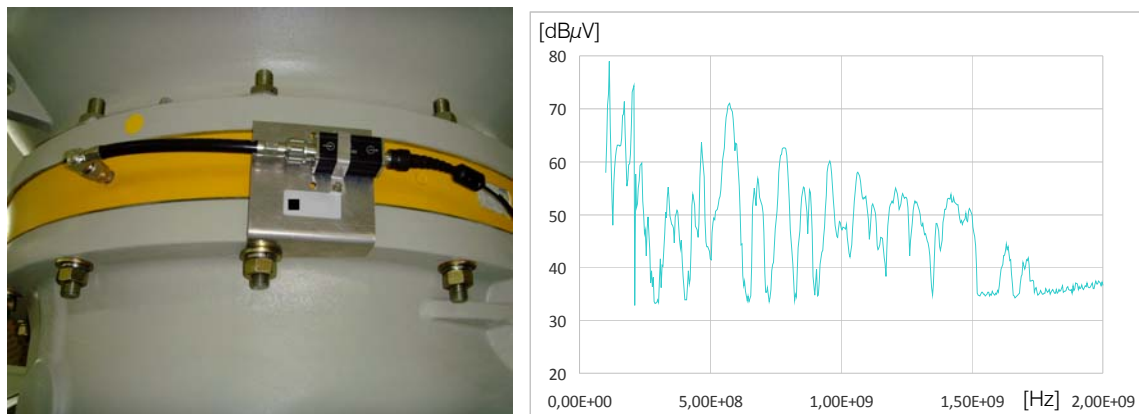


Fig. 4.12 Use of an embedded field-shaping electrode as sensor and its UHF response

Other than the comparably well-designed embedded sensor previously described, Fig. 4.12 shows an example of using shaping electrodes that were introduced in a three-phase GIS to reduce the internal electric field at the tripple point. The meander-formed wires are molded along with the support insulator disk and connected with three bolts each to the outer metallic ring.

Replacing the middle bolt by a threaded N-connector makes the wire assembly accessible as folded monopole. Besides acting as antenna with a quite resonant behavior, this monopole is the perfect antenna to capture the H_{10} mode VFT wave traveling the GIS upon a switching action²⁶.

Additionally, partly exotic antenna types – mostly wide band – can be used for partial discharge detection, if there is no electric field limiting the design. This includes spiral conical, Yagi-Uda, and bi-conical antennas.

A special role have the TEV (transient enclosure voltage) antennas. Technically, they are mostly $\lambda/4$ monopoles. They are placed outside of a transformer tank or a GIS enclosure. Especially at out-door terminations, the transient wave originating from an internal partial discharge source splits, when it arrives at a bushing (gas-air or oil-air). Part of the signal is being reflected back into the tank, another part travels the overhead line, while a third part travels the enclosure²⁷ referring to ground. The relation of the three impedances determines the percentage of the three parts.

Likewise, antennas are used for UHF detection of partial discharge in transformers. However, especially here, design limitations, as that an antenna must fit the drain valve, or that an antenna mounted into a hatch shall not disturb the internal field distribution, force using more simple antennas. Thus, drain valve sensors use mostly inductively modified $\lambda/4$ monopole antennas, while hatch sensors are often designed as simple field probes. Generally, the design limitations lead to partly resonant behavior with strongly varying return loss [Akb16].

²⁶ The typical wideband noise floor of partial discharge detecting front-ends is in the range of 100-200 μ V. Such folded monopole antenna covering 1/3 of the circumference and, hence "seeing" 1/3 of the H_{10} mode of the switching wave shows an impulse voltage 20kV and above. Protecting electronics against this, while maintaining sensitivity is demanding.

²⁷ This TEV wave is another challenge for any electronic equipment installed outside of a GIS, as the VFT of a switching action undergoes the same split into reflection, ongoing, and TEV.

4.4 Acoustic detection

The electron avalanche of a partial discharge event releases energy that cause a local heating of the gas or other material and, hence, causes a rapid local pressure increase depending on the material involved. The spectrum of the resulting sound extends into several MHz [Lun92₁]. The resulting pressure wave or longitudinal wave propagates through the medium at a certain speed, which is a property of the medium and is being influenced by other parameters, such as the temperature, for instance.

In solid materials, additionally, the transverse wave or shear wave offers transmission of the sound. However, the shear wave's transmission speed is substantially lower than the pressure wave's speed²⁸. Thus, as the shear wave arrives later, it is typically buried in the signal of the pressure wave and, therefore, usually not of importance for detection and location. Fig. 4.13 shows an example of the pressure wave and the slower shear wave acquired on a transformer tank wall (upper trace). Here, additionally, a fin-style tank wall stiffener causes the reflected signal. Acoustic location, the principles, and the limitations are discussed in depth in chapter 7.5.

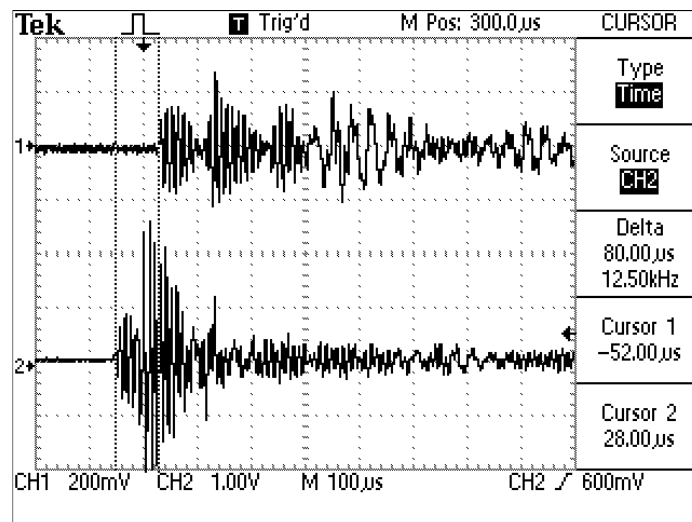


Fig. 4.13 Acoustic signal showing pressure and the slower shear wave on a transformer tank

²⁸ Steel, as used for transformer tanks, offers a pressure velocity of 5900ms^{-1} , while the shear velocity reaches 3200ms^{-1} , only [Lun92₂].

For the detection of air-borne sound of partial discharge activity different types of microphones are suitable and have been used. Typically, parabolic reflectors are used in order to amplify the usually faint acoustic signals and to obtain directivity for locating the source. Often, such devices are equipped with notch and bead sighter or a laser pointer to aim the device for identification of the source. Using higher frequencies improves the directivity, as the wavelength becomes shorter. Thus, usually, ultrasonic frequencies are used. The majority of commercially available sensors operate at 40kHz resulting in a wavelength of 4.25mm for 340ms^{-1} , which does not limit the location precision. The devices are equipped with circuits to convert the ultrasonic signal into audible sound and come with speakers or headsets.



Fig. 4.14 Ultrasonic detection of air-borne partial discharge signal using parabolic reflectors

For the acquisition of structural sound, such as with gas-insulated switchgear, cable accessories, or transformer tanks already in the 1930s stethoscope-like instruments were in use to mechanically guide and amplify sound signals (Fig. 4.15). Already then versions with rods made of insulating material were available to comparably safely investigate test objects on moderate high voltage [Gro15₁].

Nowadays, typically, piezoelectric sensors are used to acquire such signals. Jacques and Pierre Curie found the piezoelectric effect already 1880 [Cur80]. It took until 1916 that research was conducted to use the principle for detecting submarines. However, a widely industrial application of piezoelectric sensors started only in the 1950s.



Fig. 4.15 "Original Defekt Sucher", mech. instrument to investigate structural sound (~1930)

For the detection of structural sound of partial discharge activity nowadays mainly piezoelectric sensors often combined with a built-in amplifier are in use. Fig. 4.16 shows the principle of such sensors as well as a commercially available sensor. The piezoelectric crystal is protected using a ceramic wear plate, while a backing material or weight piece ensures that the crystal is able to capture the acceleration due to the incoming sound wave. This configuration is acoustically isolated from the metallic enclosure. Additionally, this acoustic isolation provides damping of the in general resonant behavior of the setup. Often, the sensor enclosure carries as well a small amplifier, which acts also as 50Ω-line-driver and which is remotely powered using a phantom supply.

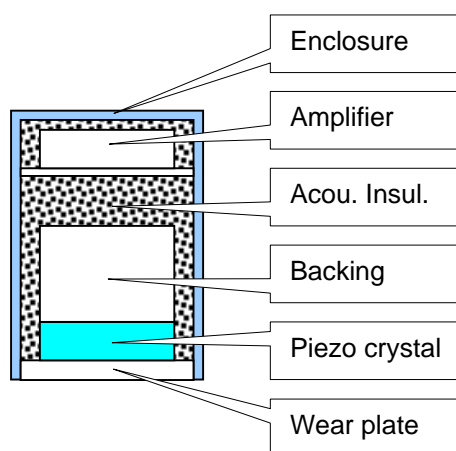


Fig. 4.16 Piezoelectric ultrasonic sensor principle and practical example with fixing magnet

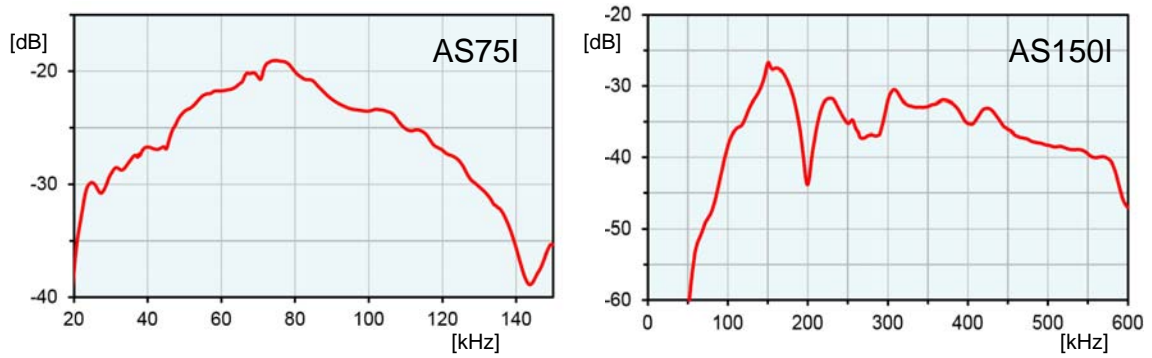


Fig. 4.17 Typical bandwidth of damped resonant piezoelectric sensors (referring to $1\text{V}/\mu\text{bar}$)

Commercially available piezoelectric acoustic sensors for the detection of structural sound reach from below 20kHz into the range of 1000kHz and above. Fig. 4.17 shows the response of two different sensors that are used for acoustic detection of partial discharge. The AS75I sensor has a resonant frequency of 75kHz and shows a bandwidth of about 20-140kHz for $\pm 10\text{dB}$. The AS150I has its resonance at 150kHz and an anti-resonance at 200kHz, while it offers a bandwidth 80-570kHz for $\pm 10\text{dB}$ with stronger fluctuation. Such fluctuation in frequency domain causes distortion of the time-domain signal, as certain frequencies are not correctly represented.

At its origin, the sound emission of partial discharge in liquids and solids can be considered as a steep impulse with a slower decay and, hence, the spectral amplitude of the resulting signal shows decaying amplitude over frequency. Thus, the highest sensitivity can be achieved towards the lower frequencies.

However, on the other hand, acoustic signals originating from mere mechanical sources show predominantly as well higher signal amplitudes in the lower frequency range. Moreover, impulse sound originating from the changing size and orientation of magnetic domains in core material, the so-called Barkhausen noise [Bar19, How78, Cla00] reaches well into several tens of kHz. Thus, selection of the proper acoustic sensor and its frequency range is always a compromise and strongly depends on the application and signal processing technology used.

4.5 Optical detection

The atmosphere under which the partial discharge occurs does not only control the rise-time of the current due to the electron avalanche, but also controls the light that is being emitted. Nitrogen, as the dominant gas in our atmosphere has several strong lines in the violet and ultraviolet range, which are responsible for the bluish appearance of so-called corona. Of course, the light emission can be used for the detection of partial discharge.

Several techniques are available for this detection. UV avalanche photo diodes can be used and offer high-speed response, but suffer from their typically small aperture. For the mere detection, photomultiplier tubes can be used in conjunction with suitable UV optics. Their aperture is typically much wider, but operation requires high voltage supply. The photomultiplier principle²⁹ is also used in multi-channel plates, where the secondary electrons are generated in tiny tube-like channels. On one side the photocathode provides the initial electron, whereas the accelerated and "multiplied" electrons hit a fluorescent layer on the other side. The channel density of modern multi-channel plates is well suited for imaging. Depending on bandwidth and processing circuits, also high repetition discharge activities can be detected optically, which cannot be separated under the regime of the IEC60270 bandwidth [Muh04, Muh06]

Finally, special versions of CCD (charge-coupled-device) as used in digital imaging extend the into the UV band³⁰. Here, special cameras have been developed to detect hydrogen fire, which emits only very little visible light.

²⁹ Comparable to the electron avalanche of partial discharge, here, secondary electrons are generated on photo cathodes to amplify the signal of initially few photons.

³⁰ In fact, all current commercial CCD imaging chips, such as in digital consumer cameras extend both into the infrared and the ultraviolet. Their range is limited to visible light by filters. Replacing this thin filter by an equivalent thin quartz window allows IR and UV images using standard cameras.

5 Bandwidth and processing circuits

The current impulse of partial discharge under a nitrogen atmosphere has a rise-time of about 1ns, as discussed in chapter 3.1. Thus, in frequency domain, the bandwidth of the signal extends into frequency ranges of 350MHz and higher with, however, decaying amplitude. Generally, the whole frequency range can be used for partial discharge detection. Each frequency range and the corresponding processing circuit have their immanent benefits and drawbacks.

All electrical methods do have in common that they are using band-pass filters to select the frequency band. Moreover, the band-pass characteristic of the coupling circuits needs to be considered as well. Thus, the signal chain contains in general complex filters of higher order. Their behavior influences the impulse properties of the signal. With the following sections the most dominant effects are described for the different techniques covered.

5.1 IEC60270

A central point of the original IEC 270 [270] and its revisions [60270₁, 60270₂] is the idea of expressing the partial discharge magnitude in terms of charge. The required integration, either by actively integrating the signal or by making use of the quasi-integration of the signal with a low-pass filter, relies on an undistorted current signal of the original discharge or its displacement current.

Thus, with the IEC60270, the frequency range is set for the so-called wide-band detection to a lower corner frequency f_1 of 30kHz to 100kHz and the upper corner frequency f_2 to a maximum of 500kHz with a bandwidth Δf of 100kHz to 400kHz. For the so-called narrow band detection the limits were agreed to be f_m between 30kHz and 1MHz with a bandwidth of Δf of 9kHz to 30kHz.

Further, for the wide band detection, the upper corner frequency was chosen not to extend into the AM broadcast frequency range, which, however, is of increasingly minor importance, as AM broadcasting is strongly decaying currently. Hence, with the standard's recent revision to IEC60270:2015 [60270₂], the inconsistency between wide band and narrow band detection was rectified and f_2 was extended to a maximum of 1000kHz with a bandwidth Δf of 100kHz to now 900kHz. The lower corner frequency remained unchanged.

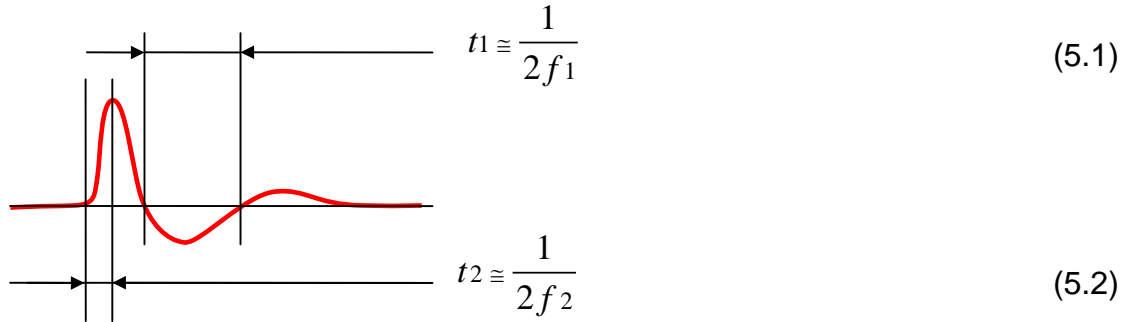


Fig. 5.1 Band-pass response – rise time, decay time, and ringing

In time domain, the upper corner frequency f_2 of a band-pass determines the rise time, while the lower corner frequency f_1 causes the pulse tail and its ringing (Fig. 5.1)³¹. This general pulse response of band-pass filters is responsible for a number of problems encountered, when acquiring partial discharge pulses.

- Pulse pile-up

In case partial discharge pulses of high repetition rate or originating from several similar spots, such as with epoxy-mica insulation systems do come in the range of the ringing of the previous pulse, so-called pulse pile-up occurs. In case, the second pulse "rides" on the ringing of the previous pulse and, hence, causes a false too high or too low amplitude of the second pulse. Depending on the processing method of the partial discharge detector, this has different consequences: Peak-detector-based instruments react with a reading of the largest pulse, i.e. with a positive superposition error, while traditional analog processing instruments may react both with negative and positive superposition errors.

³¹ The approximation for the corner frequencies given with (5.1) and (5.2) is a good estimation for $f_2 > 5f_1$. In case of smaller bandwidth, firstly the undershoot increases and comes in the range of the first pulse, while the signal becomes more oscillatory. It shall be noted that t_2 is defined as the entire pulse front. For the 10-90% rise time it would read $t_2 \cong 1/3f_2$, instead.

- Noise modulation

High sensitivity is a central goal of partial discharge measurements, especially in case of insulation systems that do not tolerate partial discharge at all, such as polyethylene. Thus, typically, partial discharge measurements are extended to the noise floor. Here, the peak amplitude of small partial discharge pulses or calibration pulses undergo the so-called noise modulation. In case, the pulse "rides" on the noise signal and, hence, the captured peak amplitude is modulated by the noise signal. This appears as a non-linearity, when the (calibration) signal comes close to the noise magnitude.

For instance, with a noise floor of 2pC, a signal of 5pC may read 6pC based on a calibration at 20pC. In return, if calibration is made based on injecting 5pC, the reading at 20pC will be 17pC, only.

Consistently, it is stated with the IEC 270 from its beginning up to the IEC60270:2000 revision in Annex C that "A detailed treatment of partial discharge measurements on objects with distributed elements, in which travelling wave and complex capacitive and inductive coupling phenomena take place, is beyond the scope of this standard". However, most vertical (product) standards adopted the IEC60270, often without taking in-depth care of the limitations.

If measuring partial discharge on a lumped component, such as a small specimen, the idea of a (displacement) current impulse remains true and, hence, this current impulse will cause a voltage drop on the measuring impedance for test circuits as show with Fig. 4.1.

If, instead, the test object is a distributed component, as a cable, rotating machine, or transformer, additionally, the effects as mentioned already in chapter 3.2 will influence the properties of the incoming impulse: Attenuation, dispersion and reflection. Here, mere attenuation only reduces the reading of the detector and makes the reading location dependent. Dispersion, instead, causes different travel times for different frequencies and, thus, will distort the shape of an impulse. The effect can be illustrated by separating the different frequency components using a Fourier analysis at the origin, which will be due to the frequency dependent travel time inconsistently recombined with a Fourier synthesis at the instrument's input.

Likewise, reflections will cause additional trailing pulses and superimposed pulses, which may affect the processing of the original impulse within the detector.

Measurement receivers and their construction pose the main heritage of partial discharge testing. Thus, the early instruments follow the heterodyne principle of such receivers. Fig. 5.2 shows the principle of a heterodyne partial discharge detector with input attenuator (1), mixer (2), local oscillator (3), intermediate frequency filter and amplifier (4), demodulator (5), meter (6), and oscilloscope (7).

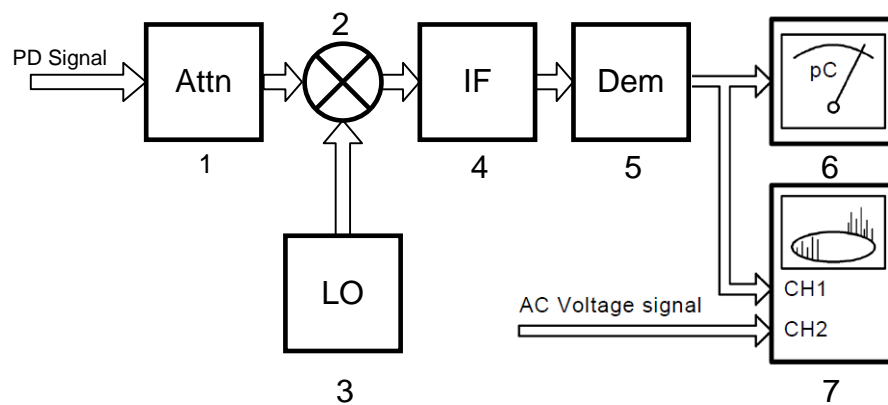


Fig. 5.2 Partial discharge detector based on single-stage heterodyne principle

With the heterodyne principle, the input signal is mixed with the signal of the local oscillator and the output of the mixer contains both the differential as well as the additive signal. However, in the AM radio range, the differential result is used and the input signal is down converted to the 455kHz intermediate. For AM radio transmission, this produces acceptable results. Likewise, for narrow band detection of impulse signals the demodulator response is reasonable stable. Here, the IF filter is the low pass filter that performs the quasi-integration.

However, if the resolution bandwidth comes into the range of 10% of the intermediate, the demodulator response becomes increasingly unstable as a function of the versus time relation of the local oscillator's period and the incoming impulse. Thus, up to a bandwidth of about 30kHz, the single stage heterodyne circuit produces acceptable results with the 455kHz intermediate frequency. For improved impulse performance generally higher intermediate frequencies are beneficial and mandatory for wide band detection.

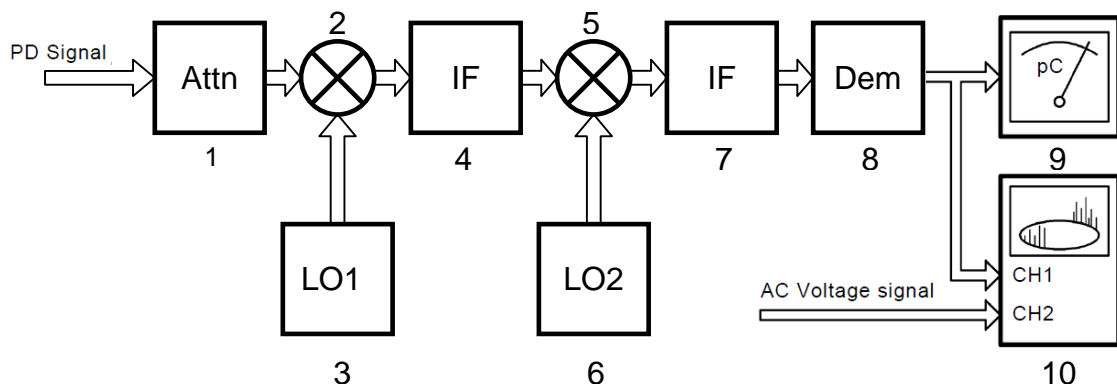


Fig. 5.3 Partial discharge detector based on double-stage heterodyne principle

In case, the circuits as commercially used for FM radio reception can be used. Fig.5.3 shows the block diagram of such two stage heterodyne circuit with input attenuator (1), first mixer (2), first local oscillator (3), first intermediate (4), second mixer (5), second local oscillator (6), second intermediate (7), demodulator (8), meter (9), and oscilloscope (10). Here, typically, because of the common use, the first intermediate is at 10.7MHz and the second is at 455kHz and, hence, allowing narrow band detection. For wide band detection the output of the first intermediate frequency stage is taken and demodulated (not shown).

Care must be taken, when designing the circuits to tolerate the comparably high energy of short pulses, if compared with standard receiver applications. Additionally, multiplying mixers offer the cleanest results and are less prone to image frequencies due to harmonics of the local oscillator, for instance.

Notably, the use of the wide band heterodyne principle is not expressively mentioned in the different editions of IEC60270. Likewise, there is no block diagram shown. The only reference that is made to measurement receivers is found in Annex D, which deals with "radio disturbance receivers" according to CISPR 16-1 [16-1]. Such receivers offer a so-called quasi-peak detection with an amplitude reading as a function of the impulse repetition rate. This weighting curve as shown with Fig. 5.4 is intended to emulate the grade of annoyance that ticking, clicking, or buzzing sounds pose in communication (!) channels. Since a single click hampers communication only negligible, it is weighted with less than 10%, while a constant buzzing comes close to 200%.

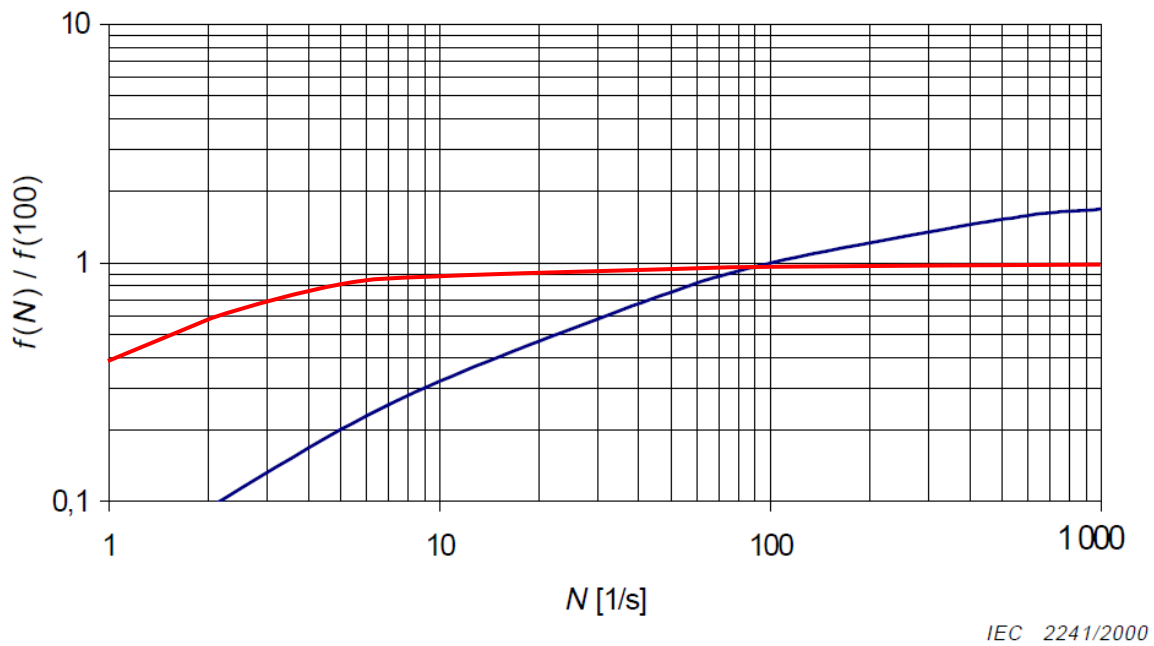


Fig. 5.4 CISPR 16-1 weighting curve (blue) versus IEC60270 weighting curve (red)

Likewise, the IEC60270:2000 sets a mandatory "pulse train response" for the meter of partial discharge detectors. Other than with CISPR 16-1, here, emphasis was put on having digital instruments behaving comparable to the inertia of pointer based earlier analog instruments. However, this goal wasn't met then (2000), as many of the old analog instruments did behave differently and were of course not forced to comply. Moreover, comparably quickly the use of such analog instruments went down during the following years.

Fig. 5.4 shows the two response curves according to IEC60270:2000 (red) and CISPR 16-1:1993 (blue). The two weighting curves are only in line, if there is one partial discharge pulse in every half cycle for a 50Hz system. Higher repetition rates make the quasi-peak detector giving up to twice the reading based on a charge calibration at 100Hz. For lower repetition rates, the reading of the quasi-peak detector increasingly decays well below the IEC60270 reading.

Thus, such "radio disturbance receivers" are not useable for this application³² and partial discharge detectors following heterodyne principles require a fresh design from scratch to fulfill the requirements.

³² Besides the widely incompatible weighting curves, also the usual narrow band detection hampers their application for partial discharge testing. Due to the narrow band intermediate of 9kHz and the general behavior of the demodulator circuits used, such detectors produce strongly decreasing readings with increasing PD repetition rate.

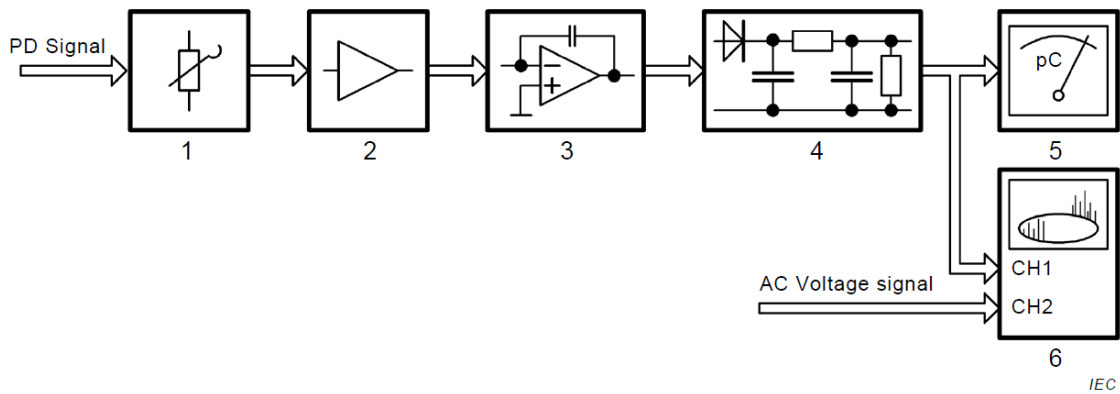


Fig. 5.5 Block diagram of an analog PD instrument equipped with an electronic integrator

For the time being, no functional or block diagrams of partial discharge detectors were given with the IEC60270. Only the recent addendum [60270₂] adds in the (informative) Annex E three block diagrams:

Fig. 5.5 shows the block diagram of an instrument with active integrator with attenuator (1), amplifier (2), integrator (3), peak detector and "evaluation unit" (4), meter (5), and oscilloscope (6). Here, the "evaluation unit" has the task to ensure the behavior according to the aforementioned weighting curve.

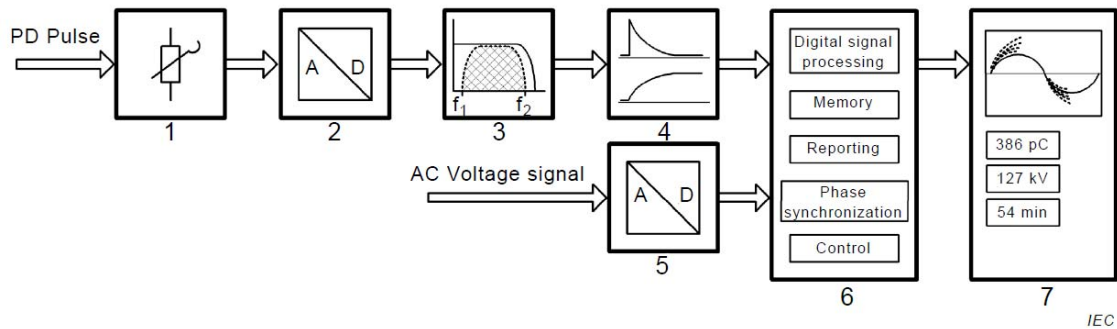


Fig. 5.6 Instrument with direct A/D conversion of the input PD pulses

The second block diagram is shown with Fig. 5.6 for an instrument with "direct A/D conversion of the input PD pulses" with attenuator (1), A/D converter for PD pulses (2), digital band pass filter (3), numerical integrator (4)³³, A/D converter for AC (5), acquisition unit (6), and evaluation and visualization unit (7).

³³ Following the ideas of the IEC60270, the so-called quasi-integration using a low pass filter is sufficient. In that sense f_2 of the filter block (3) in Fig. 5.6 takes already care of the integration. Hence, the added numerical integrator is not needed.

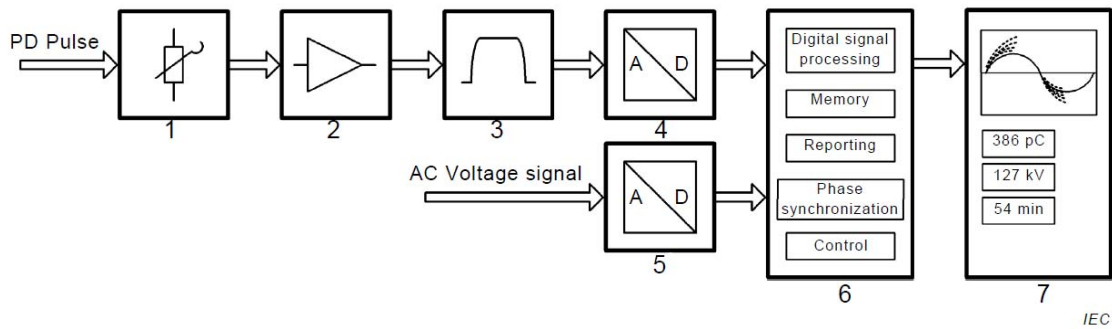


Fig. 5.7 Instrument with integration at a band-pass filter and subsequent A/D conversion

The third example is shown with Fig. 5.7 including attenuator (1), amplifier (2), band pass filter (3), A/D conversion PD³⁴ (4), A/D conversion AC (5), acquisition unit (6), and evaluation and visualization unit (7).

Besides the three block-diagrams included with the addendum (Figs. 5.5-5.7) of the IEC60270, other principles are widely in use and provide good results. Especially, the combination of analog peak detection, peak hold circuits and adequate timing provide good pulse separation for high repetition pulses under moderate requirements for the A/D conversion.

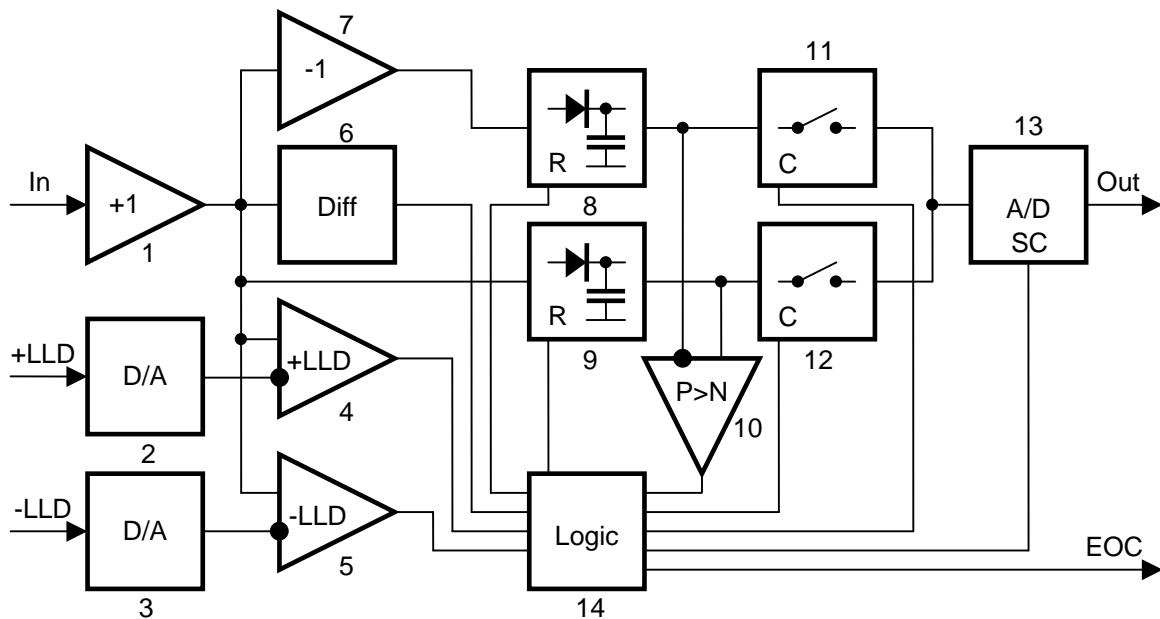


Fig. 5.8 Analog peak detection with event triggered peak/hold and A/D conversion

³⁴ To reliably capture the peak-amplitude of the band pass response, heavy over-sampling is needed. A peak with 1MHz bandwidth decays by 1%, if it is sampled about 20ns off the peak. Thus, already 0.5% accuracy requires a 100Msample conversion. Alternatively, for lower sampling rates additional high-speed computing is needed using, for instance, cubic splines for the interpolation of the estimated peak amplitude.

Fig. 5.8 shows an example of such a triggered peak detector, as it is part of a commercially available partial discharge detector (ICMsystem) [Sys16]. The amplified and filtered signal is fed to the input buffer (1). The buffered signal reaches the peak hold circuit for the positive signal (9) directly, while it is inverted (7) for the negative signal's peak hold circuit (8). Additionally, the buffered signal is compared (4) with the positive LLD (low level discriminator) threshold as received from a D/A converter (2). Likewise, the signal is compared with the negative LLD (2, 5). Additionally, the signal is differentiated to detect whether the input signal is rising or falling. The output signals of the peak hold circuits are compared (10). The logic (14) controls resetting the peak hold and directs the peak hold signals via two analog switches (11, 12) to the sample/hold A/D converter (13).

The circuit is triggered when the input signal surpasses the preset LLD trigger thresholds. In the mode "trigger on first peak" (Fig. 5.9, a), after starting with the positive LLD, a positive pulse is expected, while the differentiation of the input signal indicates that the peak occurred and, hence, the A/D conversion is started on the positive peak hold signal. The circuit is only re-armed after a certain dead time t_D to prevent acquiring undershoots. The A/D converter is a sub-ranging flash converter with $0.78\mu\text{s}$ conversion time t_C , only.

With the second mode, "trigger in time window", as well the process is started after one of the LLD thresholds is tripped. However, here, the peak hold signals are compared at the end of the time window t_W and the larger output is selected for conversion. The peak detectors are reset and re-armed immediately at the end of the time window, as the A/D converter has a sample/hold input and, thus, detecting the next pulse can be directly started. Fig. 5.9, b shows how a signal is processed that has the so-called β -response, where the main pulse follows an initial undershoot. Trigger on first peak would acquire the neg. undershoot.

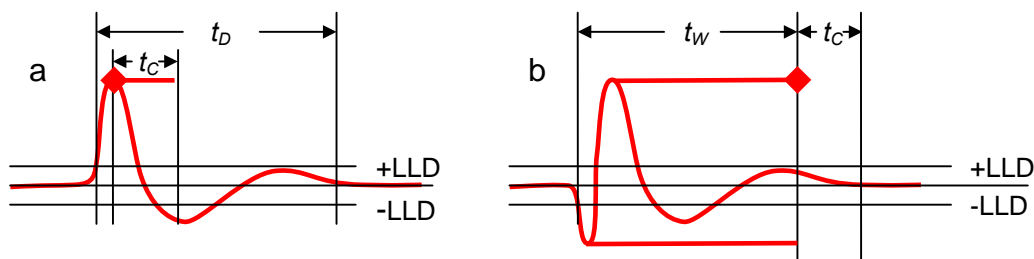


Fig. 5.9 Trigger on first peak (a) and trigger in time window on β -response (b)

The minimum dead time or time window is $5\mu\text{s}$ ³⁵ and, hence, the circuit can acquire up to 2×10^5 pulses per second. Even at high repetition rates a clear distinction of the pulse polarity is given.

The trigger in time window mode is best suited for the already mentioned β -response and for oscillatory signals. For high repetition signals this mode maintains the correct amplitude, since all pulses occurring within the time window are considered for peak detection. Hence, upon increasing repetition rate, this mode puts more emphasis on activity with larger magnitude.

For ideal signals with the so-called α -response (Fig. 5.9, a) both modes give similar results. However, for partial discharge activity with higher repetition rate, the trigger on first peak mode evenly accepts pulses of any magnitude, but may miss then larger pulses that do fall in the selected dead time.

Fig. 5.10 shows an example with high repetition rate low-level pulses, while the larger magnitudes have a comparably low repetition rate. As "trigger on first peak" takes the very next peak, it put emphasis on the high repetition rate (Fig. 5.10, a) at low levels. The mode "trigger in time window" (Fig. 5.10, b) takes the largest pulse within the window and, hence, misses most of the small pulses.

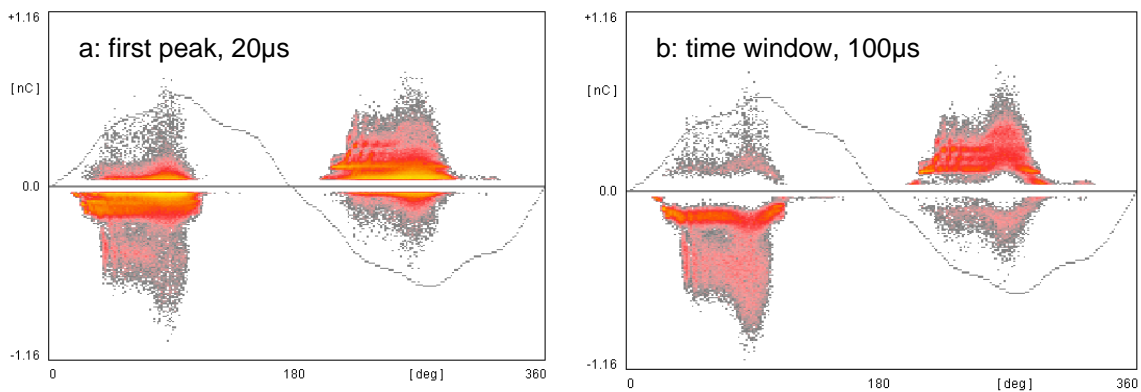


Fig. 5.10 Partial discharge pattern – trigger on first peak (a) versus trigger in time window (b)

³⁵ The $5\mu\text{s}$ dead time was intentionally chosen to match the highest lower corner frequency f_l of the IEC60270. Even a very nice band pass pulse response shows an undershoot corresponding to the lower corner frequency. Thus, the $5\mu\text{s}$ dead time is only applicable in well-controlled environments and typically, a dead time of $10\text{-}20\mu\text{s}$ would be appropriate to avoid counting oscillations.

5.2 Acoustic

The applicable frequency bands for acoustic (partial discharge) detection are similar to the IEC60270 frequencies and, hence, comparable circuits are used. Likewise, detecting acoustic emission of partial discharge concerns comparably faint signals and the input circuits must be of low-noise design.

The majority of the hand-held detectors for air-borne acoustic emission of partial discharge have selective amplifiers tuned to the frequency of the detector. This detector is often a piezoelectric microphone with 40kHz resonant frequency. To make the amplified signal audible, simple demodulator circuits and NF amplifiers are used.

Instruments that allow using wide-band sensors or sensors of different resonance frequency make use of the heterodyne principle (Fig. 5.2) with digitally adjustable synthesizer as local oscillator to shift the received signal into the audible frequency range. Again, demodulator, NF amplifier, and speaker or headphones are used.

Instruments to detect and locate structural sound emission of partial discharge on high voltage equipment having comparably poor ultra-sonic transmission properties, such as cable accessories or gas-insulated switchgear (GIS) typically come with only one sensor and location is performed by moving the sensor for spot testing. Fig. 5.11 shows instruments for on-site spot testing, which allows as well ultra-sonic as UHF detection [Aia15].



Fig. 5.11 Portable detector for on-site acoustic and UHF spot testing

For sensors with embedded pre-amplifiers, as described in chapter 4.4, the phantom supply of typically 28V must be provided. Care must be taken that any remaining high frequency components of this superimposed DC signal on the coaxial cable between sensor and instrument does not disturb the output signal of the sensor.

The frequency band of such sensors used for detecting structural sound covers 20kHz to about 600kHz, depending on the model chosen. Moreover, the signal amplitudes are comparable to electrical partial discharge detection. Thus, the same circuits for amplification, filtering, and peak detection can be used. For time domain signals, if considering the upper corner frequency of the signal band of 600kHz, sample rates of 10MHz are more than sufficient. The acoustic travel time within the materials of high voltage equipment ranging from transformer oil with 1390ms^{-1} to steel with 6000ms^{-1} (longitudinal wave) requires a storage depth of a couple of ms for power transformers, whereas for the more remote distances even lower sample rates are acceptable. Thus, a versus time storage of 8kByte per channel is sufficient for this application. Fig. 5.12 shows a typical acoustic versus time signal captured on a transformer at the sampling rate discussed.

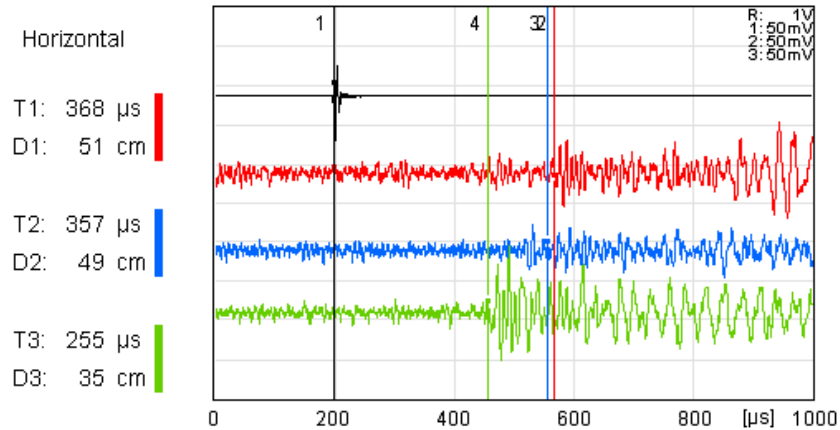


Fig. 5.12 Acoustic signals of three sensors (trace 2-4) with trigger on electrical PD signal (top)

5.3 HF, VHF, and UHF

The electron avalanche under dry air atmosphere has a rise time of about 1ns, as mentioned earlier, while a rise time of less than 200ps is found for SF₆. Thus, frequencies up to 400MHz and well above 2GHz for SF₆ are available for partial discharge testing.

Generally, the quasi-integration principle can be used at higher frequencies as well, although the IEC60270 does limit this to 100kHz lower corner frequency and 1MHz upper corner frequency. There are few conditions that must be met to extend this principle into higher frequencies:

- The applied measurement frequency or band must be well within the available bandwidth as given by the gas-discharge process as such
- The whole measurement signal chain must provide the bandwidth and the instrument shall pose the final bandwidth limiting factor
- Likewise, the used impulse charge calibrator including all means of connecting it to the test object must provide a bandwidth that extends the chosen signal bandwidth

It is obvious that these conditions are hard to meet, if the test object is a physically extended object, such as a transformer. However, for cable accessories with well-defined connection means, the applicable frequency range for the quasi-integration can be a couple of MHz, for instance [Hen96].

Generally, the larger the test object, the more complex the internal transmission properties as discussed in chapter 3.2, and the higher the chosen frequency (band), the more location dependent and the more doubtful a display in terms of pC becomes. Thus, for frequencies well out of the applicability of the quasi-integration principle, preferably units referring to the instruments input signal strength shall be used. For signal paths with linear response the reading can be expressed in mV or for logarithmic behavior in dB μ V or dBm³⁶.

³⁶ Both units are used in communication engineering, whereas dBm means dB_{re1mW} (dB over 1mW) and dB μ V means dB_{re1 μ V} (dB over 1 μ V). In a 50 Ω environment, 0dBm equals 107dB μ V. Because of $P = U^2/R$, a factor of ten is 20dB for voltage, but 10dB for power.

Given a constant amplitude spectrum up to a couple of 100MHz, the sensitivity of partial discharge measurements greatly benefits from a wider measurement bandwidth compared to the IEC60270. This is because the detected signal amplitude increases linearly with the bandwidth, while the noise signal increase only with the square root of the bandwidth. Thus, doubling the bandwidth increases the signal-to-noise-ratio (SNR) by a factor of $\sqrt{2}$, provided that linear increase of the signal amplitude is not hampered by dispersion, for example.

In terms of post processing, separating, and displaying partial discharge pulses, a resolution bandwidth of 1MHz is mostly sufficient, as the experience with the IEC60270 shows. However, there are discharge activities, such as under DC high voltage in SF₆, for instance, which partially show very high repetition rates and, hence, benefit from ultra-wide-band (UWB) or even optical detection.

Further, if the constant amplitude spectrum is given, any bandwidth limiting circuit of the post processing may provide the quasi-integration of the signal. This can be the amplitude response of a demodulator after an IF circuit or the response of a wide-band detector circuit with logarithmic gain.

Thus, different techniques are available to pre-process or down-convert wide band signals for the further processing:

- **Heterodyne circuits**

Circuits as described with Figs. 5.2 and 5.3 can be used with wider IF bandwidth as used for AM or FM reception. Those commonly commercially available component offer a bandwidth of about 10kHz (455kHz IF) or about 300kHz (10.7MHz). This technique can be implemented on conventional FR4 printed circuit boards for frequencies up to 10 or 20MHz with a dynamic range of up to 60dB, if carefully designed.

Fig. 5.13 shows such card with spectrum analyzer function. The synthesizer can be set in 10kHz steps to tune from 10kHz to 10MHz. It offers 9kHz bandwidth with and without CISPR weighting as well as 270kHz bandwidth. Additionally, the card offers 100Msampe A/D conversion with 8kByte storage. Finally, besides providing phantom supply for pre-amplifiers, the card carries the "standard" path according to IEC60270 with selectable filters for high pass (40, 80, and 100kHz) and low pass (250, 600, and 800kHz).



Fig. 5.13 Pre-processing card with spectrum analyzer, 100Msample ADC, and 60270 path

- Spectrum analyzer

Commercially available spectrum analyzers can be used for partial discharge detection. Also being in principle as well a "radio" using heterodyne principles, their design differs substantially. The main mixer resides directly at the input after a matched resistive attenuator and, hence, is prone to early damage, if used on high voltage equipment. However, other than conventional receivers, spectrum analyzers use a high intermediate referring to the additive mixer output. For the base band, for instance, the Agilent 8566B uses a 3.6214GHz intermediate. This produces absolute stable demodulator signals under pulsed input signals and makes sure that the spurious amplitude modulation³⁷, which is found with lower intermediate frequencies does not occur at all.

Sadly, designing such circuits requires a lot of shielding and makes the units comparably heavy (18kg for the Agilent 8594E). Moreover, putting such analyzer concepts with ultra high IF on standard printed circuit board level is very challenging. The Agilent 859x family is along with the 856x family the last in the line of spectrum analyzer with full analog path down to the so-called "video out" BNC connector, which represents the analog signal of the final demodulator.

³⁷ Especially for input signals containing pulses of short duration, the time of arrival in relation to the phase of the local oscillator becomes relevant. If, for instance, a pulse of 500ns duration is mixed with a local oscillator of 10.7MHz, only about five full waves do fit into the 500ns and, hence, the demodulator shows a spurious amplitude modulation for a stable pulse.

This signal can be perfectly connected to a partial discharge detector with pulse counting function and capabilities to display ϕ - q - n partial discharge pattern [Fru94₁]. Fig. 5.14 shows such analyzer and a screen-shot of control software.

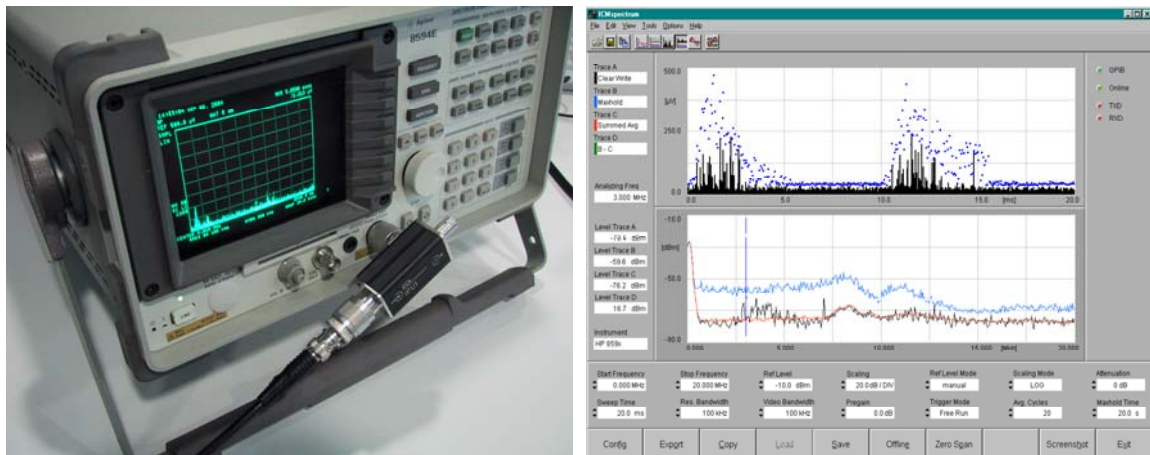


Fig. 5.14 Agilent spectrum analyzer 8594E, input protection, and control software

The control software (Fig. 5.14) allows switching between the frequency scan mode, where it shows the averaged signal (red), the life signal (black), and the peak hold signal (blue). Viewing the three traces allows identifying wide band pulse activity. Moving the cursor to such area and switching to zero-span, shows the versus phase signal at that specific frequency for further analysis (upper graph). Thus, changing between the two modes allows identifying and distinguishing areas of impulse noise, internal partial discharge, and external activity, for instance.

Due to a relative high refresh rate, the software even allows building a ϕ - q - n partial discharge pattern just from the traces received. However, the effective measurement time is relatively small and, hence, a partial discharge detector at the already mentioned "video out" connector has the better performance.

Around the year 2000, the traditional spectrum analyzers such as the 8590 or 8560 family were discontinued. Since then, high-end spectrum analyzers use digital intermediate frequency circuits. Hence, there is no longer a physical demodulator and the "video out" signal of the traditional analyzer does no longer exist and must be provided by reconverting it to an analog signal.

Tests on few modern spectrum analyzers with digital IF, although offering a lot of benefits in other fields, if compared with units having the "traditional" fully analog signal path, show that this reconverted "video out" is not suited for pulse applications. The signal especially does not have the resolution in time and amplitude, which is needed for adequate post-processing in pulse applications with short duration signals.

- Analog computation circuits

Modern monolithic and laser-trimmed analog four quadrant multipliers offer excellent bandwidth and can be used to process wide band partial discharge signals. Fig. 5.15 shows the principle of a circuit making use of such wide band multipliers.

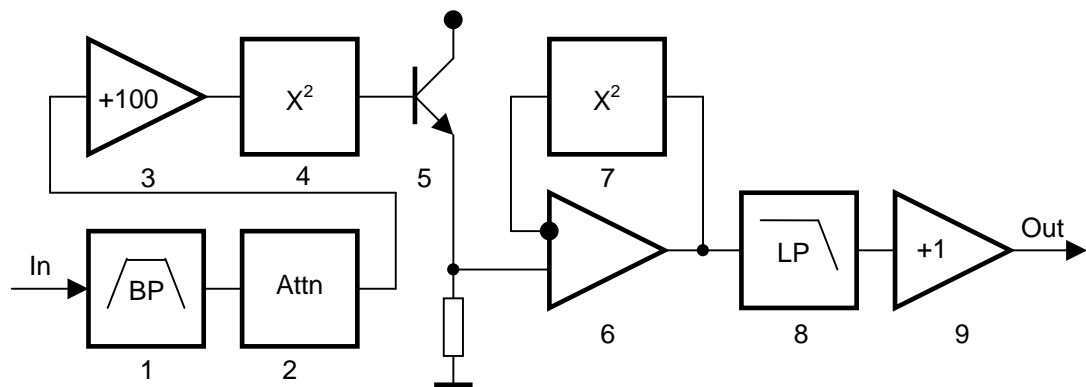


Fig. 5.15 Pre-processing using high-speed multiplier circuits

The circuit consists of a band pass filter (1), selectable attenuator (2), fixed gain amplifier (3), two multipliers connected as squarer (4, 7), voltage follower (5), operational amplifier (6), low pass filter (8), and output buffer (9). The main function is that the first squarer rectifies the signal, but with the non-linear quadratic response. Putting a squarer in the return path of an operational amplifier results in a square root function. Thus, multiplying the parabolic function with the hyperbolic function, both normalized to 1, results in a fairly linear response. The low pass filter removes the ripple of the rectified original signal to obtain the low frequency envelope of the original signal. The function of the voltage follower is to avoid any negative signal at the input of the hyperbolic circuit, which, in case, would drive it into negative infinite.

However, as the square root of 0.1 is as low as 0.01^{38} , this circuit has a comparably low dynamic range and, hence, tends to become less linear between the attenuator stages. Using appropriate components, the circuit as such is able to operate at frequencies up to 1GHz. The input band pass filters reduces the processed input signal to the desired band.

- Logarithmic detector

Integrated logarithmic detector circuits offer wide band envelope detection of signals up to the GHz range. Such circuits are based on the successive compression technique, whereas the logarithmic amplifiers go step by step in saturation, while adding the resulting currents in a row of detector cells. The input frequency of this example reaches 500MHz, while the output response offers a rise time about of 10ns. The deviation over 80dB is less than 0.5dB (Fig. 5.16).

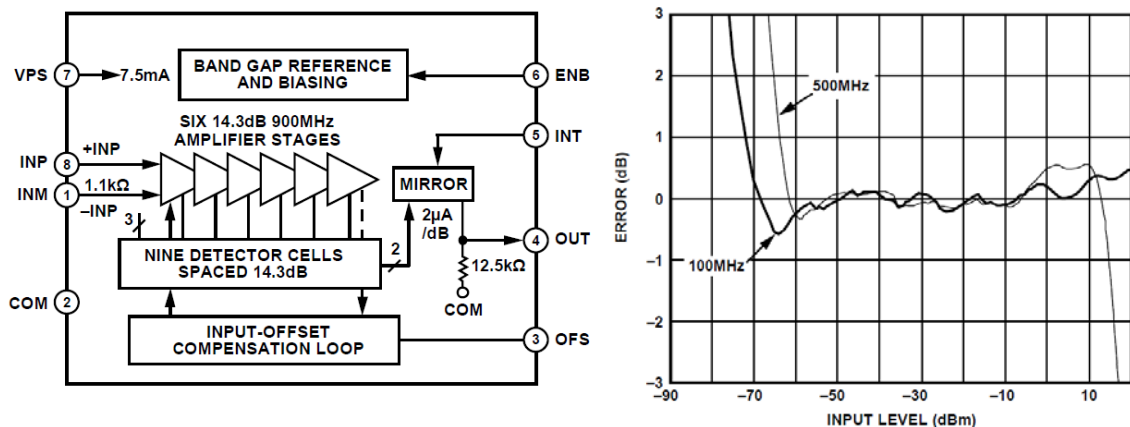


Fig. 5.16 Block diagram of a six-stage logarithmic detector (a) and its response (b)

Especially integrated circuits as such logarithmic detectors, input mixers, or amplifiers require adequate protection against surges and over voltages. For instance, just operating a breaker in a GIS starts very fast transients (VFT), which eventually are picked up by UHF sensors pose risks that are by decades higher than typical ESD definitions.

³⁸ Multipliers of that technique mostly do offer an input signal of $\pm 1V$. Therefore, at a utilization of 10%, i.e. 100mV the multiplier's output signal amounts only 10mV. Thus, if considering a squarer output signal of 1mV as the lowest practically feasible, the circuit offers a dynamic range of only 30dB. As a consequence, circuits following this principle must be combined with an adequately spaced input attenuator.

Using shields or embedded electrodes in GIS, which are not designed for this task, often produce "good" sensitivity in the lower frequency range. Thus, it is a demanding task to reliably protect input circuits, which are designed to measure very faint signals at a noise floor of $100\mu\text{V}$, for instance, against surges of 20kV . This is always a combination of several measures, as simply limiting a surge at one spot creates a strong magnetic field, which in return induces again electric surges in its vicinity.

Moreover, input circuits of such devices shall also be protected against failure of the high voltage equipment, which is even more demanding. Thus, evaluating and describing methods to reliably protect such devices is a book on its own.

6 Visualization and interpretation

Since early partial discharge detectors were based on disturbance measurement receivers, they came with a pointer-style meter showing the intensity. Moreover, many of them were equipped with speakers and/or headphones. Figs. 6.1 & 6.2 show two examples of those early narrow-band receiver-based instruments. The design of the Stoddart NM-22A unit (Fig. 6.1) dates back into the early 1950ies. It is valve operated and came with an external power supply unit (not shown). At its time in the early 1960ies, the Siemens Störspannungsmessgerät (Fig. 6.2) was quite modern being equipped with early Germanium transistors (ACY14, OC614, TF78, etc.) and optional battery operation. The unit has a weight of about 5kg and, hence, came with a shoulder strap.



Fig. 6.1 Early instruments: NM-22A, Stoddart, later unit, ~1962, succeeded by NM-25T, 1966



Fig. 6.2 Early instruments: Betriebs-Störmessgerät B83600-B40, Siemens, built ~1965

Interpretation of the results was made here based on magnitudes and interpretation of the demodulated signal made available by speaker or headphone.

Making partial discharge audible is nowadays an unjustly underrated method. An experienced operator can easily hear the inception of partial discharge with its sizzling sound even if superimposed by periodic thyristor signal or even a radio carrier. Likewise, distinguishing and separating for instance Trichel pulse of point-plane-discharge and, say, discharges in delamination of insulation material is possible, if they occur simultaneously or consecutively.

Fig. 6.3 shows a portable, battery-operated partial discharge detector for field testing, which offers besides the display also a built-in speaker to give the demodulated signal.

Generally, in measurement, human abilities to assess acoustically or visually fine deviations and judge information are underestimated. Hence, sadly, modern instruments often do not provide means to make use of such abilities.

In medicine, the very simple stethoscope can be used as an excellent example. The trained senses, especially in combination with the likewise underrated or judged old-fashioned auscultation still form an excellent diagnostic tool. However, today, there is a tendency to avoid gaining the personal experience closer at the effect and instead a preference to rely on complex apparatus that provide preprocessed and, hence, often prejudged results.



Fig. 6.3 Modern field-test partial discharge detector with speaker and headphone

6.1 Analysis in phase domain

Already with the early pointer-based instruments it was an established practice to use an oscilloscope in parallel to display the demodulated signal versus phase, if analysis was needed. Typically, with the divided signal of the high voltage on one channel and the demodulated signal on the other channel, viewing the added signal allowed to understand the phase position of the partial discharge activity.

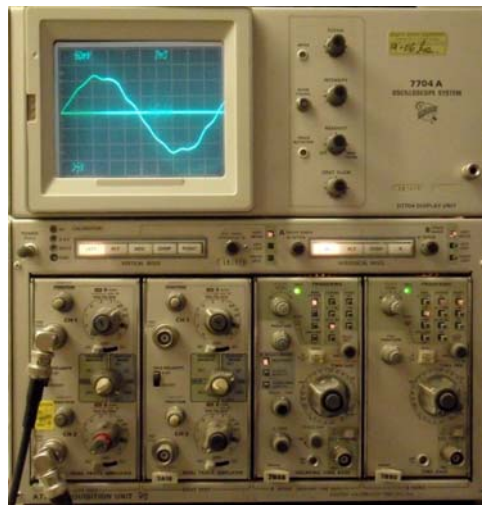


Fig. 6.4 Tektronix 7000 series oscilloscope showing AC and PD signal

During the early 1960ies, both instrumentation and standardization progressed quickly. VDE 0434 [434] was issued 1966 and the first edition of IEC270 [270₁] in 1968. Fig. 6.5 shows an early detector, which used an ellipsoid Lissajous display to indicate the phase position of the partial discharge activity.

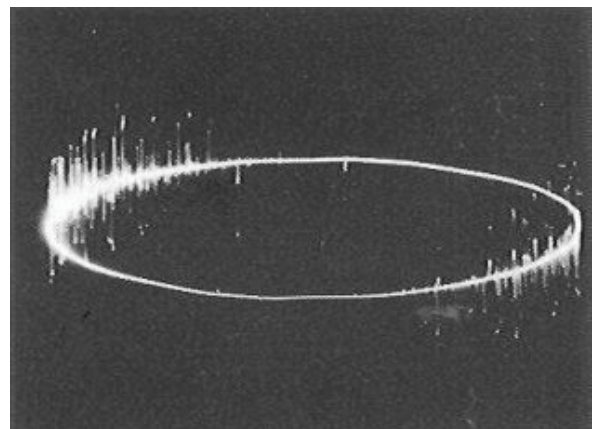


Fig. 6.5 ERA Model 3, early PD detector with Lissajous indication on round CRT screen

In parallel, guidelines to interpret the Lissajous representation were established [23-01]. Over the years many sources can be found and the general idea was used the coming two decades [Koe93]. Fig. 6.6 shows an example of such typical Lissajous signatures³⁹ for different defect types [Koe93].

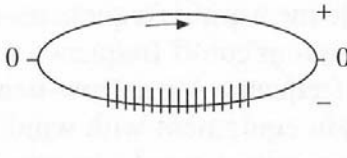
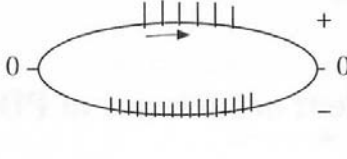
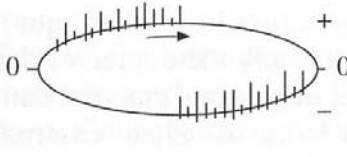
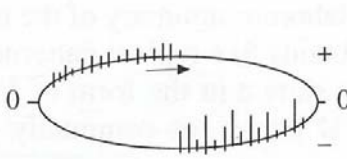
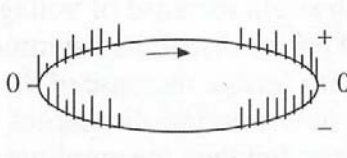
Type	Oscilloscopic picture	Description	Type of discharge
A		Pulses of equal amplitude in one half-cycle, symmetrical about the voltage maximum. With increased voltage, number increases, but not amplitude. Pulses on the other half-cycle only at higher voltage.	Sharp point against large opposite electrode in gas. Charge pulses in negative half-cycle; sharp point at high voltage potential. Charge pulses in positive half-cycle; sharp point at earth potential.
B		Pulses in both half-cycles symmetrical about the voltage maximum; smaller pulses of same amplitude. Increase in number with increased voltage.	Sharp point against large opposite electrode in liquids. Large pulses in positive half-cycle; sharp point at low voltage potential. Large pulses in negative half-cycle; sharp point at earth potential.
C		Pulses between zero-crossings and peaks of both half-cycles. On an average, pulses of the same amplitude in both half-cycles.	Voids in solid insulating materials. Gas bubbles in liquid materials. Insulated conductors in contact. Discharges on surface without metallic contact. Ungraded metallic parts.
D		Pulses between zero-crossings and peaks of both half-cycles. On an average, pulse amplitude in one of the half-cycles larger.	Voids in solid materials at the electrodes. Discharge on surfaces at the electrode. Large pulses in positive half-cycle; discharge on the high voltage side. Large pulses in negative half-cycle; discharge on the earth side.
E		Pulses symmetrical about both the zero-crossings.	Poor contact between metallic parts or between semi-conducting layers.

Fig. 6.6 Lissajous display, interpretation guidelines for typical defect types [Koe93]

³⁹ The then found signatures and the associated root cause remain of course valid and, hence, the findings can be easily translated in to the ϕ - p - n pattern of modern instruments.

Around 1990 research started at different places to assess the count distribution of partial discharge activity [Tan93, Fru92]. Mostly, multi-channel analyzers (MCA) were used as being designed to analyze nuclear decay and the energy distribution of various processes in nuclear physics. Such MCAs behave like counter arrays, whereas the impulse amplitude addressed the counters to achieve an amplitude height distribution. Additionally, with two-dimensional MCAs addressing versus time was possible and, hence, with few additional circuits, synchronization to the frequency of the high voltage applied to the test object became possible. Fig. 6.7 shows a basic block diagram of such two-dimensional MCA for PD measurements. Research instruments of those days, fully equipped 19" racks of 2m height, could be configured to allow setting a dwell time as well. Fig. 6.8 shows the unipolar ϕ - q - n (phase-charge-counts) pattern of such instrument, whereas the color represents the counts.

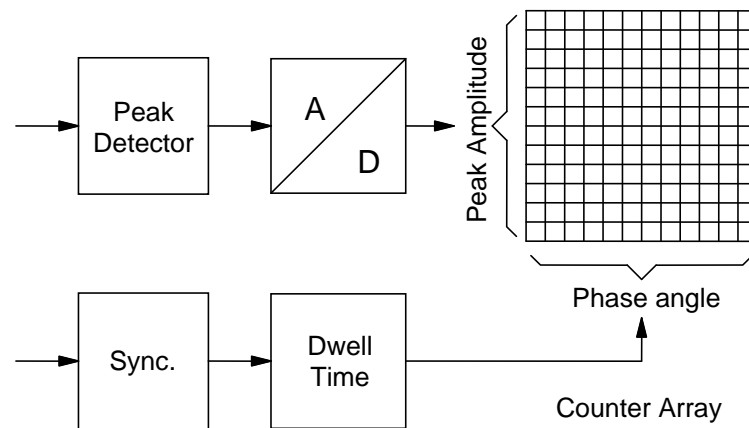


Fig. 6.7 Two-dimensional multichannel analyzer for partial discharge recording

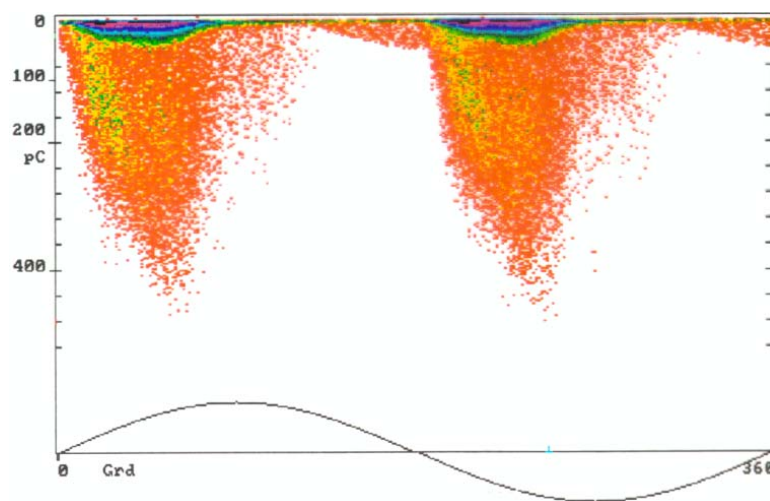


Fig. 6.8 ϕ - q - n partial discharge pattern of an early MCA-based research instrument

In January 1993 the ICMsystem, Power Diagnostix, became commercially available. At the same time the first notebook computers with color LCD became available as well. Their initially offered VGA resolution with 256 colors allowed already displaying the φ - q - n pattern in native resolution. Control and visualization of the instrument was achieved with a virtual instrument programmed under LabView[®] (National Instruments), which was introduced in 1992 for Windows⁴⁰. To suit the then new notebooks, National Instruments introduced a PCMCIA-GPIB interface, which made the instrument the first highly portable instrument for onsite online partial discharge investigations (Fig. 6.9).

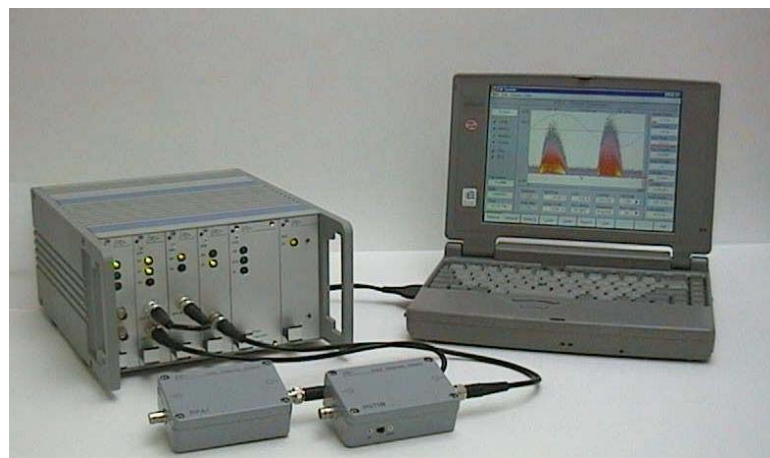


Fig. 6.9 ICMsystem, digital PD detector with preamplifiers and notebook (~1993)

The instrument offers an 8x8Bit counter array with a 16Bit depth. Amplifier and filters were designed to stay within the boundaries of IEC60270, but offering also higher upper corner frequencies for better peak recognition and pulse polarity differentiation.

In order to not load the 2nd order band-pass filter, as formed by coupling capacitor and quadrupole, i.e. inductor and damping resistor, the unit comes with preamplifiers that are directly placed at the quadrupole. Those preamplifiers are remote powered (phantom supply) and controlled in their gain. They further act as impedance converter with 10k Ω input and 50 Ω output impedance.

⁴⁰ Originally, LabView was a program offered for Apple Macintosh computers, only. It was firstly introduced by end of 1986. The first Windows version, LabView 2.5, was issued by August 1992. LabView, at that time written under Watcom C, offered a code interface that allowed writing custom code extensions, such as the display for the colored φ - q - n pattern.

Besides avoiding to load the coupling circuit, this method additionally reduces the influence of noise pick-up⁴¹ on the 50Ω connecting lead to the instrument, as the signal is already amplified at its origin (gain 1, 10, or 100).

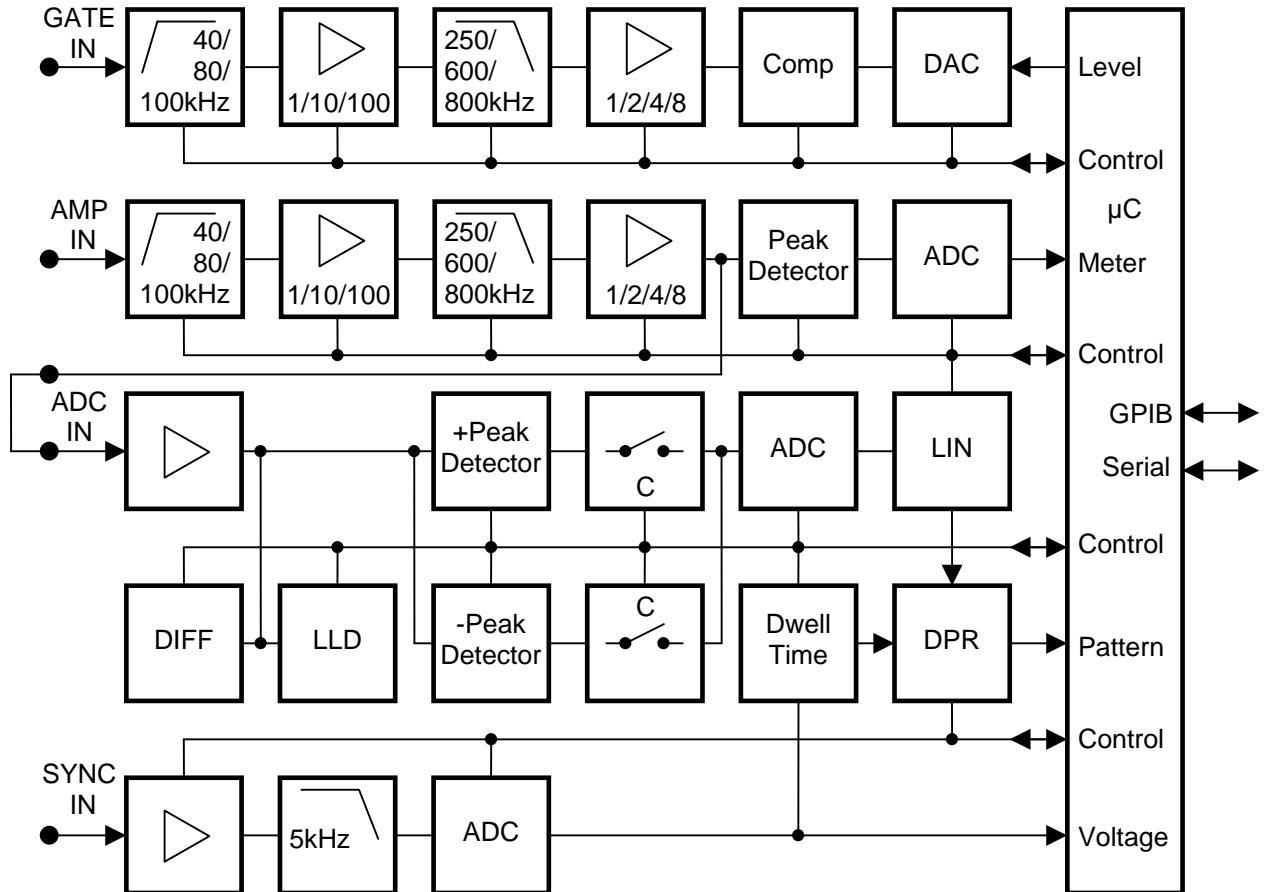


Fig. 6.10 ICMsystem – block diagram of an early single channel unit

Fig. 6.10 shows a simplified block diagram of an early single-channel ICMsystem. Both measurement and gating channel offer identical gain and filter stages. The measurement channel ends with an A/D converter for displaying the charge value on a meter according the requirements of the IEC60270 (peak hold circuits and weighting circuits are not shown), while the gating channel (upper row) has a comparator with adjustable threshold for event triggered noise gating. Gating can be set to block the amplifier stage and/or the pattern ADC.

⁴¹ Safety regulations as well as requirements to achieve signal integrity make earthing of the coaxial cable mandatory on both sides. Naturally, this causes high frequency currents on the cable sheath. Their voltage drop on the sheath resistance adds to the signal on the coaxial cable. Here, as a general precaution, clip-on ferrite cores acting as sheath current transformers reduce this effect.

The peak detector for the pattern acquisition (third and most of fourth row) allows acquiring bipolar pulse magnitude as described in chapter 5 and shown in more detail with Fig. 5.8. The linearization module (LIN) allows assigning the native 12Bit range of the ADC, a sub-ranging flash converter, to the effective 8Bit amplitude range⁴² of the φ - q - n pattern. Likewise, the dwell time counter has an 8Bit resolution. The dwell time, i.e., the time, the phase address stays on one phase slot is automatically calculated based on the frequency measurement of the synchronization voltage. The synchronization range covers 20-500Hz automatically and down to VLF frequencies (0.1Hz and below) manually.

Fig. 6.11 shows an early version of the virtual instrument to provide control and visualization of the ICMsystem. Here, the screenshot indicates alternate ways to set the low level discriminator (LLD) with a pull-down menu, typing a value, selecting a pop-up, or moving the red slider.

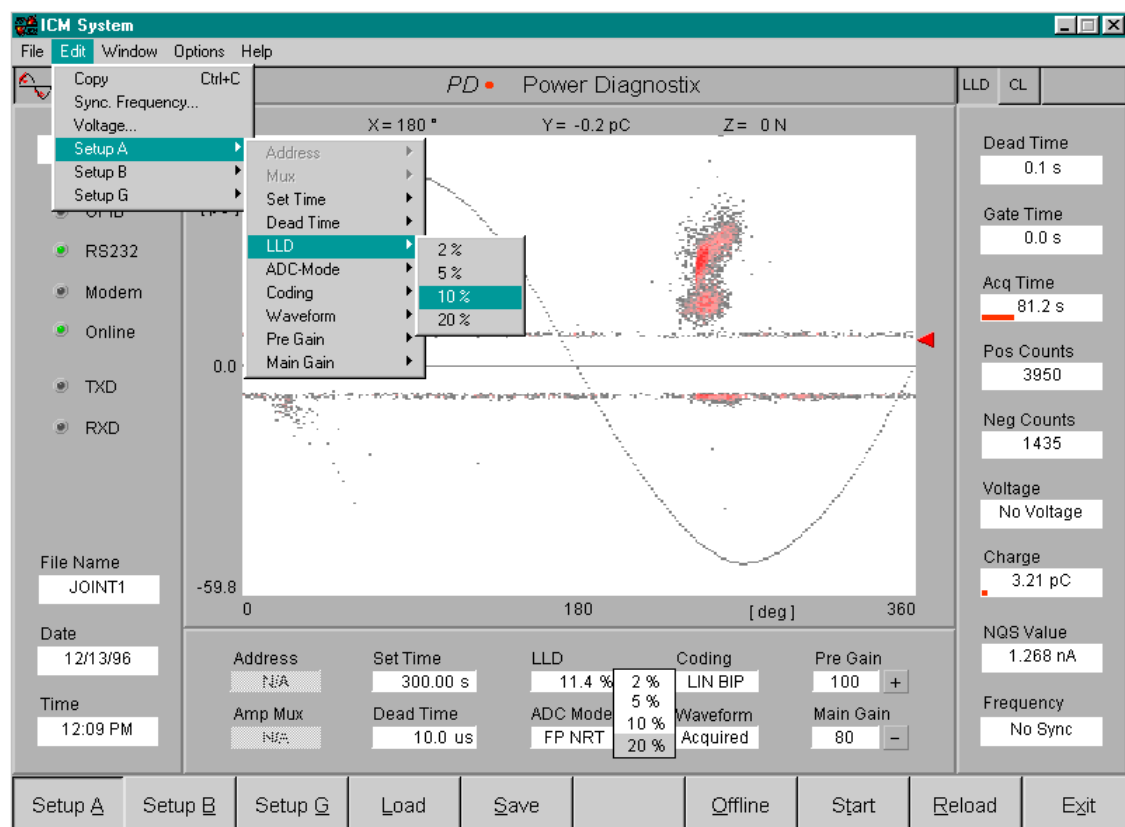


Fig. 6.11 ICMsystem – early virtual instrument for control and visualization

⁴² The local pattern storage of the instrument, which is a dual port RAM, allows storing pattern of higher resolution – both in amplitude and phase. However, tests under real life conditions have shown that uncertainties due phase jitter and (amplitude) noise modulation do not support a resolution higher than 8Bit, i.e., ~0.4% in most practical cases.

The example below illustrates the advantages of the φ - q - n pattern, if compared with traditional modes of displaying partial discharge activity. Please refer to chapter 3.1 for the basic properties of such φ - q - n pattern and to chapters 7.1 & 7.2 for transformer specific pattern. The appendix contains further examples.

Fig. 6.12 shows the discharge activity as found with tests on a single generator bar. Even a healthy resin-rich epoxy-mica-insulation may show partial discharge already in an early stage, while vacuum-pressure-impregnated (VPI) insulation systems often show massive discharge due to inherent air pockets⁴³. Here, a superimposed activity from different sources can be seen [Gro02₂, Gro03₂].

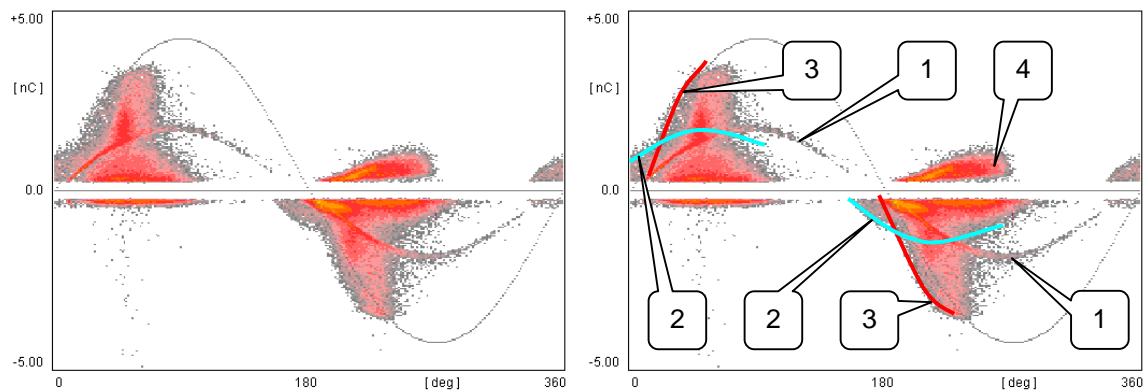


Fig. 6.12 φ - q - n pattern – epoxy-mica insulation, single generator bar with multiple defects

The different sub pattern can be easily distinguished. There is an individual larger spherical gas inclusion (void) in epoxy resin (1), several internal cavity-like discharge sources (2), and surface discharge at the field grading (3). Finally, a surface tracking type partial discharge can be identified with the coupling capacitor or its lead (4). Here, the conclusion that this is a problem of the coupling capacitor is drawn, as the high frequency return current of activity of the other branch shows up with swapped polarity (please refer to chapter 4, Fig. 4.4, which makes use of this effect).

⁴³ With global VPI insulation the taped, dry bar or coil is immersed in resin under vacuum, while the pressure is applied before and during curing. However, this impregnation naturally leaves internal air pockets, which cause initially higher – sometimes also massive – discharge activity. Generally, controlling the VPI process is demanding. This activity decays during the so-called run-in period. During this time, the discharge activity deteriorates the contributing surfaces, which increases the availability of free starting electrons and, in return, reduces the magnitude, while the frequency of occurrence increases proportionally.

6.2 Analysis in time domain

Displaying partial discharge activity versus time is used whenever there is a travel time and the need for locating with distributed high voltage equipment. Besides mere electrical signals, this also includes acoustic and optical signals. Additionally, displaying partial discharge signal versus time helps to understand effects such as dispersion, reflection, radiation, and attenuation in the time domain. This is discussed in detail with chapter 3.2 in general and 7.2 for transformers. Finally, versus time measurement are used with DC equipment.

The most prominent application for versus time partial discharge measurement is the location of partial discharge in (polymeric) high voltage cables. Here, as discussed in chapter 3.2, the stacked insulation system of inner semiconductive layer, main (almost loss-free) insulation, and outer semiconductive layer causes an increasing attenuation, when the thickness of the semiconductive layers do come in the range of the equivalent conducting layer thickness as know from the skin effect. For typical cable designs this causes a corner frequency mostly in the range of few MHz after 1km. The attenuation due to this effect increases linearly with the cable length.

As such measurements concern single-shot events, an over-sampling with respect to the signal bandwidth is needed. It was found that an acquisition of 100Msample produces sufficiently accurate results. Fig. 6.13 shows a partial discharge signal as captured on a medium voltage cable of 868m length. During calibration, the transmission speed was found to be 168.7m/ μ s.

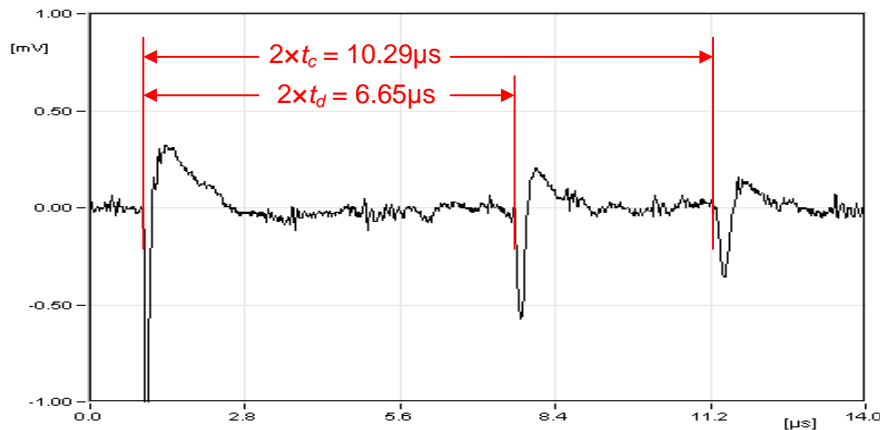


Fig. 6.13 Versus time PD measurement on a medium voltage cable of 868m length

Fig. 6.13 shows the typical trace with the initial three pulses. The first pulse takes the direct path to the coupling, but obviously has to travel the distance from the defect's site to the coupling circuit (Fig. 6.14). The second pulse is being reflected at the far end⁴⁴ with $\Gamma = 1$ and, hence, arrives the time later it takes to travel from the site to the far end and back, as indicated with Fig. 6.14. Finally, the third pulse travels the entire cable back and forth. The time that the 2nd & 3rd pulses travel additionally with respect to the 1st pulse is shown in red.

Moreover, Fig. 6.13 clearly shows the effect of the HF losses introduced by the stacked insulation system. The first peak, which in our example has already traveled $1.82\mu\text{s}$ ($t_c - t_d$), shows a high frequency content with its almost immediate increase, whereas the 3rd pulse shows a rise time of about 300ns, which translates into a remaining bandwidth⁴⁵ of approximately 1.5MHz, only.

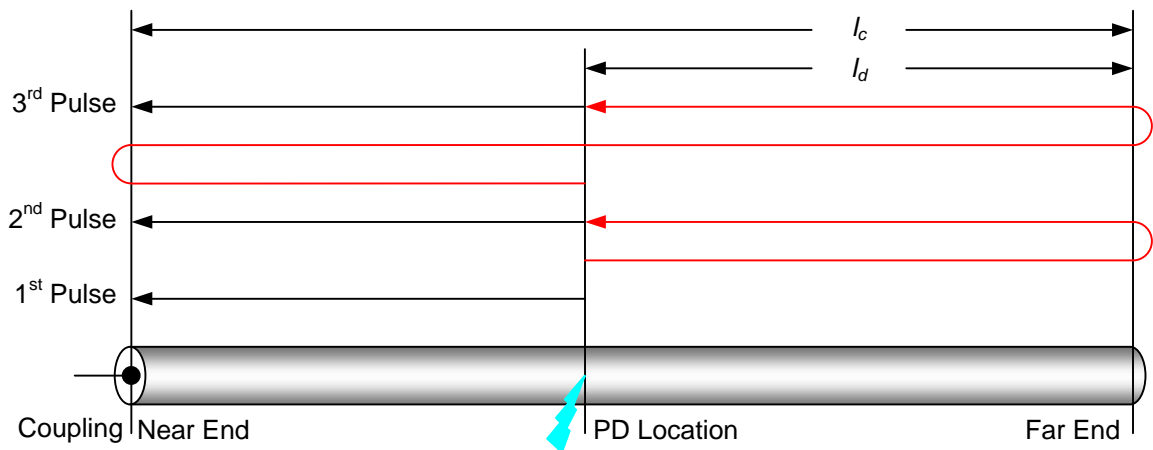


Fig. 6.14 Reflection scheme of the three initial pulses in a high voltage cable with a defect

Observing the aforementioned rise time of the first pulse helps also to identify the affected end, if the measurement indicates a PD location in one of the cable ends. If the far end is affected, the first pulse has traveled the cable already once and, hence, underwent already the reduction of its bandwidth, while in case of a location at the near end, the full bandwidth will be observed.

⁴⁴ The far end is typically left open and, hence, offers a 100% positive reflection. It is obvious that the coupling circuit at the near end has to maintain an impedance, which is large against the impedance of the cable in order to have clear reflection.

⁴⁵ This decaying bandwidth as a function of the stretch traveled makes it mandatory to put the cursor at the inception of the pulse, as the peak of the pulse is increasingly delayed, which would add unnecessary uncertainties, if the cursor would be set to the peak instead.

Likewise, electrical partial discharge signals in gas-insulated switchgear and lines can be measured and located. However, other than in polymeric cables, the velocity of propagation in GIS and GIL is close to c_0 due to the gaseous insulation. Moreover, the typical sensors that can be utilized for such investigations offer a high lower cutoff frequency (see chapter 4.3). As finally, the rise-time of the electron avalanche under SF_6 is in the range of 200ps and below, the frequency band for such location measurements ranges from approximately 100MHz into well above 1GHz. Thus, adequate coupling, cabling, i.e., low loss signal cables of identical length and oscilloscopes of sufficient bandwidth for acquisition have to be used.

On GIS, after initial investigation, typically, two neighboring sensors of the assumed defect location are used. The difference of the arrival time of the partial discharge pulse Δt_{pd} is determined and compared with the Δt_c , when injecting an impulse at one of the two sensors or at a third neighboring sensor.

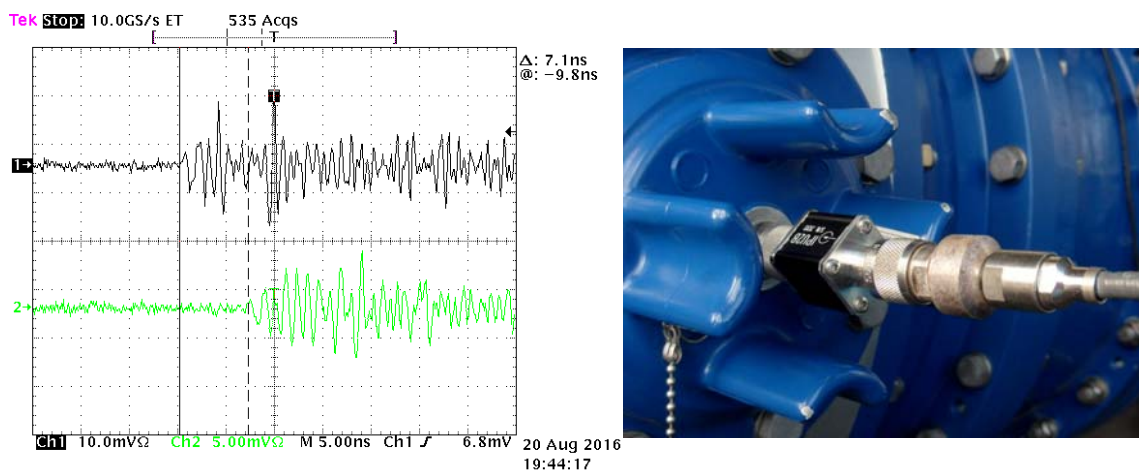


Fig. 6.15 Signals captured on two neighboring UHF sensors on a GIS

Fig. 6.15 shows the signals that were captured on a GIS with integrated UHF sensors for a signal in the range of 200pC. Here, low-loss semi-rigid cables⁴⁶ (Heliac[®] FSJ1-50A) with corrugated sheath were used.

⁴⁶ In terms of attenuation at higher frequencies, semi-rigid cables are superior to standard low-loss coaxial cables, such as the RG214U. However, semi-rigid cables do break easily. The ¼" Heliac[®] cable with its corrugated sheath and the foam polyethylene insulation is a good compromise. The cable is relatively durable and offers an attenuation of 18dB/100m at 1GHz versus about 30dB/100m at 1GHz for the RG214U. Typically, wide-band low-noise amplifiers, adequately protected against surges are used directly at the sensor for signals of smaller magnitude.

The propagation velocity c_0 translates into 3.3ns/m, however, as moving the source towards one sensor increases the difference in arrival time Δt twice, it is 6.7ns/m, approximately. Thus, every 1ns difference stands for a 15cm offset. However, in GIS, the practical precision is often not better than 15cm, as the width of an EHV GIS is larger than the shortest signal wavelength and, hence, different transmission modes cause dispersion. Additionally, depending on the design of the GIS, there may be also an irritating airborne path, if the GIS is not perfectly encapsulated in terms of UHF signals.

With partial discharge testing under direct voltage, the well understood phase relation of the discharge activity is not available and the discharge activity is recorded versus time. Generally, of course, the electrode geometry is responsible for field enhancement, as under AC voltage. However, the internal distribution of the electric field under DC within insulation materials is controlled by surface and volume conductivity, while for AC conditions the permittivity is the dominant parameter that controls the field distribution. Thus, under DC, the differential field along an insulator's surface, for instance, is influenced by the conductivity and, hence, the accumulated charge amount of the discharge activity is a measure of this process. In this sense, the Annex H of the 2015 amendment to IEC60270 [60270₂] recommends deriving the accumulated charge from the recorded activity (Fig. 6.16.)

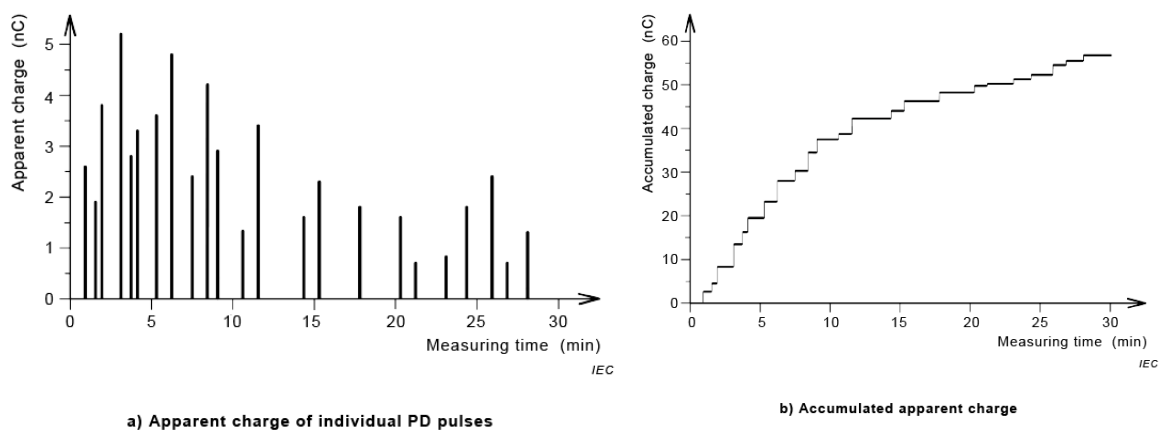


Fig. 6.16 Annex H, IEC60270:2015, accumulated apparent charge based on recorded pulses

Obviously, for a clean DC voltage the versus time record and derived quantities, such as accumulated apparent charge, the average discharge current, or $\Delta q - \Delta t$ graphs may be useful for diagnosis and interpretation.

However, for most practical setups and especially industrial applications, the observed DC voltage will show amplitude ripple originating from the conversion circuits and changes due to load variation, for example. Clearly, every such dU/dt that distorts the clean DC voltage influences the start conditions of a partial discharge activity and, hence, modulates the time of occurrence.

An oil drop under a car's gearbox can be seen as a trivial example of such effect. Here, the oil leakage (volume and surface conductivity) grows the drop, whereas its size (local space charge) and the gravity (DC voltage) determine the time the drop falls. However, the vertical acceleration (AC voltage) due to a road bump modulates the time the drop falls and, hence, many drops can be found right after the bump.

On one hand, such effects of ripple or load variation do hamper applying the methods as described above. However, on the other hand, such modulation of (known) deviations of the voltage and their impact on the occurrence of partial discharge opens additional possibilities for diagnosis and interpretation.

In case, for instance, an intended stepwise increase of the direct voltage by few percent may be used to trigger partial discharge activity. The $\Delta q - \Delta t$ graph of the provoked partial discharge pulses with reference to t_0 of the step is then used to understand the physical properties of the discharge activity.

6.3 Analysis in frequency domain

Again, partial discharge activity under nitrogen atmosphere has a rise time of approximately 1ns and, hence, at its origin a bandwidth of up to 350MHz with a widely even amplitude spectrum, as discussed earlier. Generally, high voltage equipment and the conductors used are not designed to transmit high frequency signals without losses. Moreover, several of the design elements of high voltage apparatus, such as semiconductive layers, for instance, limit the transmission of high frequency signals, as discussed in chapter 3.2.

Thus, the remaining frequency amplitude spectrum of the original partial discharge signal at a given coupling point contains vital information concerning the path the signal has taken. In fact, the spectrum that is detected at the coupling point can be considered as the result of a swept frequency response analysis, but instead of sweeping a signal generator using the broadband signal of a partial discharge event.

For example, just observing the bandwidth of an incoming partial discharge pulse at one end of a high voltage cable – derived with fast Fourier transformation (FFT) – allows a rough estimate of the distance the pulse has traveled. However, the cable's properties must be known or determined using a calibration impulse generator of sufficient bandwidth.

Likewise, on transformers, different signal paths exist, whereas each path has its own properties of attenuation, dispersion, or radiation, for instance. Firstly, some simple rules apply: If only low frequency content is remaining at the coupling point, the signal source is deeply buried in the coil stack of the transformer. If high frequency signal is dominant, while low frequency signal is missing, the source is close to the coupling point, but the signal is capacitively coupled or radiated, but not traveling a conductor. If finally, a broad band signal is detected, the source is close and reached via a conductor. In principle, this method requires a calibration with injecting broad band calibration pulses at a terminal (bushing, ground connection, core, frame, etc.) and recording the received signal at the other terminals.

Of course, such calibration measurements to understand the high frequency behavior of the transformer under test are quite time consuming, if every injection and cross-coupling point is considered. Thus, to reduce efforts, such calibration measurements shall be limited to the affected winding and the taps that do receive cross-coupled signal. Generally, all bushing taps are equipped with high frequency current transformers and coaxial cables. Coupling capacitors with such RF CTs are used at the bushing having no taps and core or frame connections, if available. Fig. 6.17 shows such coupling on the LV bushings for a 310MVA GSU transformer (generator step-up).



Fig. 6.17 Coupling capacitors with RF CT used on LV bushings of a GSU transformer.

The signal is injected into the high voltage connection and the signal on the tap or at the coupling capacitor is recorded. Fig. 6.18 shows the signal in frequency domain at the terminal on which the calibration signal is injected. Thus, this signal is predominately reflecting the complex impedance at this terminal (HV C).

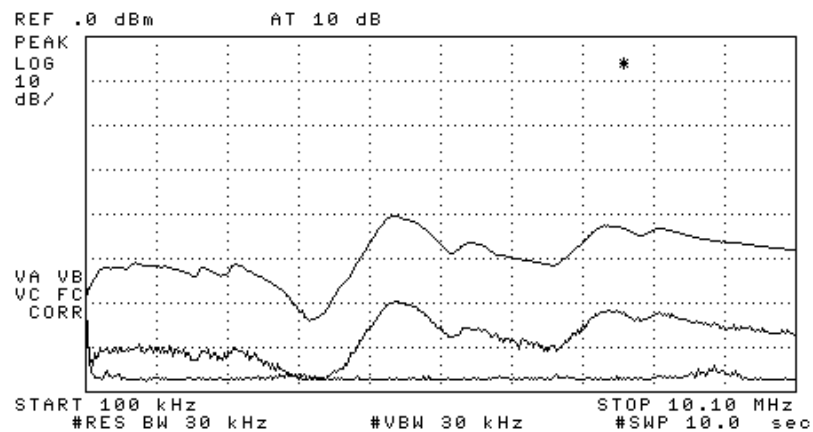


Fig. 6.18 Amplitude vs. frequency for 1000pC and 100pC injection and noise floor

A discharge activity close to this terminal would produce a comparable frequency signature. Additionally, the signals as received from the adjacent terminals are taken. Fig. 6.19, for instance, shows the situation at LV C. Here, the upper trace shows again the 1000pC signal as injected at HV C, while the middle trace shows the signal at LV C, i.e., the signal that traveled the whole coil stack. The graph shows several distinct properties of this transformer. There is, for instance, cross coupling signal at about 700kHz, 4.5MHz, and comparably strong above 7MHz.

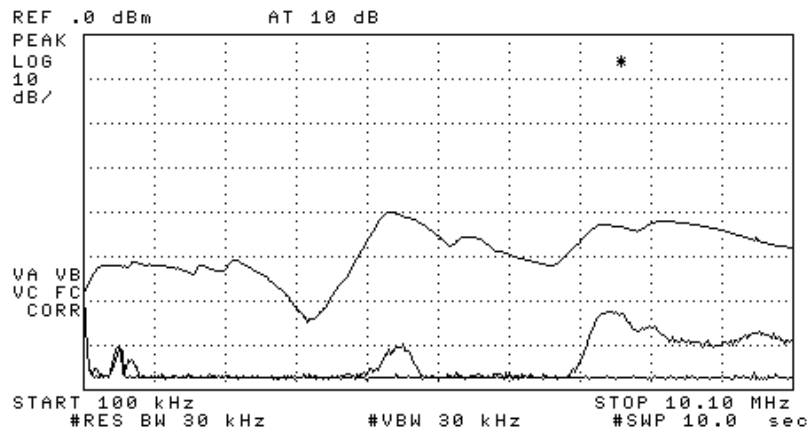


Fig. 6.19 Amplitude versus frequency - 1000pC injection at HV C and coupling to LV C

The received amplitude spectra of the partial discharge activity to be identified are then compared with the spectra taken during calibration. However, often signals on large transformers are less distinct and, hence, the analysis has to be aided by measurements in time domain and pattern interpretation.

Another analysis method both applicable for mere electrical measurement as well as for acoustic measurements is the joint time-frequency-analysis. The method, the Garbor transformation is a special case of the Fourier transformation. Its comparably narrow window allows showing short time frequency content changes of the signal. The method is especially used in speech processing. The three dimensional result is typically shown as waterfall diagram, but benefits also from a color-coded graph comparable to the φ - q - n graph of the partial discharge pattern. However, here, the t - f - a graph shows the intensity or magnitude color-coded over time and frequency. Fig. 6.20 shows an example of a waterfall diagram [Kaw00], while Fig. 6.21 shows an example of the t - f - a graph [Gao13].

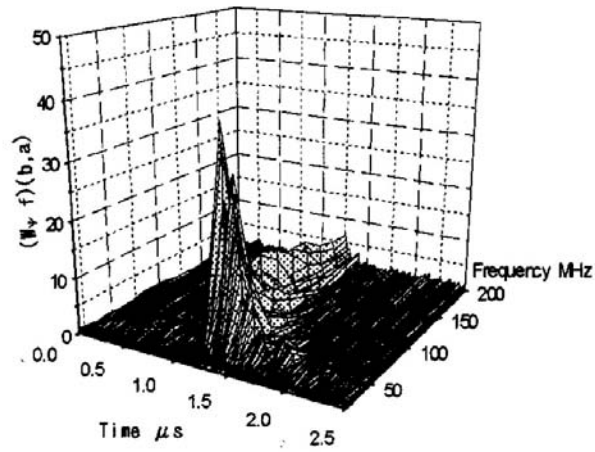


Fig. 6.20 GIS, waterfall diagram of the time-frequency signal of PD (biconical antenna)

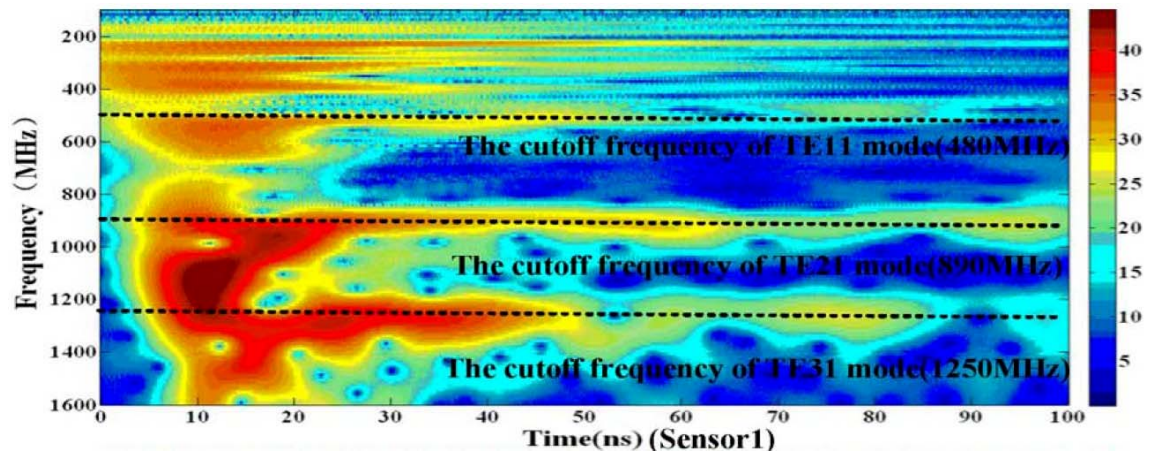


Fig. 6.21 GIS, color-coded time-frequency signal captured with an UHF sensor

7 Finding partial discharge in power transformers

Due to their basic design principles, traditional liquid-filled power transformers offer certain stability against partial discharge. The oil-paper insulation system has moreover some self-healing capabilities, as long as no carbonization on paper surfaces occurred. Likewise, traditional transformer bushings shared the oil-paper insulation system. Additionally, in the beginning, the insulation system of liquid-filled transformers was heavily over-designed.

Thus, partial discharge activity caught firstly attention with the increasing use of radio broadcasting and the disturbance of AM radio reception due to emission originating from external partial discharge, then called corona.

In order to assess the impact of "corona" on AM radio reception, disturbance measurement receivers [107₁] were used and a weighting curve based on impulse repetition rate was introduced, as described earlier. Naturally, also strong internal activity caused readings on such receivers and to also cover these activities, the acceptance levels were reduced to 100 μ V, based on narrow band detection. However, as the said weighting curve was kept, low repetition rate partial discharge was heavily underrepresented, while high repetition rate Trichel pulses, for instance, caused the highest readings.

With the wider application of the charge related partial discharge measurement based on integration or quasi-integration, this technique also made it into transformer testing. In Europe, this transition took place relatively early, while in North America this change was achieved only recently, when the IEEE standard C57.113:2010 [57113] in 2010 completely abandoned RIV testing.

Progress in signal processing, better understanding of related failure mechanism, and ongoing progress in μ controller design increasingly allows using partial discharge diagnosis as an online monitoring technique as a complement to the dissolved gas analysis (DGA) [Fru97, Sun98, Gro04₁].

7.1 Factory acceptance testing

Liquid-filled power transformers must undergo – among other tests – a partial discharge acceptance testing. Initially, this was achieved with single phase testing or using multiplexer and one partial discharge detector during three-phase induced voltage testing. During the past two decades the demand for real-time multi-channel parallel partial discharge testing increased in order not to lose any information and to reduce testing time. By end of the past century, the first true parallel partial discharge detectors appeared on the market.

Different instrument concepts and architectures have been implemented to fulfill the requirements. Haefely, for instance, combined single-channel instruments to a multi-channel instrument in a 19" rack (Fig. 7.1). The units offer as well a four-channel multiplexer to scan low voltage bushings (Fig. 7.1, lower unit).

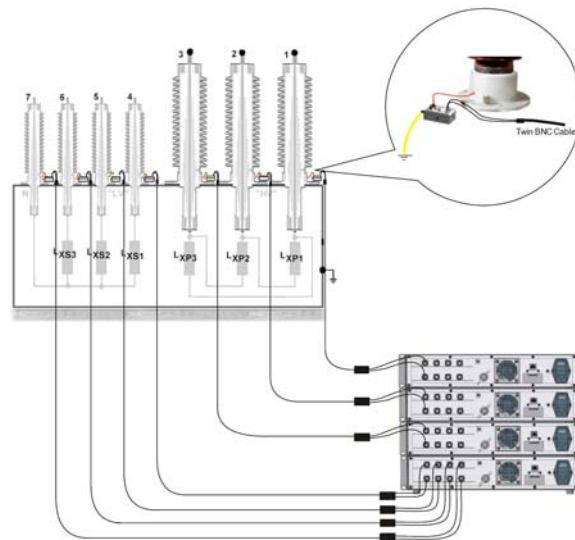


Fig. 7.1 DDX9121, Haefely – combining single channel units to a multi-channel system



Fig. 7.2 MPD600, Omicron – battery-operated acquisition units with fiber optic interconnection

The Omicron MPD600 (Fig. 7.2) follows the concept of early A/D conversion at the input and digital post-processing as described in chapter 5 and shown with Fig. 5.6. Thus, for each channel an acquisition unit and a battery pack is needed. The units are then interconnected with fiber optic cables using a proprietary protocol. The signal processing is handled by a FPGA (Field Programmable Gate Array), which is reconfigured, when changing from wide band acquisition to narrow band RIV measurement.

Fig. 7.3 shows an early version of the then eight-channel real-time Power Diagnostix parallel partial discharge detector ICMsys8 [Gro02₁] with optional eight-channel parallel RIV testing.



Fig. 7.3 ICMsys8 – eight channel parallel PD and RIV transformer acceptance testing

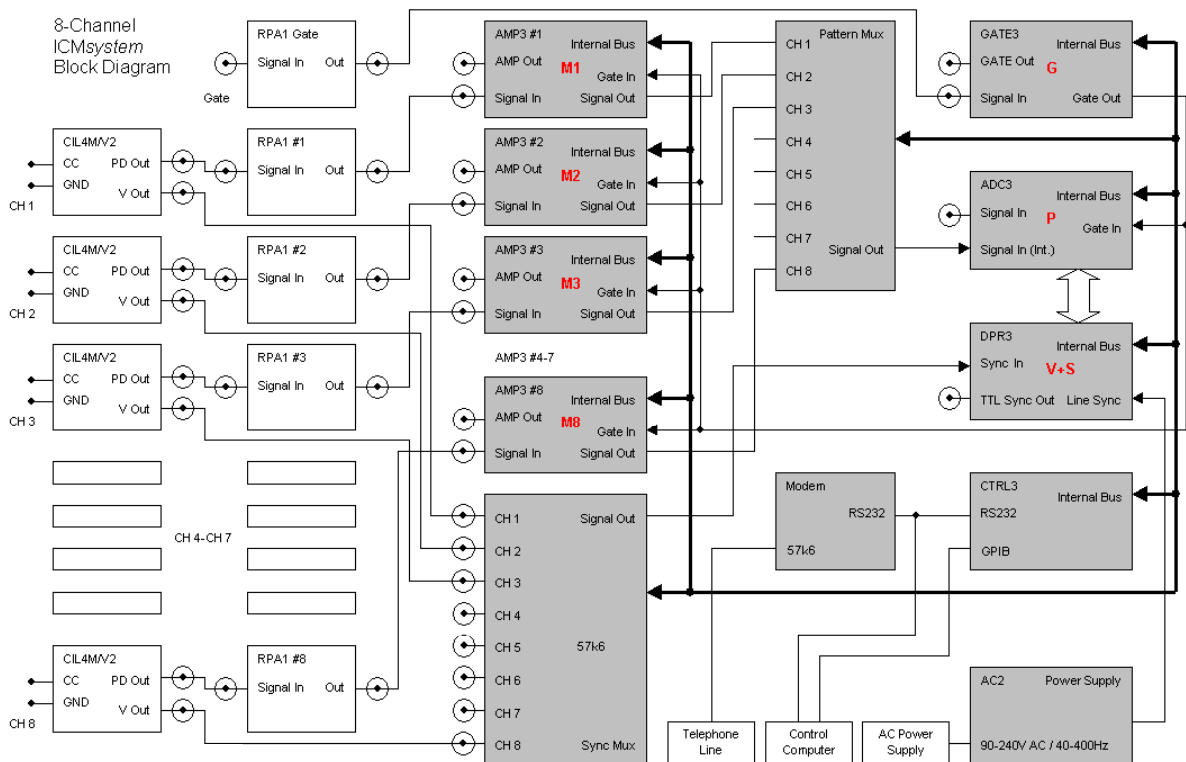


Fig. 7.4 Block diagram of an early ICMsys8 (~2000) unit with eight parallel PD channels

Fig. 7.4 shows the block diagram of the early ICMsys8 version for eight channel parallel partial discharge testing. Optionally, the unit could be equipped with a spectrum analyzer card for each or few selected ones of the eight input channel cards (the 9th, utmost left card serves as gating input). The spectrum analyzer card, equipped with a synthesizer-based local oscillator allows setting the center frequency up to 10MHz in 10kHz steps with a bandwidth of 9kHz or 270kHz. Thus, if selecting the appropriate coupling impedances, calibration sources, and center frequency, RIV testing according to the two main RIV standards [107₃, 16-1] can be conducted⁴⁷ as well.

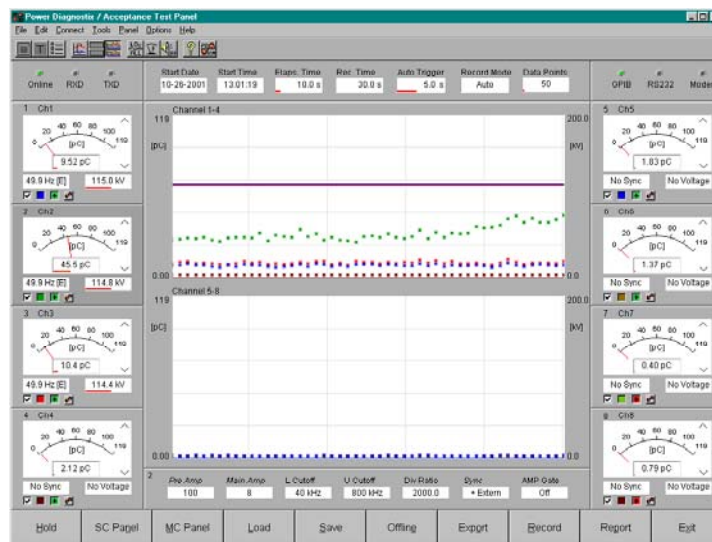


Fig. 7.5 Control panel for the eight-channel transformer PD acceptance test detector ICMsys8

Fig. 7.5 shows the control software panel for the ICMsys8 in acceptance test mode – a center strip chart or table display surrounded by meters for partial discharge, frequency, voltage, and RIV (optionally) for the eight channels.

Mostly, tests were made in a three-channel configuration on the HV or in a six-channel configuration, as with grid auto transformers, for instance. Thus, with an eight-channel instrument, the remaining two channels were available for looking at the neutral or additional taps for core or core clamps. The tertiary or a low level LV was usually not monitored during acceptance testing, as partial

⁴⁷ Both IEC and IEEE have excluded RIV testing in their current transformer testing standards [60076, 571200]. The most recent issue of the NEMA 107 [107₃] dates back into 1987 and was dropped. However, even today, there are still specifications issued by utilities including the requirement of RIV testing on transformers. Of course, transformer manufacturers try to obey customer requirements, whenever possible.

discharge measurements were only mandatory for terminals rated 115kV and above [571290₁]. As this mostly concerned the winding, which was used for applying the test voltage for induced voltage tests, likewise, noise from the supply side was comparably non-critical.

However, today, the relevant IEC and IEEE standards [60076, 571200] recommend monitoring all windings in parallel. Besides raising the need for nine or ten channel instruments, this also increases the efforts to reduce electromagnetic noise on the supply side during induced voltage tests.

Test rooms traditionally run motor-generator sets with fixed ratio to provide the elevated frequency needed to raise the induced voltage above rated voltage, while avoiding core saturation. Partly, DC motors are still in use to run the generator. The most prominent noise source concerns the excitation of the generator. Here, often, six-pulse thyristor bridge circuits provide their typical noise pattern, whereas rotating rectifiers, or the traditional DC generators on the same shaft are usually not critical in their noise emission. Besides affecting the supply cables, the switching noise of the thyristors may also be radiated, or enter the test room via a poorly installed earthing net. Fig. 7.6 shows such thyristor noise, when synchronizing on line voltage (along with calibration signal).

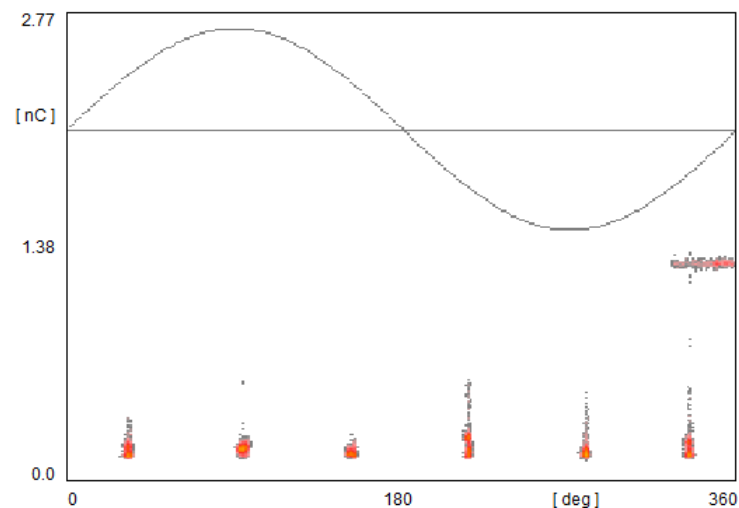


Fig. 7.6 Six-pulse thyristor noise pattern with synchronization to line voltage

However, if the synchronization is switched to the test frequency provided by the generator, the pattern usually creates one or more dotted lines due to the slip of the typical asynchronous motor or the not precise speed of the DC motor used.

As the number of available suppliers of such large motor generator sets steadily decreased, inverter based three-phase sources increasingly are used to provide the elevated frequency supply voltage for induced voltage test. Such systems do have the great advantage of almost immediate shut down, in case a current limit is tripped. Thus in case of a failure, the additional damage is very limited and allows failure analysis. Additionally, often, the operating frequency can be freely chosen, which allows minimizing the reactive power. Finally, inverter based systems can easily provide reactive power, which can become difficult with generators. However, inverter based sources are by definition noisy. Already choosing the switching frequency is a compromise. It must be high enough to support a good quality sine shaped supply with low THD, but it should be low enough to avoid its harmonics reaching into the frequency band of the partial discharge testing. Since the IEC 60270 limits the lower cutoff frequency to a maximum of 100kHz and with a typical switching frequency of 5kHz, already the 21st harmonic shows up in the relevant frequency band. Fig. 7.7 shows such typical switching pattern as caused by IGBTs and the control circuit. As the repetition rate is in the range of 5 to 10kHz and, hence, the spacing is 100 to 200 μ s, only, applying gating techniques quickly reaches its limits.

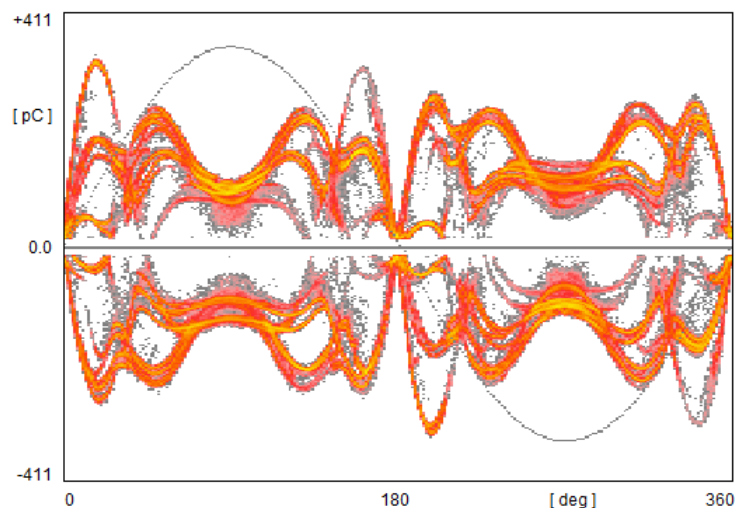


Fig. 7.7 Typical switching pattern of an inverter based power source for induced voltage tests

Thyristor pulses of the excitation system can be easily gated, as the repetition rate is low and, hence, the total loss of measurement time is negligible. However, here, it is often not easy to get a clear signal of the noise source, which shall not eventually contain partial discharge signal that shall not be gated.

Tapping the ground lead of the cabinet carrying the excitation circuits is a good try, which, however, may be far away. Both noise sources can be handled using a set of three high voltage filters in the supply line. Technically, the filters are simple T-filters equipped with damping resistors to avoid the gain at the resonance frequency. On the other hand, these resistors shall be not too small to not reduce the filter's attenuation below the resonance frequency. The use of adequate damping has been discussed already in chapter 4.1 concerning the quadrupoles and coupling circuits. Fig. 7.8 shows such high voltage filters suited for 100kV and 120A, which are mounted here upside down in an inverter based mobile power transformer test system. Here, the filter capacitors serve also as voltage dividers, whereas the AC current measurement is integrated into the filter head, while the signals are transmitted digitally via fiber optic cable. The can be moved horizontally into a parking position during transport.



Fig. 7.8 Three high voltage T-filters mounted in a mobile transformer test system

Calculating such filters in terms of power engineering requirements is comparably easy, as the formulas given for the quadrupoles in chapter 4 do apply (4.1, 4.2). However, the high frequency properties of such physically extended components are mostly controlled by their parasitic properties due to their mere size⁴⁸ given by the power engineering requirements (Fig. 7.9).

⁴⁸ The higher the operating frequency, the smaller the component, such as a capacitor or inductor needs to be to show its nominal value, only. For high voltage equipment, the creepage distance determines the size. Thus, a high voltage capacitor additionally shows approximately a series inductance of a tube or rod of the same length, depending of the capacitor's internal design. Likewise, any inductor has a winding capacitance bridging the inductor. Thus, the parasitic effects of capacitors, inductors, cages, and electrodes used for high voltage filters limit the achievable attenuation and eventually cause resonances.

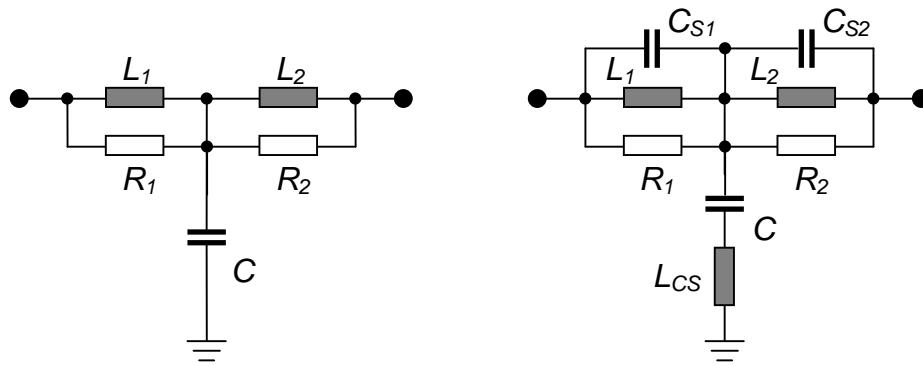


Fig. 7.9 High voltage T-filter – basic circuit and with the main parasitic components shown

For instance, a filter's attenuation cannot become better than the inductor's winding capacitance over the filter capacitor. Additionally to the winding resistance, a stray capacitance introduced by the cage surrounding the inductors to control the electric field, forms a capacitor bridging input and output. Moreover, other than in communication engineering, the transfer function instead of the insertion loss⁴⁹ has to be considered to assess the filter's properties. Finally, core materials have to be carefully selected to maintain their properties well into the range of few MHz, while tolerating the AC current without saturation.

Having now a reasonably de-noised three phase source connected to the low voltage or tertiary winding, every bushing tap that has to be monitored according to the test plan is equipped with a quadrupole and the connection to the multi-channel partial discharge detector. For the ICMsystem, a pre-amplifier as discussed earlier, is connected as closely as possible to the quadrupole to avoid attenuation due to the cable capacitance.

⁴⁹ In communication engineering filters are typically specified and tested in a 50Ω environment. I.e., the filter is inserted between a source having 50Ω and a 50Ω load – thus the name insertion loss. Obviously, this circuit considers already a plain capacitor as a good filter. In power engineering applications, the (noise) signals often arrive with lower impedance, such as with paralleled medium voltage cables, while there is often only a high impedance load for high frequency signals. Thus, the transfer function describes the real life situation closer than the insertion loss. However, the insertion loss is easier to determine and, thus, often used.

Fig. 7.10 shows such connection of quadrupole, pre-amplifier, and signal cables, whereas the quadrupole offers a selectable divider capacitance of 0.5 or 2 μ F. Together with the instrument's permissible input voltage for synchronization and voltage measurement of 200V_P, this suits the majority of modern bushings with a low C_2 value.



Fig. 7.10 Quadrupole and pre-amplifier connected to a bushing tap

In case the bushing to be monitored does not offer an accessible tap, an external coupling capacitors with built-in quadrupole is used instead, as described in chapter 4.1. Fig. 6.17 shows such coupling capacitors on the LV bushings of a generator step-up transformer.

With the IEC60270 through all issues it was clearly stated that validity is claimed only for lumped components and that the complications of measurements on cables and components having windings are beyond the scope of the standard. Due to the effects as described in chapter 3.2, 6.2, and 6.3, the signal response and, hence the calibration becomes strongly location dependent and dependent of the winding configuration of the unit under test.

Thus, in the next step, each channel is calibrated using an impulse calibrator, as described in chapter 3.3. Using a multi-channel partial discharge detector allows taking a cross-coupling matrix, which offers getting a first idea of the physical location of the partial discharge source, once incepting during test. Fig. 7.11 shows such cross-coupling matrix. Here, besides calibrating the current channel, also every other reading is taken and, as the calibration progresses, weighted with the calibration of each channel.

	H1	H2	H3	-	X1	X2	X3	-
H1	100.0 %	6.6 %	2.5 %	N/A	14.0 %	3.1 %	3.0 %	N/A
H2	6.8 %	100.0 %	6.6 %	N/A	4.1 %	13.0 %	3.1 %	N/A
H3	2.9 %	7.0 %	100.0 %	N/A	2.5 %	3.7 %	13.2 %	N/A
-	N/A	N/A	N/A	N/A	N/A	N/A	N/A	N/A
X1	51.1 %	9.2 %	4.3 %	N/A	100.0 %	14.7 %	6.9 %	N/A
X2	10.0 %	47.7 %	8.9 %	N/A	14.9 %	100.0 %	15.2 %	N/A
X3	8.4 %	12.0 %	62.9 %	N/A	9.2 %	16.8 %	100.0 %	N/A
-	2.2 %	2.2 %	2.1 %	N/A	2.0 %	2.0 %	2.0 %	N/A
Date	02-21-09	02-21-09	02-21-09		02-21-09	02-21-09	02-21-09	
Time	11:47:49	11:48:20	11:49:00		11:50:26	11:51:25	11:52:15	
Cal Channel	Cal. Charge	Pre Gain	Main Gain	Charge	Table			
No. 1	500.0	10	20	0.00 pC	Relative			
Clear	Copy	Print		CAL pC	CAL nC			Close

Fig. 7.11 Cross coupling matrix as acquired during multi-channel calibration

With this example, for instance, a typical low cross coupling for a star configuration is seen on the high voltage connections H1-H3 with only few percent. The readings for the X1-X3 terminals – the calibration concerns an autotransformer – are somewhat higher, as here the leads of the tap winding to and from the tap changer add additional coupling.

In a similar way, using the same connections and the same equipment, the calibration for the RIV measurement, if included in the test plan, is performed. Depending on the applicable (discontinued) standards, different calibrators have to be used. If calibrating according to NEMA publication 107 [107₃], a calibrator with voltage output of 100 μ V and 1MHz with an impedance of 50 Ω is used. The calibrator is connected to a second channel to assess the influence of the load (i.e. the bushing and the winding). The lowered signal is compared with the signal at the bushing tap equipped with a quadrupole having 150 Ω impedance and a correction factor is found. If calibrating according to CISPR 18-2 [18-2], the calibrator behaves as high frequency current source with an impedance of more than 20k Ω at nom. 500kHz. With a quadrupole having an impedance of 300 Ω , the reading can be taken directly without the need of a reference channel. Both methods allow deviations of the center frequency and other parameters upon agreement of test room manager and customer witness. Again, none of the RIV standards for power transformer acceptance testing are active any more, but remain applied frequently. The manual of the *RIVmeter*, a stand-alone instrument to cover both standards, gives an overview of the deviations [Riv13].

With a valid partial discharge and RIV (if applicable) calibration of the overall system, the long duration test is then started according to the relevant standards, or superseding customer specification. For a unit of 230kV nominal voltage, for instance, the sequence according to IEEE standards [57113, 571200, 571290₂] is to start with 50% of the rated value, i.e. 66.5kV and record the background noise level for 60s per channel. After this, the induced voltage is raised to the 1h value, which is 210kV phase-to-ground for at least 1min, or until the partial discharge magnitude has stabilized (below the acceptance level of 500pC). Then, the induced voltage is raised to 240kV (180%) for 7200 cycles and immediately lowered again to the 1h value of 210kV (156%) and held for 1h. During this 1h duration, the readings are recorded at 5min intervals. The test is passed, if the partial discharge activity stays below 500pC, the increase over time is below 150pC, there is no steady increase over time, and there is no "sudden sustained increase in the levels (...) during the last 20min of the test" [571290₁].

The requirements for the corresponding IEC standard [60076] are comparable. However, the values and procedures differ slightly. After switching on with a level smaller than $0.5 \times U_m / \sqrt{3}$, the voltage is raised to $1.1 \times U_m / \sqrt{3}$ and held for 5min (Fig. 7.12, A). The voltage is then raised to $U_2 = 1.5 \times U_m / \sqrt{3}$, while the inception voltage of partial discharge activity is recorded (Fig. 7.12, B). The voltage is then raised to $U_1 = 1.7 \times U_m / \sqrt{3}$ for 5min without recording partial discharge.

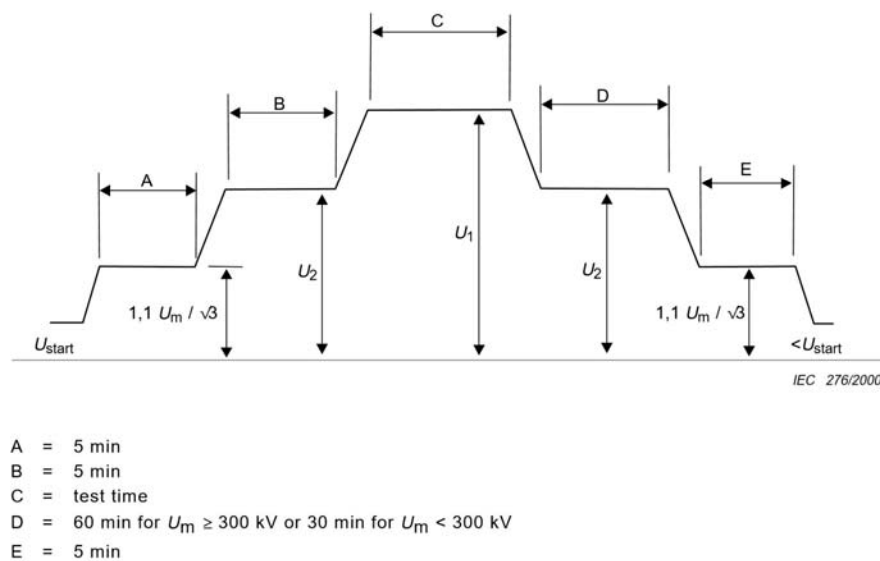


Fig. 7.12 Test sequence long duration test according to IEC 60076-3 Ed.3:2013 [60076]

After this enhancement level, the voltage is lowered back to $U_2 = 1.5 \times U_m / \sqrt{3}$ and kept for 60min (Fig. 7.12, D). During this period, the partial discharge activity is recorded every 5min and shall not exceed 500pC. Finally, the voltage is lowered to $1.1 \times U_m / \sqrt{3}$ (Fig. 7.12, E) and kept for 5min. Here, the partial discharge magnitude shall not exceed 100pC. The standard allows increasing U_1 to $1.8 \times U_m / \sqrt{3}$ and U_2 to $1.6 \times U_m / \sqrt{3}$, which is then almost identical with the IEEE requirements, as mentioned above. Reference is also made to the 150pC increase, as mentioned in the corresponding IEEE standard [571290₁].

Fig. 7.13 shows a strip chart of a successfully completed *short* duration acceptance test according to IEC60076, while an excerpt of the records around the enhancement level is shown with Fig. 7.14.

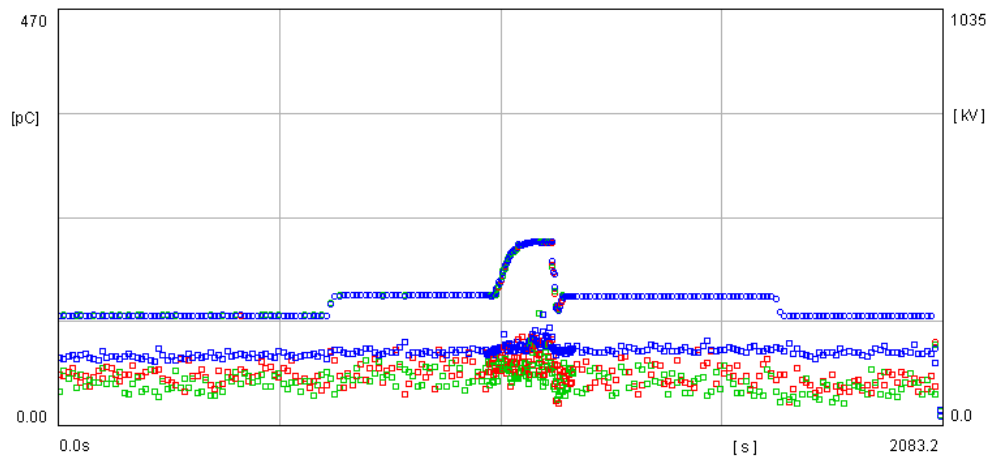


Fig. 7.13 Strip chart of a short duration acceptance test according to IEC60076:2013

Elapsed Time	HV U			HV V			HV W		
	PD	Voltage	RIV	PD	Voltage	RIV	PD	Voltage	RIV
1087.9 s	90.3 pC	447.4 kV	22 μV	63.5 pC	447.1 kV	23 μV	85.0 pC	448.4 kV	44 μV
1089.9 s	70.3 pC	447.4 kV	23 μV	57.3 pC	447.8 kV	22 μV	90.5 pC	447.7 kV	45 μV
1093.1 s	99.8 pC	448.9 kV	24 μV	63.4 pC	449.3 kV	23 μV	88.3 pC	449.1 kV	46 μV
1095.4 s	77.0 pC	450.3 kV	26 μV	60.6 pC	450.0 kV	25 μV	84.5 pC	449.9 kV	47 μV
1097.9 s	63.0 pC	451.1 kV	32 μV	69.7 pC	451.5 kV	29 μV	85.3 pC	451.3 kV	49 μV
1100.2 s	87.4 pC	451.8 kV	34 μV	55.6 pC	452.3 kV	30 μV	82.7 pC	452.0 kV	50 μV
1102.2 s	63.6 pC	453.3 kV	34 μV	68.3 pC	453.0 kV	30 μV	87.5 pC	452.8 kV	49 μV
1104.6 s	86.2 pC	453.3 kV	32 μV	59.3 pC	453.0 kV	28 μV	84.5 pC	453.5 kV	47 μV
1106.7 s	56.1 pC	453.3 kV	32 μV	46.3 pC	453.0 kV	28 μV	93.0 pC	454.2 kV	47 μV
1109.0 s	71.5 pC	454.0 kV	31 μV	53.5 pC	454.5 kV	28 μV	87.0 pC	454.2 kV	49 μV
1111.0 s	56.3 pC	454.0 kV	32 μV	92.2 pC	454.5 kV	29 μV	94.8 pC	454.2 kV	49 μV
1113.2 s	99.9 pC	454.8 kV	33 μV	95.1 pC	454.5 kV	29 μV	85.9 pC	455.0 kV	49 μV
1115.8 s	68.7 pC	456.2 kV	29 μV	81.8 pC	456.0 kV	27 μV	102 pC	456.4 kV	48 μV
1117.7 s	84.3 pC	457.0 kV	29 μV	66.3 pC	456.0 kV	27 μV	95.7 pC	456.4 kV	47 μV

Fig. 7.14 Excerpt of records of a short duration acceptance test according to IEC60076:2013

Generally, based on the mechanism of partial discharge inception of some of the defects as found in liquid-immersed power transformers, preferably, long-duration acceptance tests shall be conducted. Especially discharge originating from remaining humidity due to improper drying of the unit before filling and discharge originating from voids in casein glue and polymeric materials of composite bushings, for instance, may have an extended statistical delay to incept [Car03]. Experience with numerous long duration acceptance tests shows that such effects have the tendency to show up towards the end of the one-hour test sequence, which is the reason for the emphasis on the last 20min [571290₁].

If at this point the transformer has successfully passed the acceptance test, the partial discharge episode is at its end for this unit. If, however, the test was not completed successfully, the more demanding part of the partial discharge investigation to identify and find the source starts.

7.1.1 Narrowing the location of the source

The first indication concerning the location is the cross coupling ratio to other phases or terminals of the same coil stack. Besides directly indicating the affected coil, further understanding is gained, when comparing the ratio of the calibration cross coupling (Fig. 7.11) with the cross coupling of the partial discharge to be identified [Gro15₁]. In order to assess this effect, the ratio r of the ratios r_{pd} and r_{cal} is determined (7.1).

$$r = \frac{r_{pd}}{r_{cal}} = \frac{\frac{Q_{pd}}{Q_{pd_{cc}}}}{\frac{Q_{cal}}{Q_{cal_{cc}}}} \quad (7.1)$$

Whereas Q_{pd} is the magnitude at the dominant terminal, while $Q_{pd_{cc}}$ is the cross-coupled magnitude to the neighboring terminal. Likewise, Q_{cal} is the calibration magnitude, whereas $Q_{cal_{cc}}$ stands for the magnitude cross-coupled to the neighboring terminal during calibration.

In case $r \cong 1$, the location is close to the bushing, where the dominant signal was detected, while it is physically closer to the other terminal, if r is substantially larger than 1 (chapter 10 list few cases making use of this method).

The next step is to identify the physical appearance of the partial discharge source by analyzing the properties of the partial discharge pattern. Most of the partial discharge activities that occur in liquid-filled power transformers, such as spherical voids, paper layer delaminations, flat air pockets in glued spacers, etc., have quite distinct partial discharge pattern. However, some activities change their appearance during the partial discharge activity. Partly, this is due to "polluting" the contributing surfaces with free electrons and partly, this is due to gases generated by the partial discharge activity, which change, for example, an activity at a sharp edge into flat gas pockets in paper layers. Therefore, it is essential to capture and store partial discharge pattern at their inception voltage and shortly after incepting to get the activity of the underlying defect and not the subsequent activity [Gro06], which may camouflage the root cause.

Multi-channel versus time measurements is another helpful method to gain a better understanding of the situation at the source and to narrow the possible areas, where the partial discharge originates. In case, the pre-processed and amplified partial discharge signal of the dominant phase and terminals showing substantial cross talk are fed to a small "lunchbox" oscilloscope. Since its market introduction, the ICMsys8 [Sys16] offers such BNC output jacks for this post-processing analysis. In its latest version, the instrument contains for every channel a 100Msample DSO, which can be used for this task and which makes an external oscilloscope obsolete. The idea behind this method is to trigger on the dominant signal and compare the response of the other terminals. If all signals are in phase, the partial discharge impulses are only cross-coupled. If, however, one or more signals do show the opposite polarity, the leads or components of this terminal act as high frequency return path for the partial discharge signal. I.e., in other words, the location of the partial discharge source must be between the leads or components of the dominant terminal and the one with the swapped polarity. The appearance of this effect is comparable to the use of a second test object as coupling capacitor, as described in chapter 4.1 and shown with Fig. 4.4. Fig. 7.15 shows a screen shot of such a measurement. Here, the upper trace shows the dominant signal on X1 terminal, while the 2nd trace with the swapped signal belongs to X3 with the signals of tertiary Y1 and Y2 below [Gro15₁]. The unit is an autotransformer YN0d1.

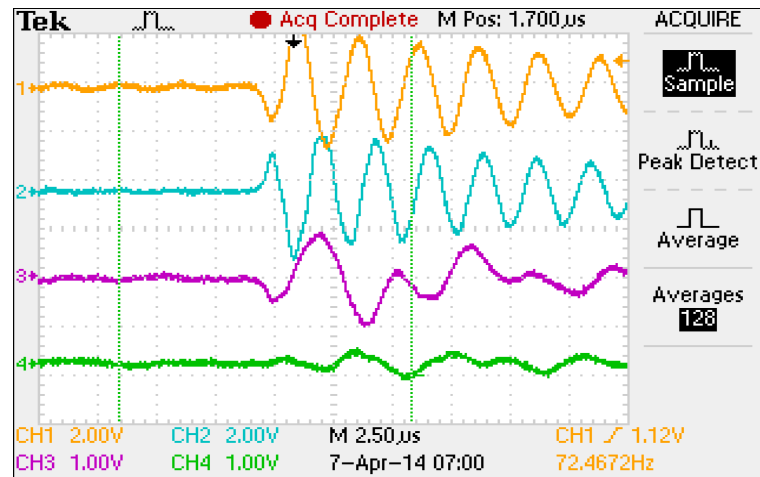


Fig. 7.15 Versus time signal of common X1, swapped X3, Y1, and Y2 (top to bottom)

The finally identified location of this case was close to the tap changer, where tap leads of both X1 and X3 did meet too close. In a practical application, of course, the partial discharge magnitude varies and the scope display jitters accordingly. Thus, the scope is re-armed few times in single shot until a clear screenshot can be taken for analysis.

7.1.2 Identifying and separating different sources

Often, there is not only one source active, but several sources contribute to the partial discharge activity at the same time. Mostly, identification of such multiple sources is already possible, when carefully observing the discharge activity and the partial discharge pattern during the increase of the test voltage. In some cases it is obvious, when looking at the partial discharge pattern that there are several activities of the same type active (Fig. 7.16).

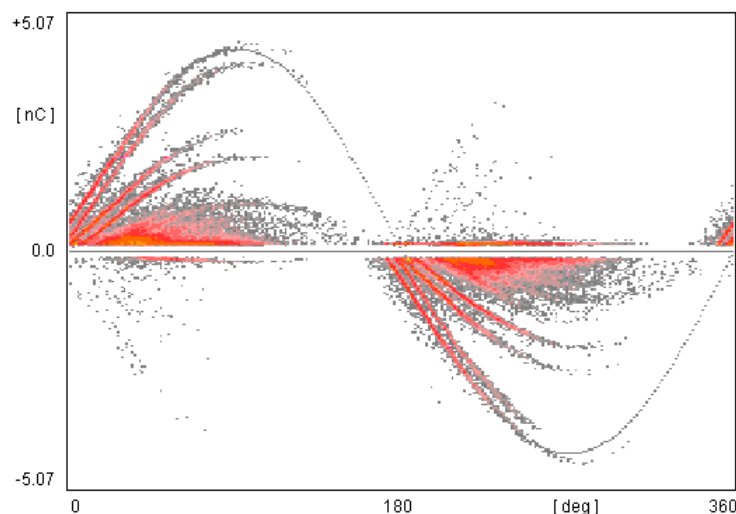


Fig. 7.16 Discharge activity of several independent voids of different sizes

Fig. 7.16 shows the activity of several spherical gas inclusions (voids) in polymeric material. They are similar, but have different sizes and/or efficiency of coupling to the electrode under test. Moreover, they are statistically independent, which can be seen at the scattered pulses in the opposite polarity⁵⁰.

In fact, it is not uncommon, to have similar defects in nearby locations, if, for instance, production procedures were applied inadequately. If, for example, a stick on barriers on top of a static shield was glued improperly, it is likely that it wasn't the only one.

Likewise, having different activities, as well does show up in the versus time measurements, as mentioned in the previous chapter. Fig 7.17 shows another screenshot as taken during measurements on the same YNa0d1 unit as shown with Fig. 7.15. However, here, the superimposed activities can be seen. The traces start with the same activity and its typical cross coupling, but after 7 μ s the second activity superimposes the signals. This second activity has a much sharper increase on common X3, which means a higher content of higher frequencies. Thus, this screenshot definitively proves that there are two activities.

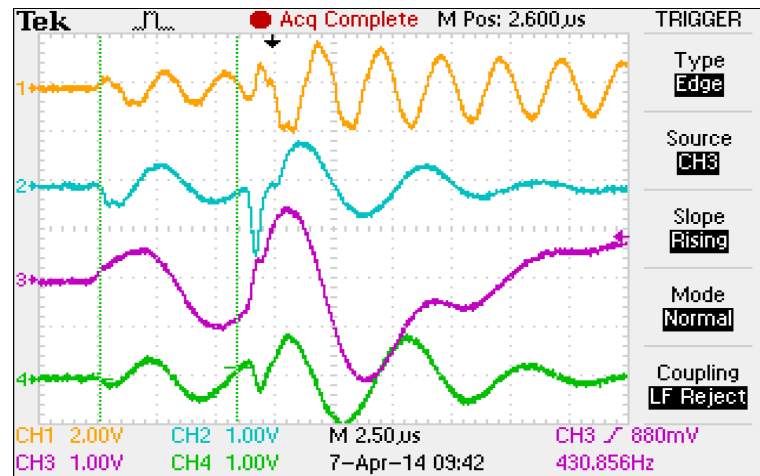


Fig. 7.17 Superimposed versus time signal of two independent activities

⁵⁰ The count rate of the overall activity is relatively small. The acquisition was taken for 100s and the accumulated dead time was only 1.7s (~8500 counts @ 20 μ s). However, as the discharge activity of each void is statistically independent, it may happen that the discharge pulses of two different voids occur almost at the same time. In case, the first peak of the later pulse is blocked and the pulse undershoot is taken instead. In fact, just by comparing counts, one can estimate the accumulated dead time versus overall acquisition time. Moreover, comparing magnitudes of the main pattern and of the scattered image allows estimating the percentage of the undershoot amplitude. In fact, partial discharge pattern do tell a lot!

Of course, it is essential to have a clear assignment of the signals to the different defects, as especially averaging techniques are heavily hampered, if not completely impossible, if two or more signals are "fighting" for the trigger.

Thus, in the first place the goal is to separate the activities by their inception voltage, or by switching to a single-phase excitation. Likewise, identifying cross coupling to other terminals, where only one activity predominately shows up, helps to not jeopardizing averaging techniques, as they are needed for acoustic triangulation at high sensitivity [Gro15₁].

7.1.3 Using a two-dimensional φ - q trigger matrix

Difficulties to apply the aforementioned strategies to separate different sources and to achieve a clear trigger, led to the idea to make use of the distinct partial discharge pattern properties that several defect types can have and evaluate the use of a φ - q trigger.

The idea of the φ - q trigger is to compare the phase and amplitude of a partial discharge pulse with a user-defined area in the φ - q plane during the process to increment a specific φ - q -counter cell [Gro15₁]. Technically, the 16Bit φ - q address (8Bit charge, 8Bit phase) of the pulse being acquired at the moment is used to check the content of a 16Bit \times 1Bit trigger pattern. In case of "1", the trigger is released and blocked in case of "0". If then the whole size of a φ - q - n pattern of 128k is taken, 16 such independent trigger areas can be stored and compared. The input of one 16Bit φ - q address causes then an output of a 16Bit trigger word. Each individual trigger is then used to store and preferably average the traces of the built-in 100Msampe oscilloscope. This can be used for separating and averaging the electrical cross talk between terminals of a power transformer, but predominantly allows averaging acoustic results of different sources.

Practically, in the first place, a partial discharge pattern is taken at a terminal giving the largest response or showing a distinct pattern at a stable voltage. In the graph of this pattern then the identified different sub pattern are marked and assigned to different trigger classes. Those trigger classes are then assigned to individual averaging baskets.

Fig 7.18 shows the screenshot of the user interface of the ICMsystem with a partial discharge pattern combining different activities, which was already given as example in chapter 6.

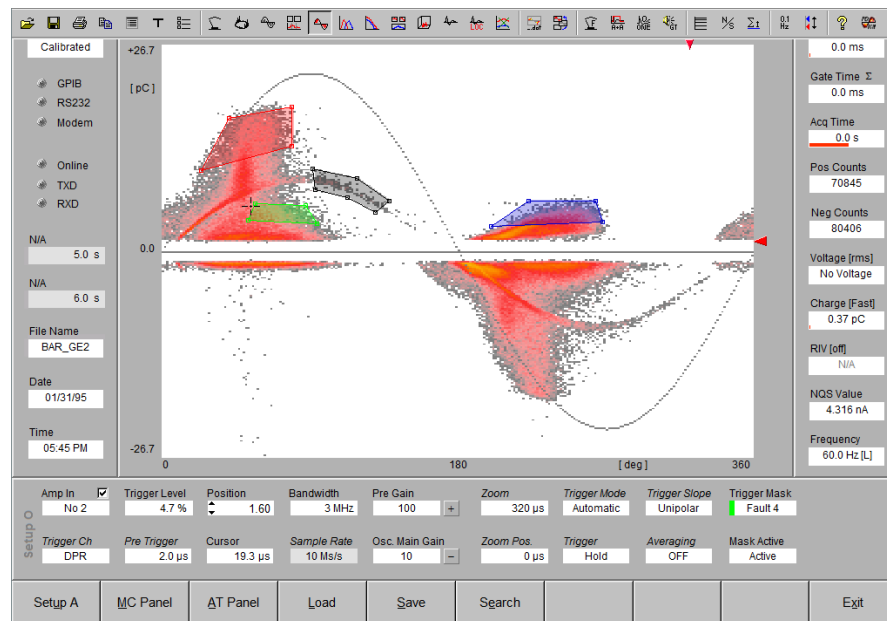


Fig. 7.18 ICMsystem – defining the φ - q trigger areas

It is essential, when defining the trigger classes, to allow only as little as possible overlap with other activities, as this would lead to a certain amount of acquisitions belonging to another activity. However, if using the averaging function, few additional "wrong" acquisitions do not substantially hamper the averaging process. Fig. 7.19 shows a screenshot displaying results of two trigger classes.

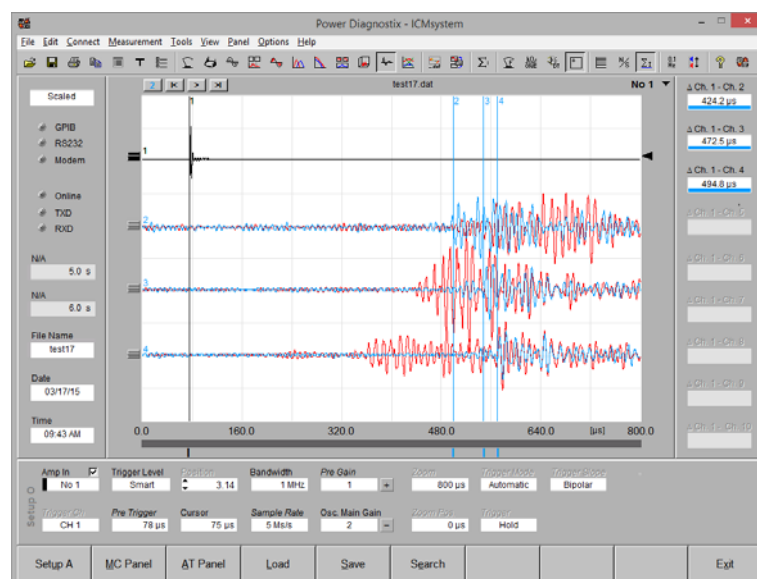


Fig. 7.19 ICMsystem – displaying results of two different trigger classes

Comparing this new pattern based φ - q trigger for oscilloscope signals with the standard only level based trigger of an oscilloscope, several strong advantages, including combinations of these advantages can be seen:

- Low repetition rate partial discharge activity can be recorded and averaged in the presence of high repetition rate activity
- Low level partial discharge activity can be recorded and averaged in the presence of high level activity
- Several different partial discharge activities, even in close vicinity can be separated and averaged individually
- Time consuming and laborious changes in the test setup (three-phase to single-phase excitation, for example) to separate activities "fighting" for the level based trigger can be avoided

The above list concerns the generic advantages to separate activities. Further advantages related closer to the acoustic location of partial discharge are discussed towards end of the following chapter.

7.1.4 Acoustic location

Generally, pulse-like acoustic emission due to partial discharge activity does travel well in liquids, such as the oil of a liquid filled power transformer. In liquids, the pressure wave travels with a spherical wave front. As any radiation with a spherical wave front, the acoustic signal undergoes the free space path loss (FSPL), provided that there are no obstacles. However, in fact this distance depending decrease is not a loss, but a decrease due to the fact that the signal power is spread over the increasing surface of the spherical wave front (7.2).

$$S = P_t \frac{1}{4\pi d^2} \quad (7.2)$$

Whereas S is the power per area at a sensor in the distance d of a source with the power P_t . Transmission, attenuation, acoustic impedance and further relevant acoustic signal parameters are comprehensively discussed in [Lun92₁].

Given a homogeneously liquid filled tank, whereas the tank wall is by its acoustic properties a thin membrane without any lateral transmission ability, the "text-book" triangulation to find a pulse like acoustic emission source becomes possible. Fig. 7.20 shows this tank and the three sensors S1-S3 placed on three orthogonal faces of the tank.

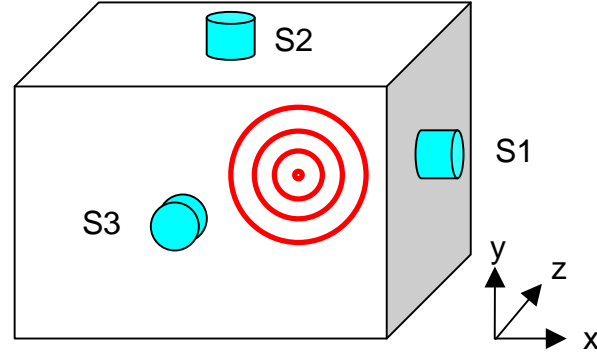


Fig. 7.20 "Textbook" triangulation – tank homogeneously filled and wall as thin membrane

With such an "ideal" tank, finding the location requires only to solve the sphere functions (7.3) based on the differences in arrival time, while knowing the transmission velocity v of the medium [Mar05].

$$(x - x_1)^2 + (y - y_1)^2 + (z - z_1)^2 = vt_1^2$$

$$(x - x_2)^2 + (y - y_2)^2 + (z - z_2)^2 = vt_2^2 \quad (7.3)$$

$$(x - x_3)^2 + (y - y_3)^2 + (z - z_3)^2 = vt_3^2$$

However, in most cases, real-life transformers do not comply with the conditions being mandatory for applying this method. First of all, transformers are usually full of material that hampers the free transmission of the compression wave and, if reaching it at all, other, longer paths may be taken to reach a remote sensor. Secondly, the tank wall is usually a thick steel plate having its own lateral transmission properties and, eventually, can cause that signals originating from laterally displaced sources do reach the sensor faster than expected, based on the assumed oil transmission velocity.

Thus, whenever applied on real-life transformers, the so-called "all acoustic method", i.e. based only on the time of arrival at three orthogonally placed sensor and upon assuming a uniform propagation velocity, suffers from strong uncertainties and partly misleading results for not considering tank wall signals.

Additionally, systems based on the "all acoustic method" cannot distinguish between mechanically induced clicking and ticking sounds and sound originating from partial discharge within the transformer. Moreover, correctly assigning a triplet of pulses arriving at the three sensors to derive a location result is quite demanding, if the reciprocal of the repetition rate comes in the range of the travel time to be considered. If complementing the acoustic detection with a trigger signal derived from a bushing tap, t_0 is defined and any mere mechanically induced sound sources are excluded.

The typical speed of propagation for transformer oil is 1415ms^{-1} at a temperature of 20°C [Lun92₁]. However, the propagation speed has a substantial negative temperature coefficient, which is typical for most liquids and, hence, the speed of propagation goes down to about 1200ms^{-1} for transformer oil at 80°C .

Other than liquids, solid materials not only allow propagation of the compression (longitudinal) wave, but offer as well propagation of the so-called shear (transverse) wave, whereas typically the compression wave has a substantially higher transmission speed than the shear wave (approx. by a factor of two). For steel, as used for transformer tanks, the compression wave travels at a speed of 5900ms^{-1} , while the shear wave travels at about 3200ms^{-1} [Lun92₁, Lun92₂].

Moreover, some of the solid insulating materials used in liquid filled power transformers, such as wood or pressboard are not amorphous, but show internal orientations of the fibers and, hence, show different propagation speed depending on the fiber orientation.

Based on the properties of steel used for transformer tanks, the propagation in clear oil space can only assumed, if the signal arrives straight or within a corner angle given by the formula below (7.4). Thus, the typical aperture angle 2α is about 28° , only, if choosing $v_{oil} = 1415\text{ms}^{-1}$ and $v_{steel} = 5900\text{ms}^{-1}$.

$$\alpha = \arctan \frac{v_{oil}}{v_{steel}} \quad (7.4)$$

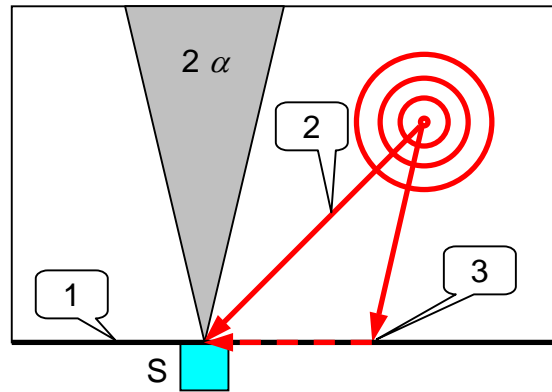


Fig. 7.20 Compression wave at a tank wall – aperture angle, possible travel paths

Fig. 7.20 shows the situation with a sensor S placed at a tank wall (1). Only for signal sources within the aperture angle 2α , the direct oil path provides the signal arriving firstly. For any laterally displaced source, as shown, the direct oil path signal (2) arrives later than the fastest signal possible, which arrives under the critical angle α at the tank wall (3) and travels with the high-speed compression wave the tank wall to the sensor.

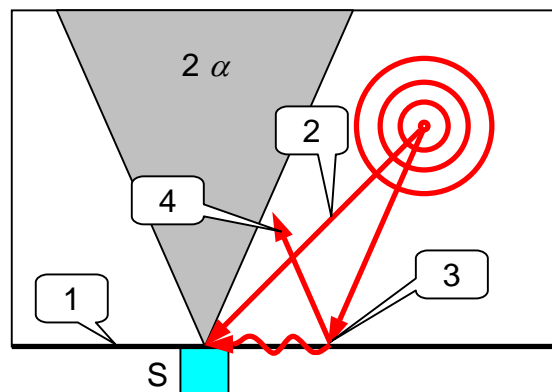


Fig. 7.22 Shear wave at a tank wall – aperture angle, possible travel paths

If considering the slower shear wave in the tank wall, the aperture angle 2α becomes wider, within which the direct oil path signal (2) arrives the earliest. The situation at a tank wall (1) is shown with Fig. 7.22. Here, for the shear wave traveling at $v_{steel} = 3200\text{ms}^{-1}$ in steel, the critical angle is about 24° . Hence, the aperture angle 2α is about 48° . The shear wave is the more dominant propagation mode for thinner tank walls, as found with smaller transformers, whereas the compression wave dominates with thick steel walls. Above the critical angle, total reflection dominates the signal path (4).

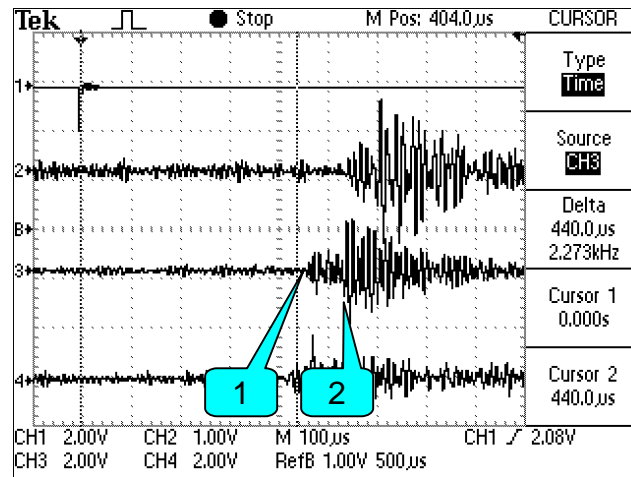


Fig. 7.23 Arrival of different wave fronts – fast tank wall path (1) and straight oil path (2)

However, in most cases, the direct oil path signal, although arriving later, can be clearly identified, since the faster tank wall signal shows clearly smaller amplitudes. Fig. 7.23 shows a screenshot of such signal arriving from a laterally displaced source. Here, the sudden increase of the signal after the initial small amplitude of the fast tank wall signal (Fig. 7.23, 1), when the straight oil path signal arrives (Fig. 7.23, 2), can be clearly seen.

The clear oil path signal is given for investigations to cover leads, mechanical structures, such as brackets, fiber nuts and bolts, tap changers and any other unobstructed elements outside of the coils. However, even here, external structures, such as flanges, hatches, fin or dome like stiffeners – the latter sometimes filled with sand – hamper proper placing of the sensors. Moreover, magnetic wall shunts attenuate acoustic signals or even block them entirely, if they are mounted on rubber to additionally correct a sound problem (Fig. 7.24).

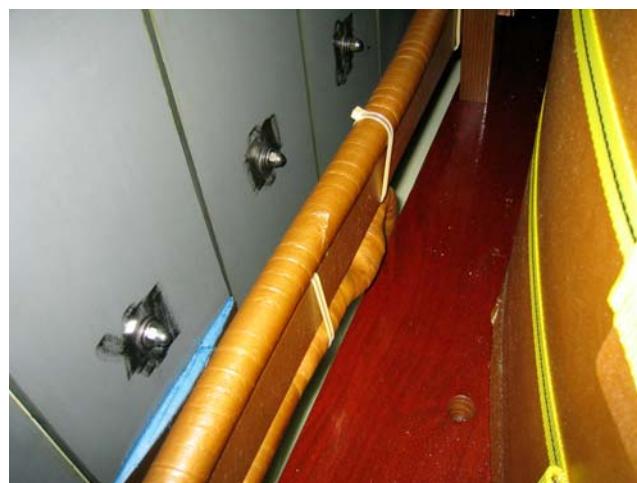


Fig. 7.24 Bolted magnetic wall shunts seated in rubber block acoustic signals almost entirely

For partial discharge activity inside a coil stack, in barrier cylinders, or other structural material deeply buried inside the transformer structure, location is difficult, if the signal is detectable at all. However, as every transformer needs to have oil channels of sufficient cross section to provide the cooling needed, even in hopeless cases sometimes surprising results can be achieved.

Fig. 7.25 illustrates such case, where the source is hidden within a transformer structure (1), but the acoustic signal makes it to the sensors through oil channels. Of course, after exiting the oil channel (2), we do have again the different propagation paths, such as straight oil path and shear wave in the tank wall. In the first place, of course the operator assumes an overall straight signal path, which in this example surprisingly points to a location outside of the tank (3).

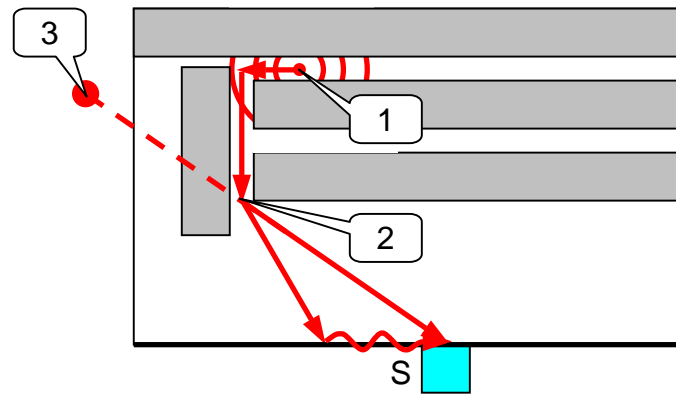


Fig. 7.25 Hidden partial discharge source – signal paths and assumed location

Thus, upon observing the indications of a shear wave, the operator will move the sensor (S) to the left and the location referring to the total path traveled is moving. Thus, whenever attempting to locate partial discharge acoustically, drawings should be at hand or at least an understanding of the internal life of the unit has to be gained from the external indications, such as drive head of the tap changer, position of bushings, tank form, etc.

Based on long-term experience with iterative single sensor and multi-sensor measurements along with electrical trigger, a software aided iterative method was developed. The early version of this software used a "lunchbox" oscilloscope, such as the Tektronix® TDS224 as acquisition unit, while the signal-processing path of the ICMsys8 was used along with special preamplifiers [Gro12].

The software supports solving "flat problems". I.e., after an initial scan of the suspected transformer areas and with a first found correlation of the electrical signal and the acoustic signal as derived from one of the sensors, three sensors are placed in a straight row. If possible, the sensors are placed evenly spaced, whereas the distance between the sensors corresponds to the initial found distance to the source. Thus, upon considering the critical angle of the shear wave, the sensors are spaced up to half of the initially found distance (Fig. 7.26).



Fig. 7.26 Evenly spaced acoustic sensors to capture the horizontal data

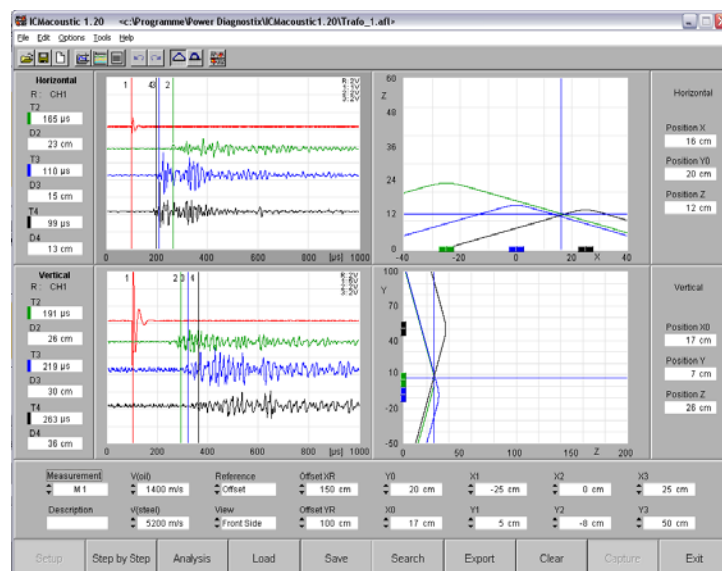


Fig. 7.27 S/W aided acoustic location based on iterative horizontal and vertical measurements

The software (Fig. 7.27) allows capturing the measurement results from the oscilloscope into the left-hand screen areas for horizontal (top) and vertical measurements (bottom). Both scope displays offer setting cursors with reference to the electrical signal serving as trigger (top trace in red).

In the right hand display area, the positions of the sensors are set either with reference to the lower left front corner of the tank or a nearby point on the tank wall. Depending on the values being set for v_{oil} and v_{steel} in the lower section of the software panel, the distance that corresponds to the respective cursor position is displayed as circle up to the calculated critical angle and from there on as line. If tank wall signals can be neglected or if the cursors are placed to the assumed arrival of the oil path signal, the display can be changed to mere circles. As the software is solving just "flat problems", they may be tilted to an initially unknown angle. However, when firstly changing from horizontal to vertical at the initially found vertical position, the previous plane is tilted to the newfound horizontal position and the indicated depth is corrected accordingly. Subsequently, with every new result, the previous result is slightly corrected and, hence, its precision increases iteratively.

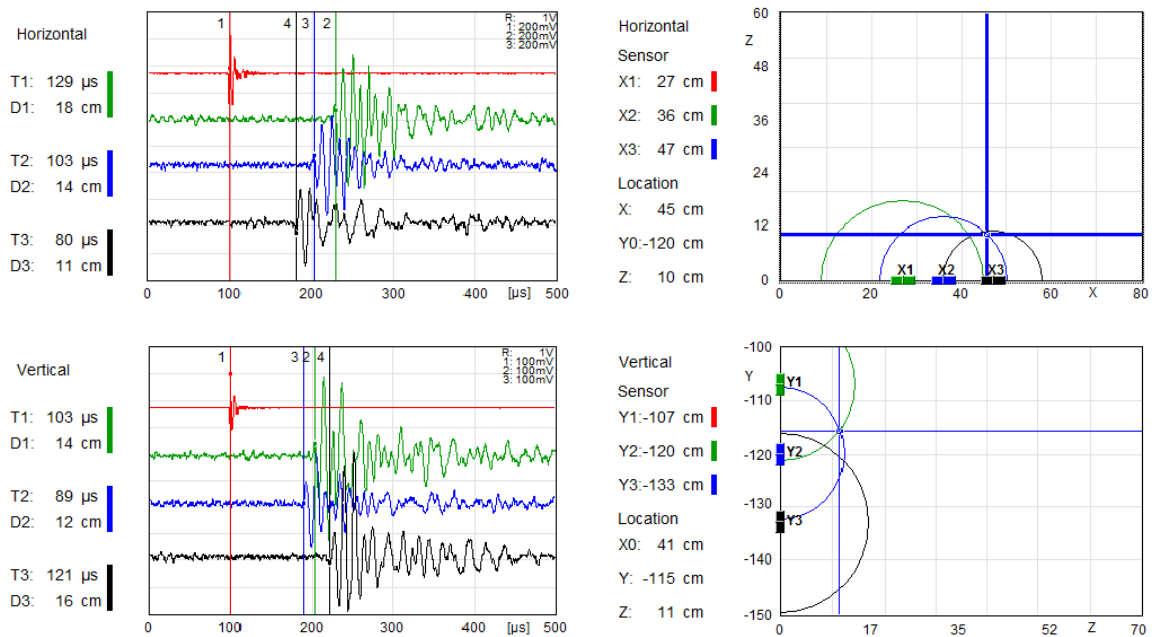


Fig. 7.28 Set of scope screenshot, cursor positions, sensor positions, and defect location

Fig. 7.28 shows a set of final graphs after the said iterative procedure. Here, displaying the circle was used, as the location was best determined with the two sensors close to the defect. The typical precision that can be reached for such acoustic location is in the range of few percent (2-4%). However, it is essential to determine the oil temperature, as the propagation speed has a temperature coefficient of about $-2.5 \times 10^{-3} K^{-1}$. A calibration measurement helps, if possible.

Additionally, besides talking to oscilloscopes, this software also controls the FOS4, a fiber-optically isolated multi-channel acquisition system that extends the acoustic location into impulse testing including testing with chopped wave. Fig. 7.29 shows the battery operated fully remote controlled transmitter unit and the receiver rack, which is equipped here with four channels.



Fig. 7.29 FOS4 – fiber-optically isolated acoustic acquisition system

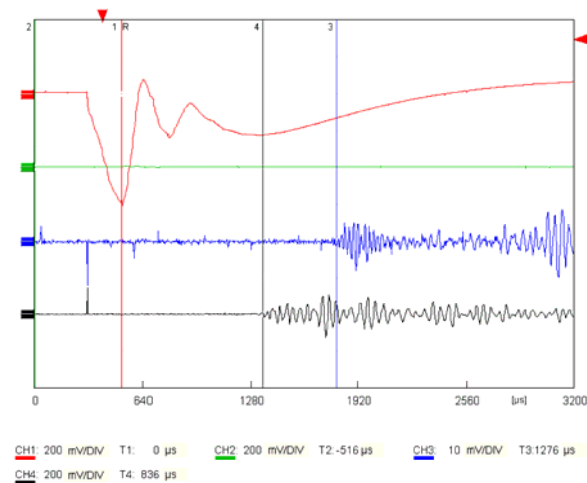


Fig. 7.30 Screen shot of an acoustic acquisition during impulse testing

Of course, during impulse testing measurements do not concern faint partial discharge pulses, but signals of partial flashover having much stronger amplitudes (Fig. 7.30). Thus, instead of using the built-in preamplifier of the acoustic sensor, the sensor AS75I/C is used in passive mode at 20dB lower sensitivity.

Another use of a combination of three nearby acoustic sensors was firstly suggested and used by Tord Bengtsson in the mid 1990ies [Ben97]. Here, a fixture holding three sensors evenly spaced by 15cm in a triangle was used (Fig. 7.31).



Fig. 7.31 Three-sensor-fixture – sensors evenly spaced by 15cm in a triangle [Ben97]

Using an oscilloscope along with electrical trigger, one can derive both distance and angle in one measurement. Moving then the fixture to a better place, the found location results then in several pointers that ideally all meet at the location of the source. Using the principle without electrical trigger would still give the direction, however, at a much lower sensitivity as the precise averaging based on the electrical trigger is lacking.

All above-mentioned acoustic methods with electrical trigger greatly benefit from the φ - q trigger, as described generally in the previous chapter. Of course, the standard oscilloscope level-based trigger is fine, if there is only one predominant partial discharge activity and if there is no noise at a level higher than the partial discharge. However, for every other case, having the ability to exclude certain φ - q areas covered with noise or clearly external signal greatly improves selectivity. Likewise, having the ability to separate two or more internal activities, which can be assigned to different averaging baskets based on their different φ - q trigger properties is a great help in case of demanding investigations on faulty units. However, in any case, although opening additional possibilities to cope with demanding cases, setting up the φ - q trigger and successfully using it remains to the well-experienced expert.

7.2 Onsite testing

Technically, nowadays, all methods and techniques as described in the previous chapters concerning acceptance testing, diagnosis, and acoustic location can be performed onsite as well [Bra00, Hae03, Fuh04, Gro12]. Here, again, as noise is an issue, if not benefiting from a shielded room, the ϕ - q trigger helps to apply sensitive acoustic location under non-ideal conditions.

However, if the full acceptance test program shall be conducted onsite, which, of course, is a vital condition for successfully doing onsite repair on large power transformers, the adequate power supply must be on site. Earlier attempts used motor-generator-set, step-up transformers, and controls distributed over several standard freight containers. Progress in power electronics of the recent decades made electronic sources an option. Fig. 7.32 shows an example of such a mobile, inverter based, transformer test system during a test on a 660MVA generator step-up transformer in a thermal power plant.



Fig. 7.32 Mobile transformer test system – 500kV, 2MVA series resonant reactor moved out

The mobile test system is built into a standard 40" high cube container and stays within the limitations of a regular roadworthy truck. The unit offers three 450kW IGBT based inverters (Fig. 7.33, a), inductive and capacitive compensation, a step-up transformer consisting of three single-phase transformers with several taps in a common tank, and a 500kV, 2MVA reactor for series resonance operation for applied voltage testing [Wer10, Gro12]. The unit is supplied with three phase 400V at 2kA. Additionally, there is a 55kW generator on the truck's power take-off for self-contained operation up to 400kVA capacitive.

The three single phase transformers having taps both on low voltage (inverter side) and on the high voltage side. The maximum output voltage can be chosen in relatively fine steps by setting jumpers, as all high voltage taps are evenly accessible. This setup allows as well changing from delta to star, running all phases in parallel, or running two phases in 180°. Thus, the full scale three phase output voltage ranges from 8.5kV to 90kV at up to 2MVA. Fig. 7.8 shows this step-up transformer along with the high voltage filters.

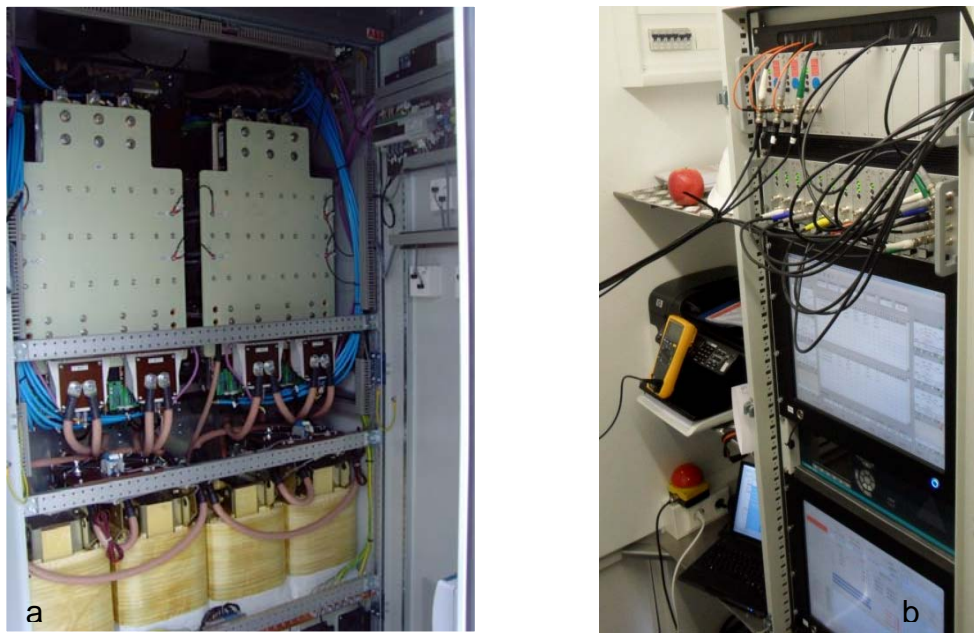


Fig. 7.33 Two 450kW water-cooled inverters (left) and control room instrumentation (right)

Additionally, the container comes with a control room equipped with the instrumentation needed: Fiber-optically isolated current measurement, voltage measurement, power analyzer, partial discharge detector, and control software to run the IGBTs as well as auxiliary circuits (Fig. 7.33, b).

The output frequency can be freely chosen between 20 and 200Hz, which allows minimizing the power requirements and transformers can be tested in their self-resonance frequency. If testing mere capacitive loads, an inverter-based source comes in the efficiency range of a resonant test set. With this unit, the (active) power requirements for capacitive loads can be estimated to be 1/10 of the (reactive) power supplied, which makes the small generator on the power take-off an option for medium capacitive loads. However, for no-load-loss tests and load-loss tests, a diesel generator of up to 2MW is mandatory.

Thus, most of the dielectric tests and associated power test, but, of course, with limitations concerning load-loss and heat run, can be conducted onsite, if the unit is taken out of service. Typically, a complete set of tests is done within few days. Especially, before and after onsite repair, this is a very cost-saving method, since the time to dismantle a unit, the transportation⁵¹ costs, bringing it to the factory, and returning it on site, easily supersedes costs of onsite repair and testing [Wer10].

Likewise, in-depth investigations become possible, if a transformer that has given troubling DGA results or has even tripped a Buchholz relay. Here, the ability to slowly increase the test voltage, while observing the partial discharge reading, is very helpful. Upon partial discharge inception, attempts to acoustically locate the source can start. In this case, there is basically no difference to the situation in a test room of a transformer factory.

Onsite investigations under service voltage do lack this ability to find an inception voltage and, if above service voltage, to determine the safety margin. On the other hand, no or little preparations are needed to do such onsite online testing. Ideally, of course, coupling circuits are in place at the bushing taps and the leads are wired to an accessible point. Few utilities took this action as a general policy – to be prepared for an online, onsite partial discharge measurement⁵². Besides the preparation for partial discharge measurements, those units are equipped with a Hydran[®], a simple DGA monitor to record the Hydrogen content. In one case, the displayed hydrogen content steadily made it up to 200ppm – 100ppm is usually considered as an alarming level. The online partial discharge investigation, however, did not show any partial discharge activity that could explain the increase observed.

⁵¹ As the trailer is packed with permanently installed measurement and power engineering equipment and, hence, is no longer suited for transportation of goods or people, the trailer can be at least in Germany registered as a "working machine". Taking this option, exempts the unit including the truck from driving hour limitations, road tolls, and the Sunday driving ban for trucks in Germany. This substantially simplifies service jobs on short notice.

⁵² Often the term "monitoring" is used in a confusing way. To me, "monitoring" shall be used only for continuous online monitoring, while everything else, such as schedule-based online or temporary online investigations shall be kept under "measurements".

Thus, as the Hydran[®] readings continued to rise, oil samples were taken and sent to two different labs, whereas both labs reported normal hydrogen levels. Finally, it was found, that a membrane in front of the sensor of the unit did break under some pressure impulse and the massive software post-processing of the unit camouflaged the otherwise step-wise increase of the reading to appear as "natural" increase due to a partial discharge problem.

Of course, acoustic investigations are feasible under onsite, online conditions as well. However, normally, no variation of the voltage is possible. Only, if the unit is connected on one side to the grid, little variation of the voltage becomes possible, when using the tap changer. Theoretically, depending on the configuration, also island operation at lower voltages would be possible, but this usually is sadly conflicting with standard utility operation principles.

Concerning acoustic location, of course, running the unit at service voltage and grid frequency causes much higher sound disturbance due to Barkhausen noise [Bar19] and, to a lower amount also magnetostriction, since the flux in the core, as well as stray flux in tank walls and other ferromagnetic material is much higher than in a test room environment at elevated frequency. Thus, piezoelectric sensors with higher resonance frequency are frequently used to stay away from these disturbances. Applying the "all acoustic method" under online condition relies on such sensors to avoid the signals of the Barkhausen noise.

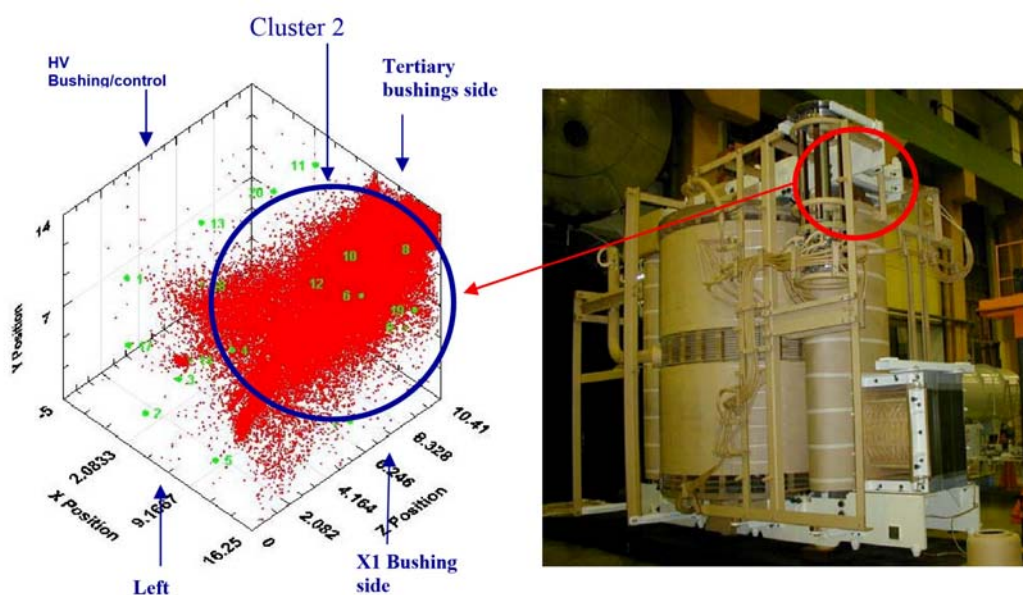


Fig. 7.34 Location results for an "all-acoustic" test with reference to a production photo

Naturally, as using averaging techniques are quite limited without electrical trigger, only based on the acoustic signals, this method focuses on higher sound magnitudes. Fig. 7.34 shows the location results of such a case as included with the appendix of the "IEEE Guide for the Detection and Location of Acoustic Emissions from Partial Discharges in Oil-Immersed Power Transformers and Reactors", C57.127-2007 [57127]. The mapped location results also show difficulties of the algorithm to correctly combine acoustic signals from different sensors to one event, when the t_0 information of the electrical trigger is missing.

Reported results often show such massive internal deterioration or mention very high hydrogen and acetylene content that it is advisable better to stay out of the vicinity of such transformer. Fig. 7.35 shows the located area (Fig. 7.34) few weeks after the measurement, when the transformer tested failed in service.



Fig. 7.35 Damage at the located area after failure of the tested unit [57127]

However, besides avoiding the pulse-like Barkhausen noise, also the sensitivity concerning partial discharge signals is substantially lower, since its acoustic spectral density shows a typical decay over frequency. Therefore, preferably averaging techniques based on an electrical trigger shall be used to maintain sensitivity and to reduce the impact of stochastic pulse-like noise.

Additionally, due to the clear t_0 information, precise spot location of the partial discharge source becomes possible, if the aforementioned limitations due to competing propagation paths, different propagation modes and velocities are considered.

Thus, with online acoustic measurement identifying and deriving the electrical trigger signal is the initial challenge, if no bushing couplers were preinstalled, as taking a unit out of service just for a provisional installation of bushing couplers is usually not an option. Coupling methods that can be used onsite online:

- Tapping the neutral connection in case of star configuration of the transformer's high voltage side with an RF current transformer (CT)
- Tapping the main ground of the transformer using an RF CT
- Using a connected high voltage cable as "coupling capacitor" by tapping the high frequency currents with an RF CT (refer to Fig. 4.6 as well)
- Inserting an UHF antenna into a drain valve of the transformer

Typically, the neutral bushing of a Y-HV is connected to ground via an isolated cable. Fig. 7.36 shows on the left the application of a clip-on CT to such neutral cable just at the power frequency CT installed for protection purpose. On the right hand side, using this type of CT on the main ground connection is shown.



Fig. 7.36 Tapping the neutral connection of a Y-HV (left) and the main ground (right) with a CT

Often, the high voltage cables connected to substation power transformers are only short connections to a switchyard or a more conveniently located overhead cable connection. Here, the cable screens are typically only terminated on one side, while the other side is left open, or is connected via a surge arrester to ground. This allows using the cable capacitance (estimation for short connections) or impedance (estimation for longer connections) as coupling. Fig. 7.37 shows on the left hand side this application. On this side, the cable is left ungrounded and the CT "sees" the full HF current (and the load current).



Fig. 7.37 Using a HV cable as coupling capacitor (left) and UHF drain valve sensor (right)

For calibration or better estimation of the discharge magnitude, a calibration impulse generator is fed in a loop through the CT as well [Fig. 7.37, left], as there are of course no other means of calibration in an onsite online situation. Fig. 7.38 shows the partial discharge pattern for that case along with the signal of the injected calibration pulse of 1nC.

The main task of the drain valve sensor, as shown on the right hand side of Fig. 7.37, is in the first place to be oil tight. After installing it on the flange of the drain valve with the central pipe moved back, vacuum is pulled to confirm that it is tightly installed and to avoid bringing air inside of the transformer in service. With then the drain valve slowly opened, the central pipe is moved inwards to have the antenna protruding a few centimeters beyond the inner tank wall.

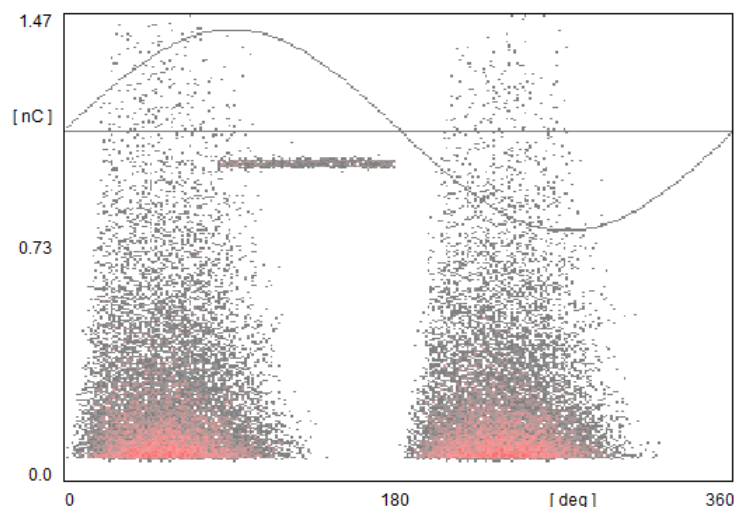


Fig. 7.38 Partial discharge captured with the setup of Fig. 7.37, left, and 1nC calibration signal

Adequate processing of the signals is needed, to ensure that signals from the internal activity are clearly captured. This has to be confirmed with the φ - q - n partial discharge pattern. For the case as shown with Figs. 7.37 left and 7.38, for instance, it was confirmed that the neighboring cables did show the same partial discharge pattern, but at a fraction of the amplitude (<20%) and that there was no further activity, whatsoever.

Having now a clear partial discharge pattern and, hence, a clear trigger signal, the suspected areas of the transformer are scanned for acoustic signals correlating with the trigger, i.e., growing out of the noise signal with applying averaging. Fig. 7.39 shows the provisional setup of the measurement equipment (left) and acoustic sensors installed for scanning (right). Fig. 7.40 shows a partial discharge pattern as it was used for trigger, but here afterwards marked with φ - q trigger areas that would have made life easier, if it was available then.



Fig. 7.39 Provisional setup of measurement equipment (left) and acoustic sensors (right)

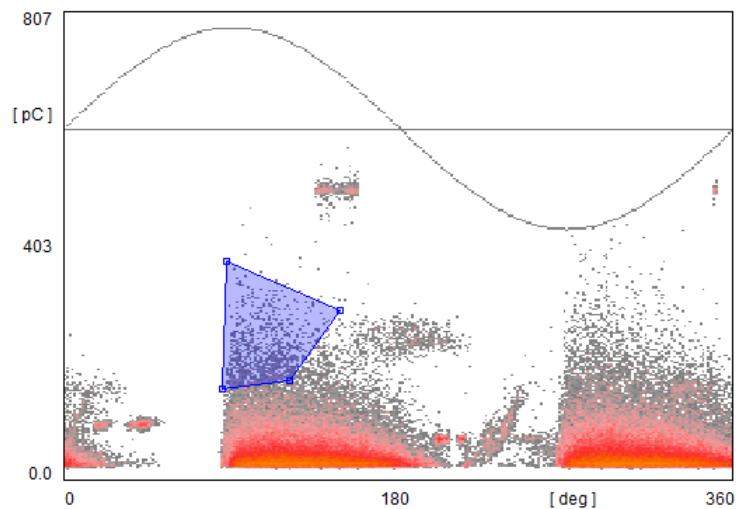


Fig. 7.40 Partial discharge pattern as used for trigger marked with φ - q -trigger area

7.3 Online monitoring

For continuous online partial discharge monitoring all previously discussed methods can be used in principle, if the practical design of couplers and circuits provide the durability, as needed for permanent installation outdoors.

Using the bushing taps, of course, is the most prominent method. Fig. 7.41 shows an example of a bushing adapter to match threads and contacts of the tap and to provide the final protection of the bushing tap with built-in gas gaps and the subsequent bushing coupler unit that carries divider capacitor, high frequency current transformer and (optionally) a quadrupole, if this unit shall be prepared for partial discharge acceptance testing as well.



Fig. 7.41 Bushing tap adapter BA and bushing coupler unit BCU on a Micafil® bushing

This separation reduces the modifications needed to the bushing adapter and keeps the bushing coupler a standard component, as there are many different designs for bushing taps and no standardization in sight.

Modern substations with GIS equipment have the transformers connected directly to the GIS or via comparably short high voltage cables and the connection to overhead cables is made with a bushing on the GIS. In those cases, using the bushing tap for coupling is an almost noise free and convenient way for monitoring. However, with traditional air insulated switchyards, noise interference can be quite strong and selecting a proper frequency and applying gating techniques can become demanding [Rob95, Gro04₁]. This is especially the case, if overhead cables have been installed sloppily, with leads pointing out of clamps and where corona rings have not been installed adequately.

Alternatively, UHF sensors can be used for partial discharge monitoring. Fig. 7.42 shows an example, where a spare flange of a pressure relief valve has been used to install an internal UHF sensor. It should be kept in mind that the rise time of the electron avalanche under Nitrogen (and other electro-positive gases) is in the range of 1ns and, hence, the relevant frequency band extends to about 350MHz, as mentioned earlier.

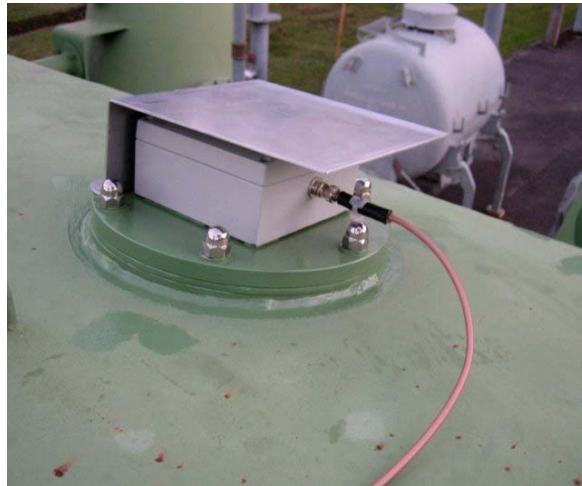


Fig. 7.42 UHF sensor installed on a spare flange for a pressure relief valve

Likewise, other hatches and openings of a transformer can be used to install an UHF sensor. Again, first of all those things installed must be durable and oil tight, before high frequency properties are discussed, for instance. The permanent use of drain valve sensors is not advisable, if the valve has not been planned exclusively for this task and the sliding mechanism of the drain valve sensor is designed to permanently withstand the oil pressure.

However, signal transmission inside of a transformer tank in the VHF (30-300MHz) to UHF (300-3000MHz) range is not uniform and has several limitations. If measuring the signal in narrowband regime with a bandwidth of, for instance, 300kHz, which is sufficient for partial discharge detection, standing wave effects create "blind spots" as a function of location and frequency. While sources in the free oil space transmit fairly well, signal originating from locations deeply buried in the winding, do suffer strongly from attenuation. As the antennas have to be fulfilling also the high voltage requirements to not disturb the electrical field, applicable designs are limited [Akb16] and a calibration, even in the comparably weak sense of partial discharge calibration, is not possible.

Thus, when using such antennas, displaying readings in μV or dBm should be preferred. However, using VHF (and UHF) signals in transformers for the mere detection of activity, rough location of such activity, and as trigger for acoustic measurements make this technique a valuable tool.

The signals derived from the aforementioned sensors are then fed to an acquisition instrument that permanently processes the signals and their pulse content. Often, the partial discharge monitoring is used as subsystem to an overall transformer monitoring system, which also takes care of temperatures, flow, dissolved gases, and other parameters. Fig.7.43 shows two examples of such monitoring systems with the partial discharge monitoring as a subsystem.



Fig. 7.43 Transformer monitoring with PD monitoring subsystem – Koncar (left), Alstom (right)

Data communication is possible on different integration levels and ranges from mere transmission of values to a full control of the instrument. However, also a direct integration using IEC61850 protocol is possible.

8 Résumé

The aim of this chapter is to give an overview of the work, the structure of the thesis, and the findings in their logical steps. This thesis covers partly work of the past more than twenty-five years, recent achievements, and new findings.

Although the work covers "only" acquisition and location of partial discharge in transformers, this cannot be seen isolated from the historic and economic context. Generally, development of technology does not move steadily into one direction, but changes focus according to needs, knowledge, and technical possibilities as time goes by.

Thus, this thesis starts with an historic overview of partial discharge as a threat for the integrity of high voltage insulation systems, as well as its increasing use for diagnosis over the decades. It is interesting to learn that the knowledge of basic gas discharge physics was already available, when the industrial use of high voltage technology started [Tow15]. Likewise, the impact of "corona" on the design of such insulation systems was understood early [Pee15].

However, besides just using the senses to "detect" partial discharge by its visible or audible effects or by the smell of ozone, the only early instrumentation was the loss measurement, which, however, is also detecting mere insulation resistance and polarization effects. From on the 1930s, also disturbance receivers were used. Modern partial discharge testing starts with the impulse charge based partial discharge measurement as proposed by F. H. Kreuger in the 1960s [Kre64]. The proposed principles made it quickly in an international standard [270₁] that is still maintained [60270₂], as the basic principles still apply.

At first sight, coupling circuits, such as quadrupoles, current transformers, and others look trivial (chapter 4). However, care must be taken to fulfill the power engineering requirements, safety issues, as well as the high frequency and sensitivity needs, which is not trivial at all. Likewise, the mere size of high voltage equipment introduces parasitic effects to be considered.

In a similar way, just using the basic processing circuits, as known from communication engineering, does not work in the first place and adequate modifications are needed. Here, for instance, understanding the signal properties of the partial discharge pulses is needed to design adequate processing circuits. Likewise, for impulse application, heterodyne circuits as known from broadcast application need to be modified.

Understanding the non-ideal transmission properties of leads and conductors in power engineering equipment (chapter 3.2) is needed to assess the limitations of partial discharge measurements due to attenuation, dispersion, reflection, and antenna effects [Gro03₁]. Moreover, the impact of resonant behavior especially in light of calibration of larger equipment needs to be considered.

A larger section (chapter 3.1) covers the gas-discharge physics background and its influence on the appearance of φ - q - n pattern. Especially, the impact of charge carrier generation, electron avalanche behavior, recombination, and polarization is discussed [Nie95, Hei99]. Additionally, the influence of electrode geometry, surface properties, and (surface) conductivity is outlined. Several examples of φ - q - n pattern are presented.

Acoustic emission from partial discharge in liquid-filled power transformers allows location of the source. However, a real-life transformer does not support the requirements of "textbook-triangulation", which is based on a homogeneously filled tank, whereas the tank wall behaves like a thin membrane without lateral transmission properties [Gro15₁]. Thus, in chapter 7.1.4 the limitations are discussed and strategies presented to cope with the resulting problems. Here, especially, the "all-acoustic-method" has strong weaknesses, as the lacking t_0 information of an electrical trigger adds interpretation ambiguities. However, competing acoustic travel paths, non-uniform travel speed, and tank wall signal hamper as well triangulation based on electrical trigger.

Several independent partial discharge sources are often active simultaneously in large power transformers. Thus, it is essential to separate the different sources by their pattern properties, different cross-coupling behavior to other phases, different behavior in time domain, or in frequency domain.

However, when the electrical signal that is intended to be used as trigger for the acoustic location is containing high repetition noise or signals of other sources with higher magnitude, which cannot be separated by using another bushing tap or non-conventional coupling, also this method fails. Here, the main problem is that the different sources are "fighting for the trigger". This is a problem because the acoustic triangulation needs averaging techniques to reach an acceptable sensitivity and in case of multiple sources, the averaging result entirely blurs.

Thus, a new trigger method was developed in this work. This new φ - q trigger is based on the partial discharge pattern of the desired trigger signal (Fig. 8.1). Here, the different identified sources can be marked to form different trigger classes. These color-shaded areas form then a 1-Bit trigger pattern [Gro15₁].

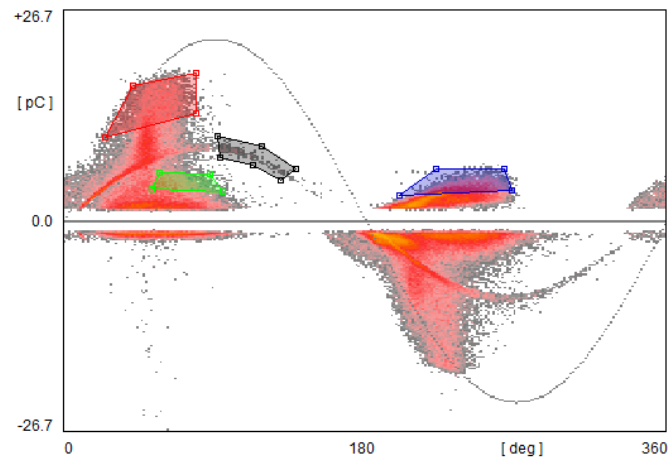


Fig. 8.1 New φ - q trigger – defining trigger classes in a φ - q - n pattern

Based on this 1-Bit trigger pattern, a trigger will only be released, if a partial discharge pulse is falling in the marked area. In case, current traces of the acoustic channels are put to the related averaging basket. As discussed in chapter 7.1.3, this method allows triggering to signals and deriving valid averaging results and, hence, valid triangulation results for situations that did not allow reliable measurements before:

- Low repetition rate partial discharge activity can be recorded and averaged in the presence of high repetition rate activity
- Low level partial discharge activity can be recorded and averaged in the presence of high level activity

- Several different partial discharge activities, even in close vicinity can be separated and averaged individually
- Time consuming and laborious changes in the test setup (three-phase to single-phase excitation, for example) to separate activities "fighting" for the level based trigger can be avoided

Besides serving for acoustic triangulation, this new φ - q trigger allows as well reliably attributing electrical time domain signals to a certain portion of the partial discharge pattern. Before, this was a guesswork that required a lot of experience, if possible at all.

This new method is especially helpful under the demanding non-ideal condition for onsite and/or online testing, where disturbance conditions are not as nicely under control as in a shielded test room. Here, as well, coupling methods and strategies are presented and discussed as well. The application of a 1.35MVA mobile test system for onsite three-phase induced voltage (up to 90kV) and applied voltage (up to 500kV) is presented.

Partial discharge monitoring on transformers, the permanently installed coupling methods and the system integration is only briefly addressed in chapter 7.3.

Finally, few cases of successful location of partial discharge sources in liquid-filled power transformers are presented in chapter 10, the appendix. In order to protect the owners of the units being covered in the cases presented, drawings are only given as principle sketch and the use of photographs is avoided. The appendix ends with a small catalog of different φ - q - n pattern.

9 Summary

This thesis covers techniques and strategies to acquire and locate partial discharge in liquid-filled power transformers. There was remarkable progress in partial discharge testing since the introduction of the modern charge-based partial discharge measurement technique in the 1960s.

However, it is still demanding to acquire and locate partial discharge in large transformers. The situation in a well-maintained shielded test room is quite predictable, but even here separating multiple partial discharge sources is difficult. Moreover, the non-ideal conditions with onsite and online testing would benefit from improvements. Thus, the research tasks for this thesis were:

- To develop strategies to locate partial discharge sources in transformers under the non-ideal conditions of real-life transformers,
- To identify, interpret, and separate partial discharge activities that occur simultaneously, and
- To find methods to reliably separate and acoustically locate partial discharge sources that occur simultaneously.

However, additionally, this thesis covers an historic overview of partial discharge testing in chapter 2. Here, further, the development steps over the decades as well as the changing industrial requirements are outlined.

Chapter 3 covers in the first part the different partial discharge processes and their impact as well as the impact of electrode configurations on φ - q - n pattern. In the second part the high frequency signal transmission of partial discharge signals in power engineering equipment is discussed, while calibration of the measurements is discussed in the third part.

Chapter 4 covers a discussion of the different circuits that can be used as coupling device for partial discharge measurements. Here, additionally, applicable bandwidth and achievable sensitivity are discussed, for instance.

Chapter 5 covers the different frequency bands and the applicable detection circuits according to the standards as well as outside of the standards.

In chapter 6 the different ways of visualization of measurement results and their interpretation are discussed.

With chapter 7 then the application of the previously described techniques on power transformers is discussed. Here, the difficulties of applying simple triangulation techniques, the strategies to identify and locate partial discharge, and how to apply this under field conditions are discussed. Further a new trigger technique based on the φ - q - n pattern is presented. This new two-dimensional φ - q trigger allows separating different sources by their phase-resolved pattern properties, which allows assigning signals in time domain to individual defects for further interpretation. Additionally, this φ - q trigger offers dedicated averaging of acoustic signals in the presence of electrical noise signals, or signals originating from other defects. Previously, such separation was only possible by finding a bushing tap that shows the wanted signal exclusively.

Further, there is chapter 10 as an appendix following Résumé (8) and Summary (9). This appendix contains few cases of partial discharge location in large power transformers. Regrettably, these cases have to be presented in a more generic form. However, care was taken to not hide the strategy as such that allowed solving those diagnostic tasks.

Finally, there is a small catalog of φ - q - n partial discharge pattern including a very brief description. Besides covering transformer partial discharge pattern, there are also examples of more generic partial discharge pattern included.

10 Appendix

The following pages cover cases of liquid-filled power transformer having had partial discharge problems. The units were investigated and the root cause was identified. Aim of this appendix is to illustrate the method and strategy. Thus, focus is put on how the task was solved. However, care is taken to avoid disclosing the owner of the specific unit and, hence, photos are not presented.

10.1 Grid transformer with cable box

This case covers a grid transformer that is connected to polymeric cables on both sides. On the high voltage side, firstly an oil-oil bushing is installed followed by an oil-filled duct to the cable box, which is separated from the main oil reservoir. A while after commissioning, oil samples were taken and analyzed. The oil sample taken from one cable box showed a hydrogen content of a couple of hundred ppm. For the onsite investigation under online conditions no measurement taps were available. Thus, after making sure that the cable's ground connection was made outside of the cable box, a high frequency current transformer offering an opening of 100mm was used on the high voltage cable as explained in chapter 7 (Fig. 7.37).

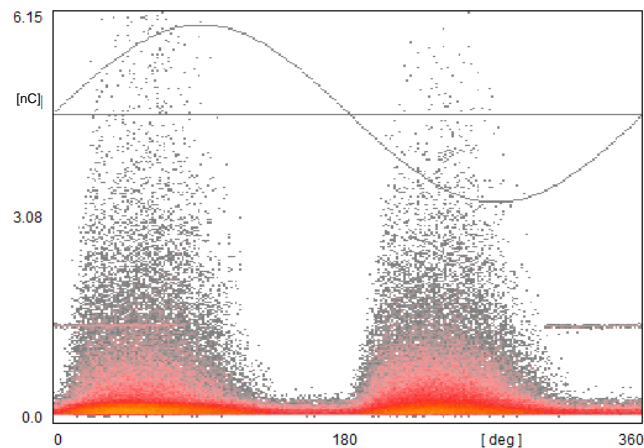


Fig. 10.1 Partial discharge pattern of paper layer delamination (flat gas-filled pockets)

To estimate the sensitivity, a calibrator signal was fed through the CT opening parallel to the cable (Fig. 7.37). Fig. 10.1 shows the signal of the partial discharge activity along with a calibration signal of 1nC. Thus, the magnitude of the activity is in the range of $5nC_{iec}$. The pattern as such shows the typical properties of large flat air pockets between insulation layers.

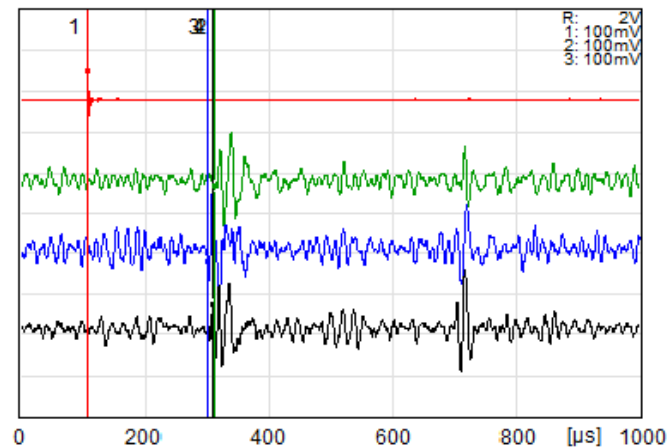


Fig. 10.2 Signal of the acoustic sensor based on electrical trigger signal (red)

Likewise the other cables were checked as well as the accessible neutral connection and it was confirmed that this was the only activity. Thus, acoustic location was attempted using the electrical trigger. Fig. 10.2 shows the signals as captured using three sensors. The acoustic signals arrive about 200μs after the electrical trigger, which corresponds to about 26cm. Here, it is interesting to see that the signal is also being reflected from the rear side of the pipe having a diameter of 600mm and, hence, the reflected signal arrives after about 600μs.

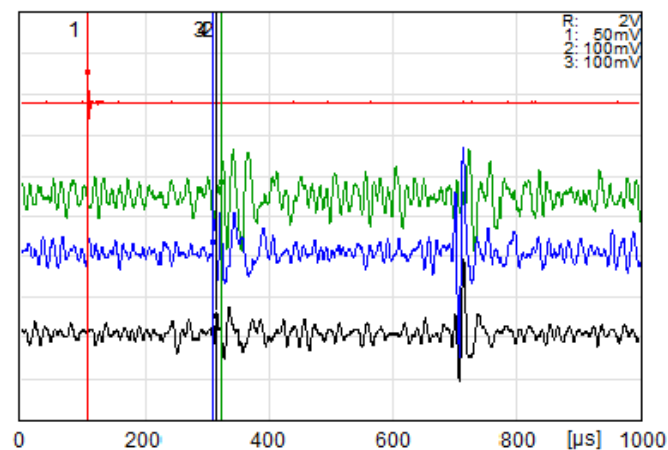


Fig. 10.3 Signal of the acoustic sensor, but placed on the left side of the duct

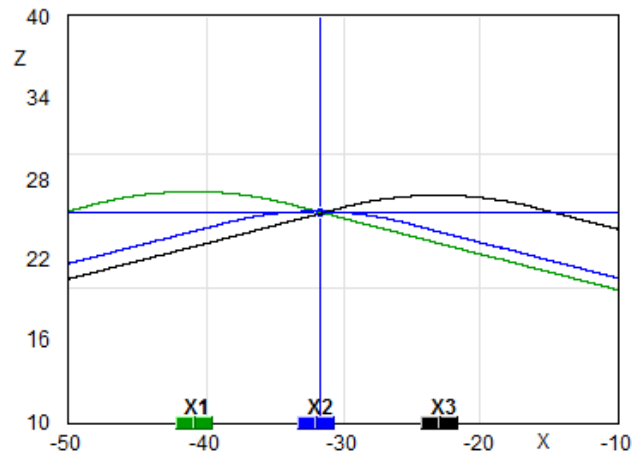


Fig. 10.4 Triangulation result of the measurements as shown with Fig. 11.3

Fig. 10.4 shows the triangulation result with reference to the centerline of the pipe that heads the cable (Fig. 10.5, red line). It turned out that at this location a flexible link is inserted into the connection between cable bushing and oil-oil bushing, which apparently has been bent during installation. When placing the sensors on the rear side of the duct (Fig. 10.3), a similar result is found. However, the reflection is stronger on the left side. Thus, it can be assumed that the activity is stronger on the right side of the duct.

The resulting field enhancement started partial discharge and gases were accumulated between the paper layers. The lead has been replaced and the unit was tested having no partial discharge afterwards. Fig. 10.5 shows the principle of the cable box for this unit and the location of the source (red circle).

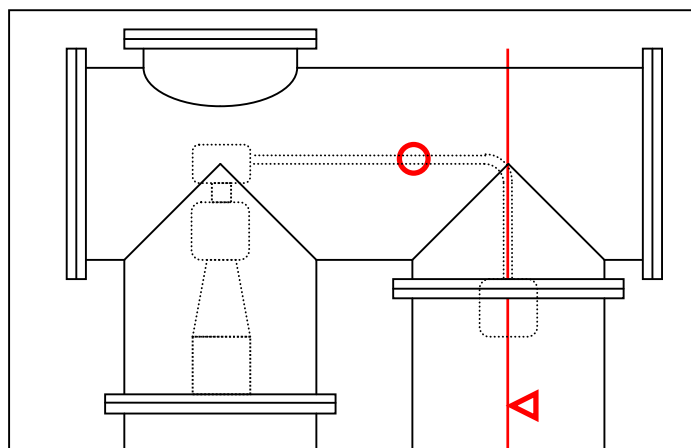


Fig. 10.5 High voltage cable box and found location of the partial discharge activity

10.2 Grid autotransformer

A large grid autotransformer failed the partial discharge acceptance test. The unit showed the highest partial discharge magnitude on X2 with about 1.2nC (Fig. 10.6). Here, the pattern shows the typical shape of a void partial discharge, but the pattern changed during the test also to flat delamination partial discharge. This indicates that gases are produced and eventually, a bubble slips out and stays a while attached to the conductor. Cross coupling to H3 was relatively high with about 40% and much larger than during calibration.

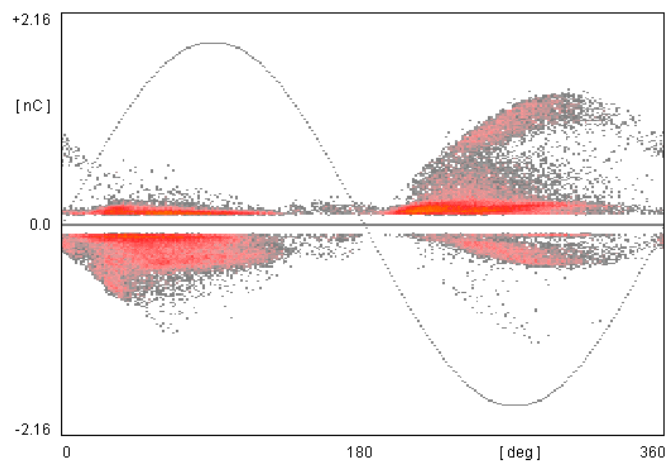


Fig. 10.6 Partial discharge pattern on X2 – spherical gas bubble

Thus, attempts to acoustic triangulation started on the LV side, where both HV potential (center part of the coil) and X2 common potential do meet (tap leads and tap changer). However, no signal was captured on the side. Instead, signals could be captured from underneath the tank (Fig. 10.7).

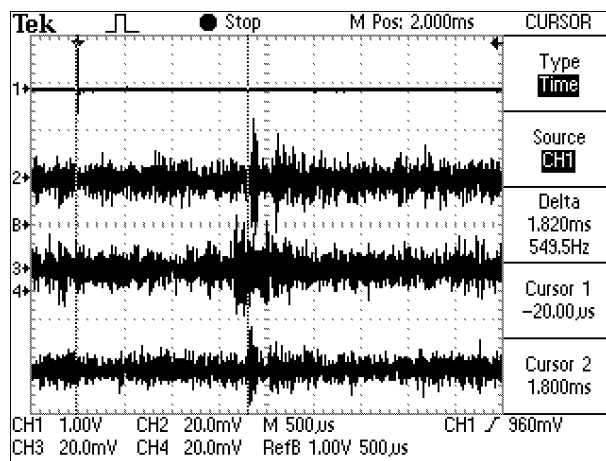


Fig. 10.7 Acoustic location results on X2 LV with sensors placed underneath the tank

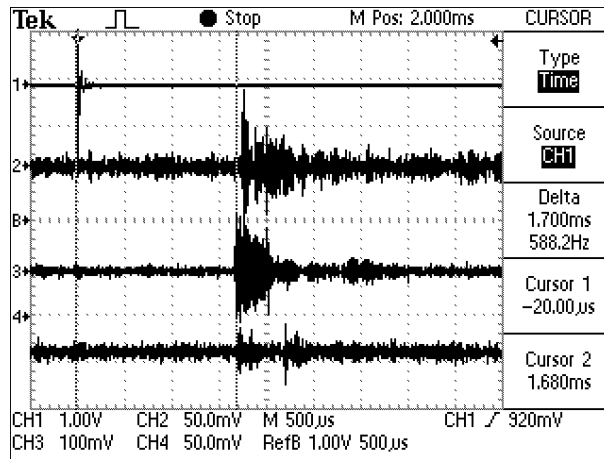


Fig. 10.8 Acoustic location results on X2 LV with sensors placed on top of the tank

Moreover, even clearer location results were obtained from the top of the tank (Fig. 10.8). It shall be noted that the distance the acoustic signal travels is about 250cm, which is in light of the "free space path loss" of the spherical wave front a remarkable distance (7.2). A direct measurement in front of the tap changer was hampered by massive magnetic wall shunts at the side walls of this unit.

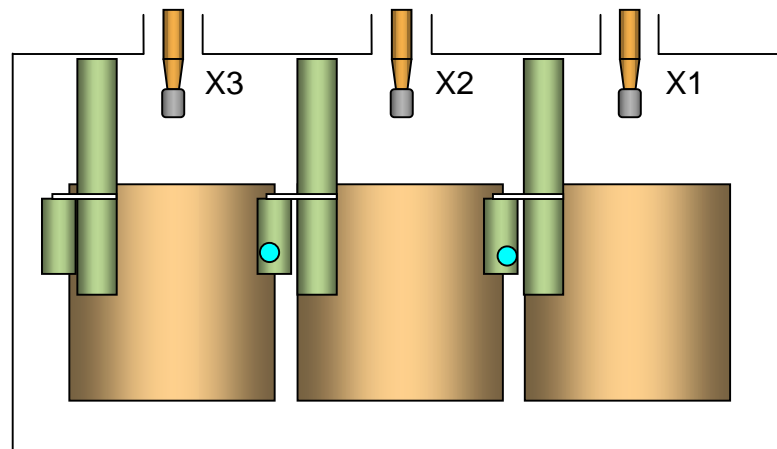


Fig. 10.9 Identified locations on the reverse switch of tap changer X1 and X2

Likewise, a similar defect on X1 was found at the identical position of the tap changer's reverse switch (Fig. 10.9). With X1, as well, location was possible from top and bottom. However, after knowing the exact location of the X2 activity, very faint signals were finally found directly in front to the identified location (Fig. 11.10). It shall be noted that not only the strong attenuation due to the wall shunt hamper measurement, but also strong flux in those shunts cause Barkhausen noise, which the averaging technique can not remove entirely.

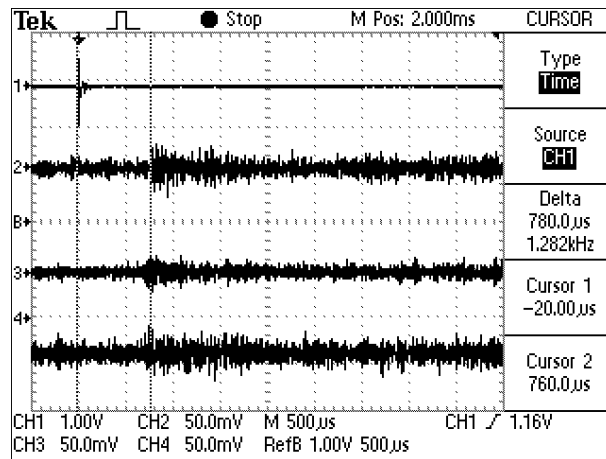


Fig. 10.10 Faint acoustic signals in front of X2 tap changer – wall shunt attenuation

As the tap changer of phase 3 does not have the proximity to a neighboring phase, signals of X3 did show only cross coupling. After untanking, the leads at the tap changers of phase 1 and 2 were improved and the unit successfully passed acceptance.

10.3 Large shell-type autotransformer

Generally, shell-type transformers are very difficult candidates for attempts of acoustic location, as the core rests horizontally on a frame and shields most of the winding. Access from top and bottom is also difficult, as there is often structural material to keep the coils in place. Thus, access can be tried from the sides above and below the core. Knowledge concerning the internal life is more needed than for core-type transformers, as for the latter the tank and position of construction elements on the tank tell about the internal life. With shell-type transformers even the orientation of the coils is not necessarily clear, as there are also variants like a horizontal five-limb core (Fig. 10.11, b).

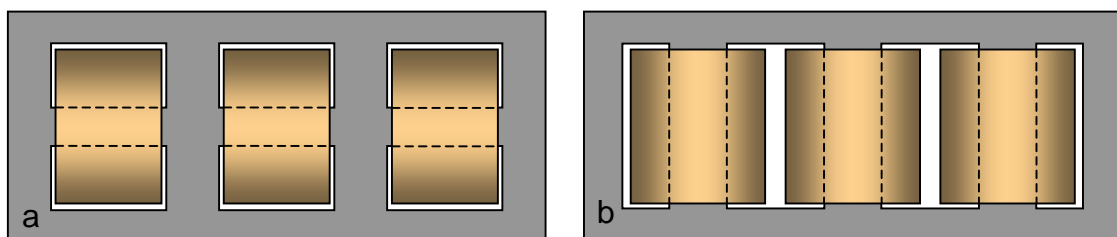


Fig. 10.11 Shell-type core styles (top view) – standard (a) and five-limb variant (b)

The unit, a large grid transformer (YNa0d11) showed discharge of a floating potential on one phase at 20% during acceptance testing after repair (Fig. 10.12). The unit underwent repair of a short circuit damage on this specific phase. The core was of the horizontal five-limb style and the problem was on C coil. Thus access was possible from HV side, LV side, and the narrow side.

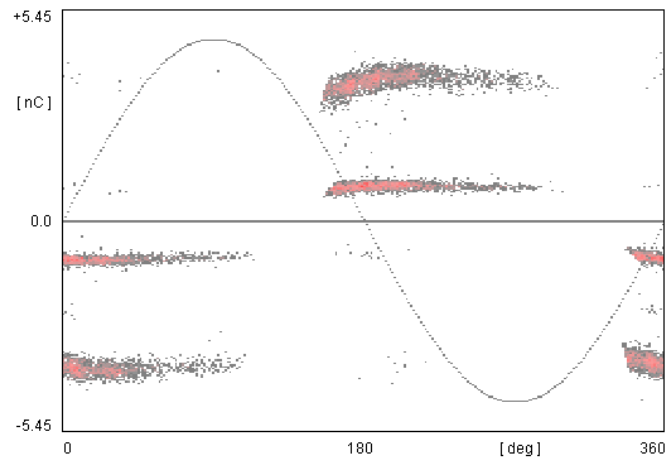


Fig. 10.12 Partial discharge of a floating potential on HV C phase.

Almost 5nC magnitude offers some possibilities for acoustic location even on a shell-type unit. The electrical signal from HV, MV (common), and LV (tertiary) indicated that the signals are cross-coupled (no polarity swap) and that the source should be electrically close to MV C. Acoustic scanning of the assumed areas of internal leads was not giving results. Finally, a very faint signal was detected below the core in only a confined area on the HV side (Fig. 10.13).

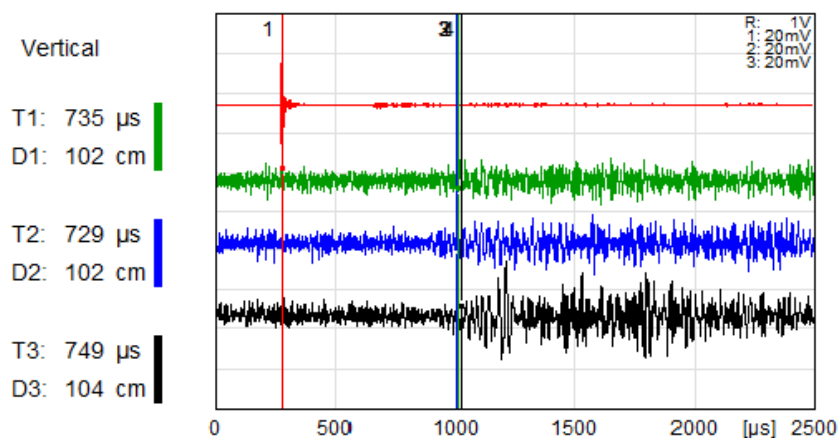


Fig. 10.13 Faint acoustic signal as captured on the lower part of C coil

The rough distance of the signal source is 100cm away from the tank wall. The fact that there is only a slow increase of the acoustic signal indicates that there are competing signal paths due to the spacers and oil channels of the pancake coil stack. This circumstance is also responsible for the only confined area in which the signal could be detected.

Subsequently, the voltage was increased and a similar activity of a floating potential inception with more than double the magnitude (12nC) at 150%. The location result was at about 170cm depth on the HV side. Based on this result, also the LV side was scanned and there was also a depth of about 100cm found, which corresponds to the tank width of 270cm.

No drawings were available at the time of the test. However, the discharge type and location fits to the location of a laminated static shield between high voltage coil and common coil. As the coil is symmetrical, the first location result concerns the static shield facing to the HV side with the low inception, while the second activity stands for the static shield on the MV side (Fig. 10.14).

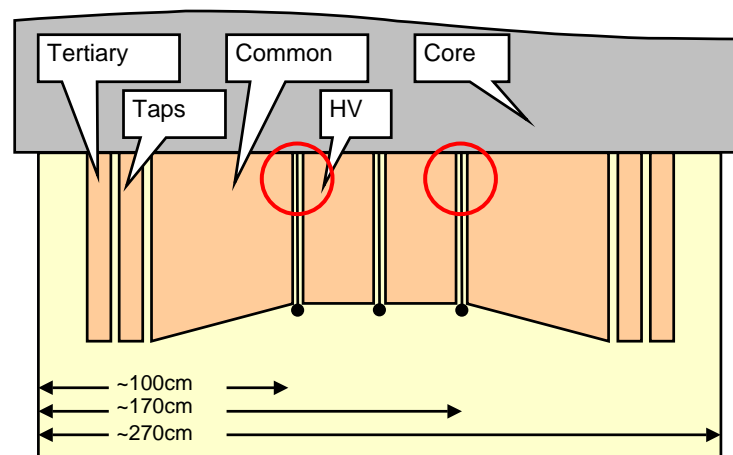


Fig. 10.14 Assumed construction of the coil stack and location of the static shields

With this case, no follow up information is available. However, repairing of the laminated static shield between common and high voltage coil would be very laborious, as this would mean a complete disassembly of the core and the pancake coils. Besides hampering acoustic location, this is one of the general drawbacks of shell-type transformers, but on the other hand, they do offer compact design and excellent short circuit behavior.

10.4 Large grid autotransformer

When attempting an acceptance test on this unit partial discharge inception with a delay of few minutes. The pattern properties and the cross coupling to other phases indicated that there were two independent activities on the same phase. Here, further identification was obtained, when viewing the signal in time domain. Subsequently, the signals of the two sources were clearly separated by choosing the most prominent cross coupling that did show the smallest response of the other signal. Thus, it is essential to always have a look at the cross coupling signals in time domain. Obviously, this case would have clearly benefited from the new φ - q trigger.

One signal gave a clear cross coupling to the common potential of the neighboring phase including a polarity swap, which makes a problem with the leads – including the tap leads – the most prominent root cause. This problem was then quickly located at the tap changer at one of the connections, while using the common of the other phase as trigger for the triangulation.

The other problem did show both a cross coupling to the core as well as to the tertiary of the said coil. Here, the ratio between calibration ratio and partial ratio (Chapter 7.1.1) was larger than 5. This already indicates clearly a location inside the coil. Thus, the trigger signal for triangulation was taken from tertiary Y1 and the top of the coil was searched, as this was the Y1 end of the tertiary. Correlating signals were found just under the top pressure disc (Fig. 10.15).

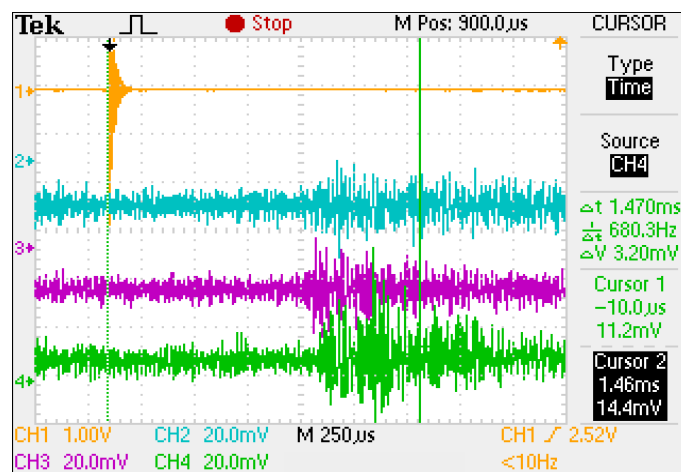


Fig. 10.15 Acoustic signals as found at the top of coil 1

The acoustic signals show a slow increase, which indicates competing travel paths for the acoustic pressure wave. Moreover, as the signals were captured just under the upper pressure disc, they had to follow the paths given by the radial placed sticks to form the oil channels between the said disc and the coil stack, as indicated with Fig. 10.16. Here, the red arrows show the position of the acoustic sensors. When moving the sensors, the identified location moves as well, because during triangulation a straight path is assumed, where the line with the total distance points to the oil channel, where the signal exits.

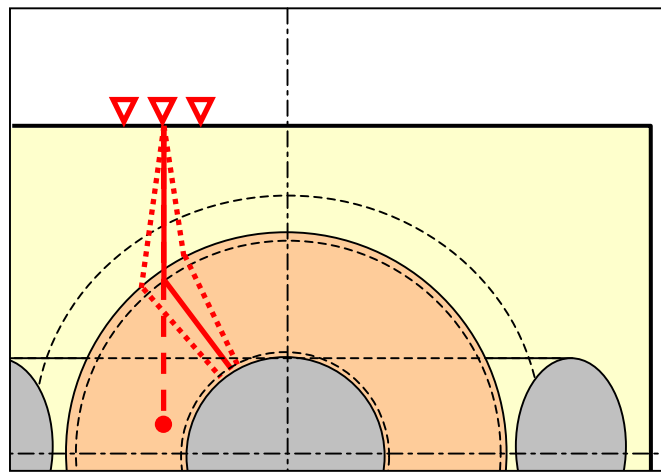


Fig. 10.16 Path of the of the acoustic signal through the oil channels under the pressure disk

Based on the acoustic travel time, the distance was calculated to 137cm, which would be close to the centerline, if assuming a straight path. Even when assuming the path along the radial sticks, there is still 27cm additional travel path. Fig. 10.17 shows the situation in a cut view along the acoustic travel path.

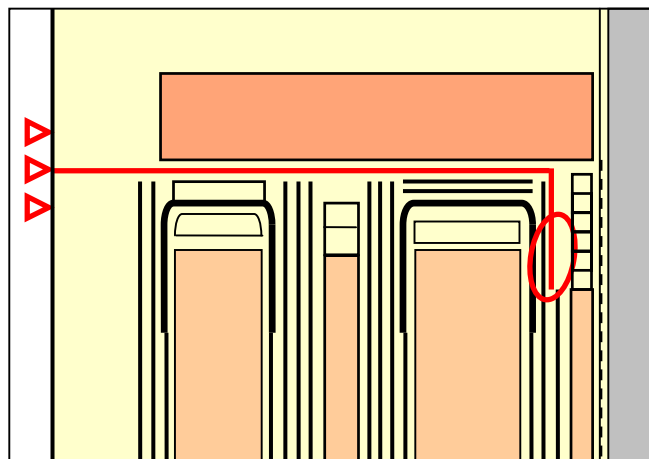


Fig. 10.17 Travel path of the acoustic signal through the oil channels deeply into the winding

However, at this position, in the interface between common, core, and the recesses tertiary, the cross coupling is possible exactly as observed. In this specific area, the comparably high field of the common potential "views" the core and the insulation stack on top of the shorter tertiary.

However, sadly, fixing the problem required untanking, removal of the yoke, and the pressure disc to redo the insulation stack on top of the tertiary.

10.5 Partial discharge pattern

The following pages list a catalog of partial discharge pattern as typical examples for common defects or over stresses of electrical insulation. Mostly, they have been already mentioned with the previous chapters to illustrate the theoretical background, for instance. In case, the page and the figure number are listed for further information.

The aim of this pattern catalog is to give a condensed overview along with a brief explanation. Naturally, such catalog builds on nice examples, as found during many years. However, sadly, real testing life often confronts one with less nice and moreover ambiguous examples.

Discharge of spherical cavities (voids) in polymeric material have plenty faces depending on the material properties, the irradiation, and the de-trapping statistics among other effects. Thus, the catalog starts with such void discharge.

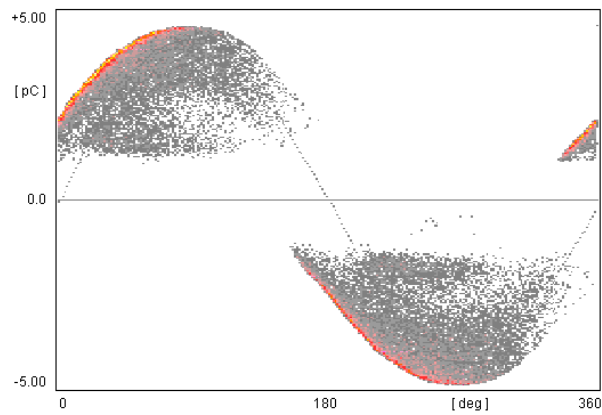


Fig. 10.18

Generic

Single void in epoxy resin
Average charge carrier generation

Fig. 3.13, p. 25

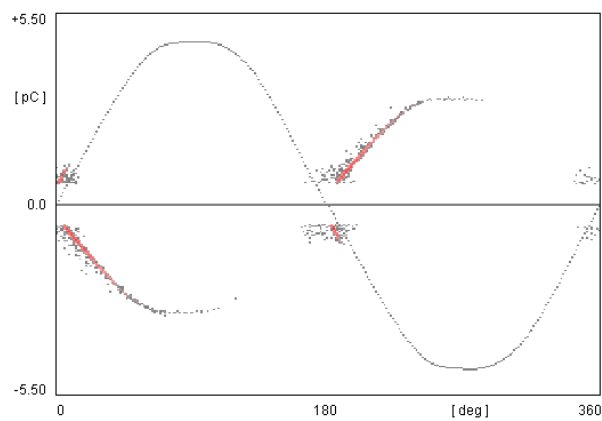
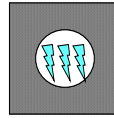


Fig. 10.19

Generic

Single void in polymeric material
Low charge carrier generation

Fig. 3.15, p. 26

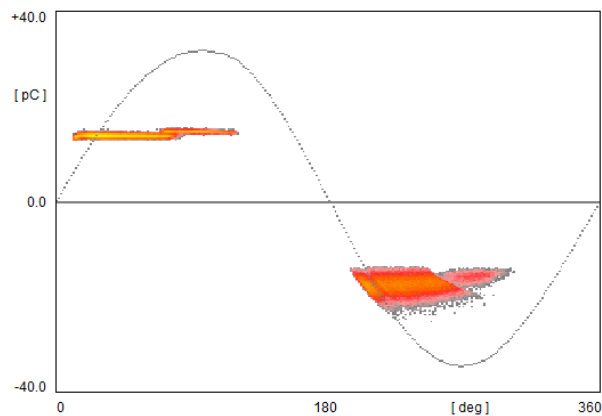
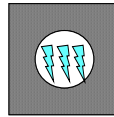


Fig. 10.20

Generic

Single void in glass bead
High charge carrier generation

Fig. 3.7, p. 19

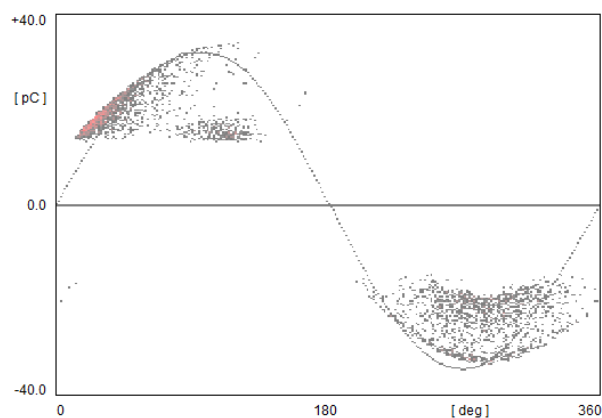
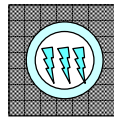
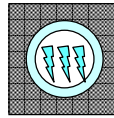


Fig. 10.21

Generic

Single void in glass bead
Low charge carrier generation

Fig. 3.11, p. 22



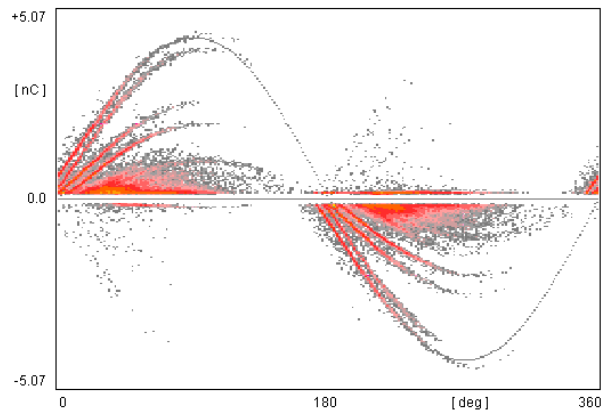


Fig. 10.22

Generic

Multiple voids in epoxy resin
Low charge carrier generation

Fig. 7.16, p. 117

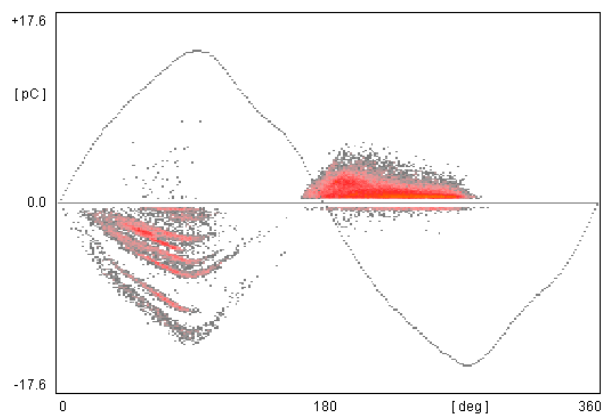
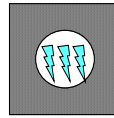


Fig. 10.23

Generic

Voids in polymeric material, semi-conductive interface, 3rd harmonic

Fig. 3.16, p. 26

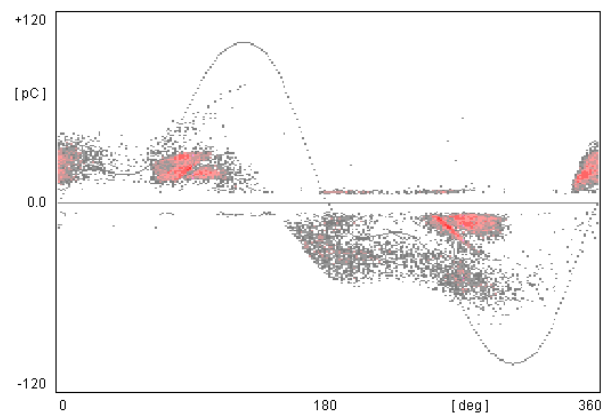
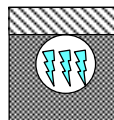


Fig. 10.24

Generic

Multiple voids in voids in instrument transformer, 2nd harmonic distortion

Fig. 3.17, p. 27

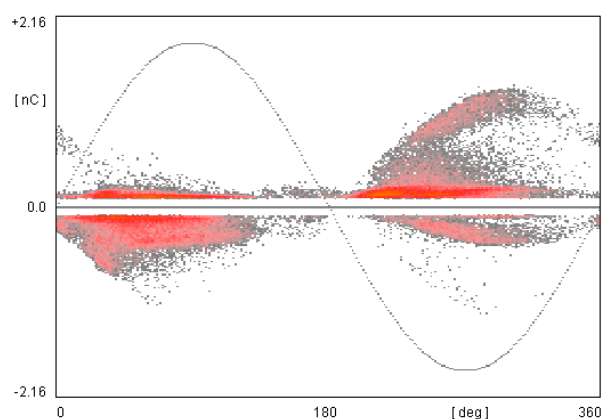
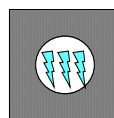
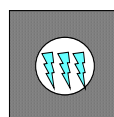


Fig. 10.25

Transformer

Gas bubble in oil attached to conductor paper layer delamination

Fig. 10.6, p. 150



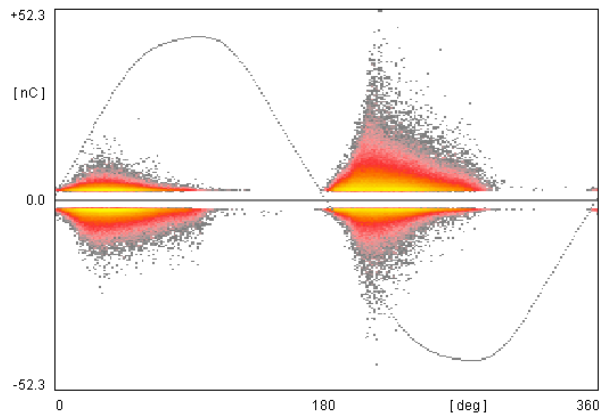


Fig. 10.26

Generic
Surface discharge
Fig. 3.20, p. 29

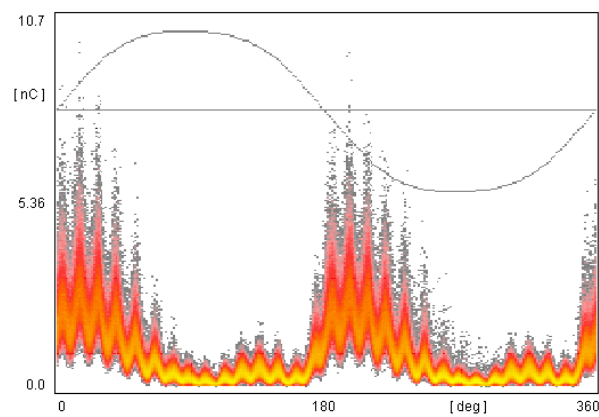
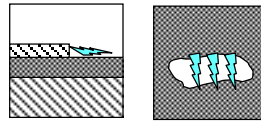


Fig. 10.27

Hydro generator
Service aged insulation with typical
triangular pattern, 29th harmonic
Fig. 3.21, p. 30

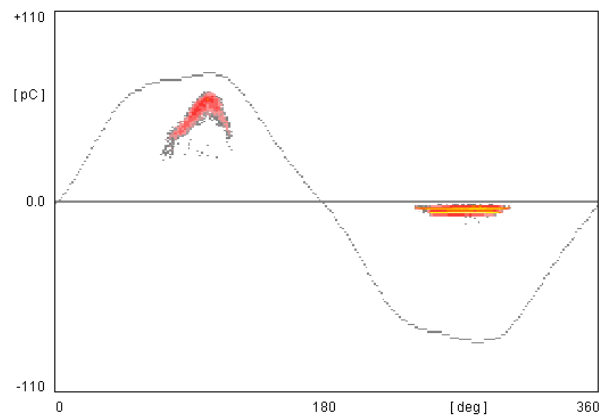


Fig. 10.28

Generic
Sharp point in air, streamer discharge in positive half cycle, Trichel discharge in negative half cycle
Fig. 3.22, p. 31

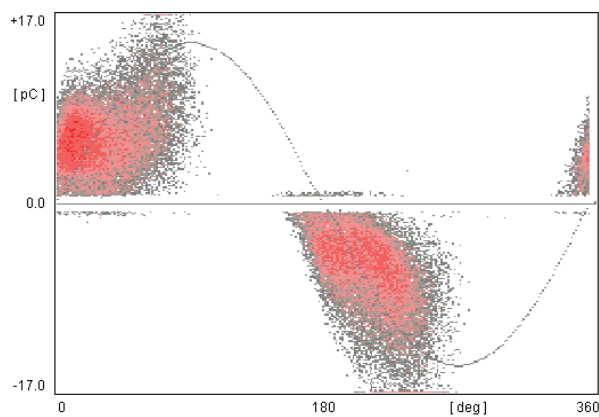
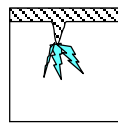
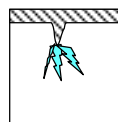


Fig. 10.29

Generic
Treeing in polyethylene
Fig. 3.25, p. 32



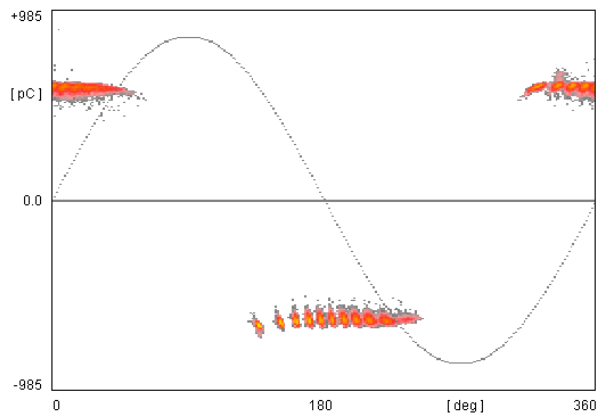


Fig. 10.30

Generic

Floating potential with metallic gap

Fig. 3.23, p. 31

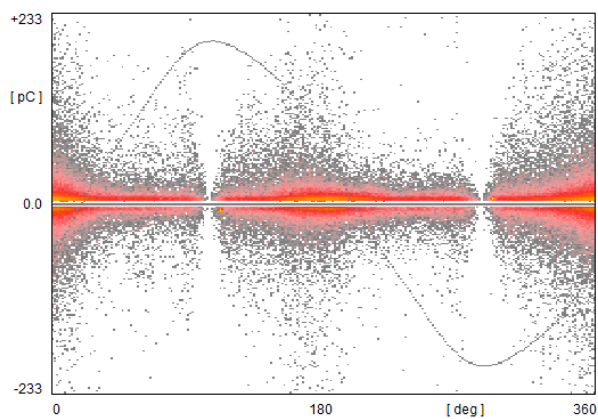
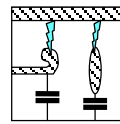


Fig. 10.31

Generic

Floating potential with isolation covered gap

Fig. 3.24, p. 32

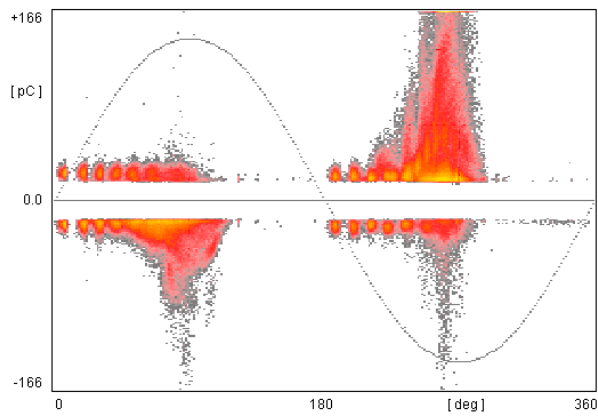
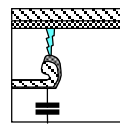


Fig. 10.32

Bushing

Internal contact problem at the tap electrode

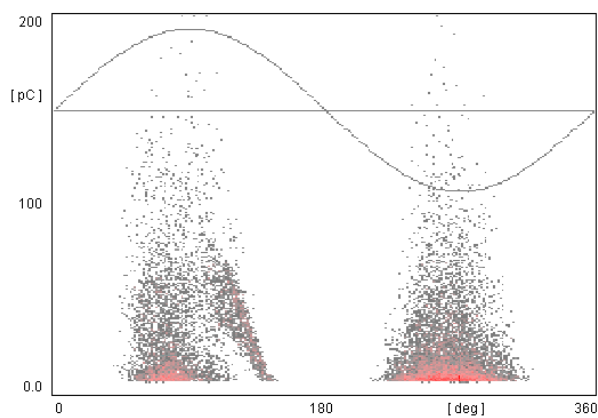
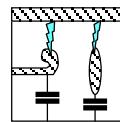
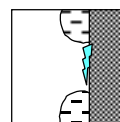


Fig. 10.33

Bushing

So-called corona discharge under light rain



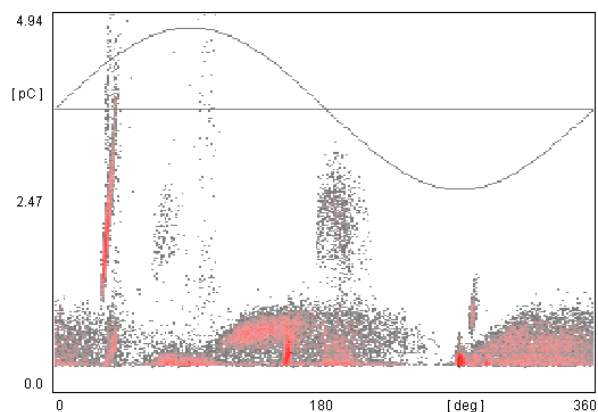


Fig. 10.34

Transformer

Internal discharge superimposed with so-called corona discharge

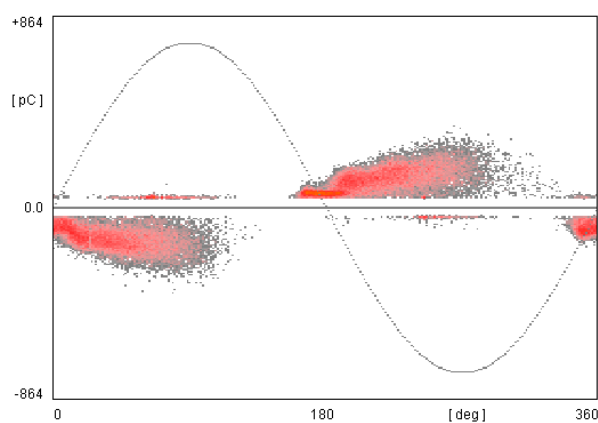
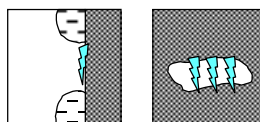


Fig. 10.35

Transformer

Gas pocket between paper layers

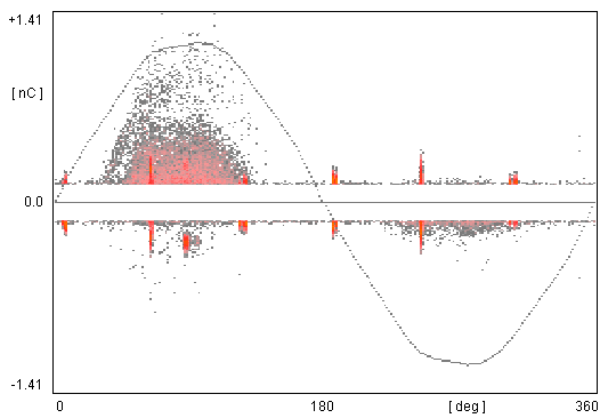


Fig. 10.36

Transformer

Point-plane-discharge under oil

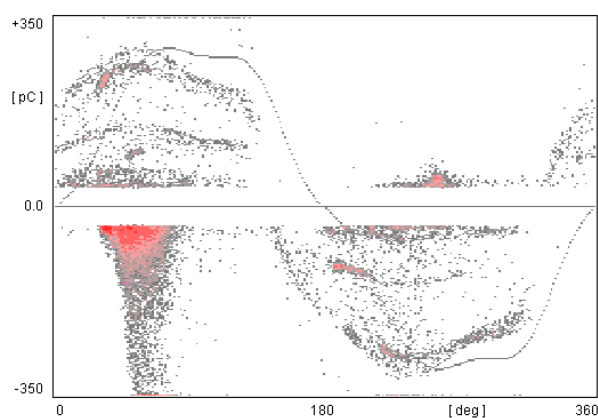
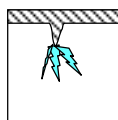
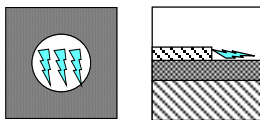


Fig. 10.37

Instrument transformer

Several voids and surface discharge under harmonic distortion



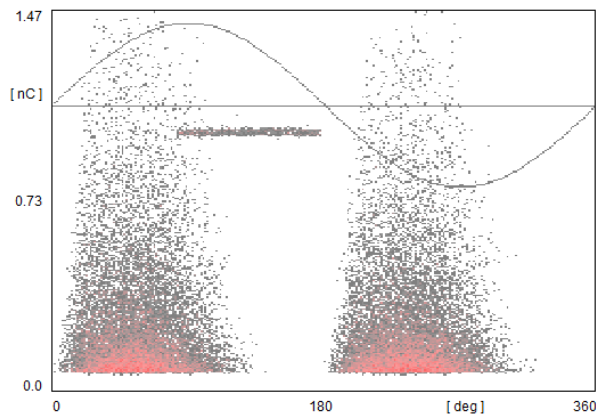


Fig. 10.38

Transformer

Paper layer delamination and superimposed calibration pulse
Fig. 7.38, p. 137

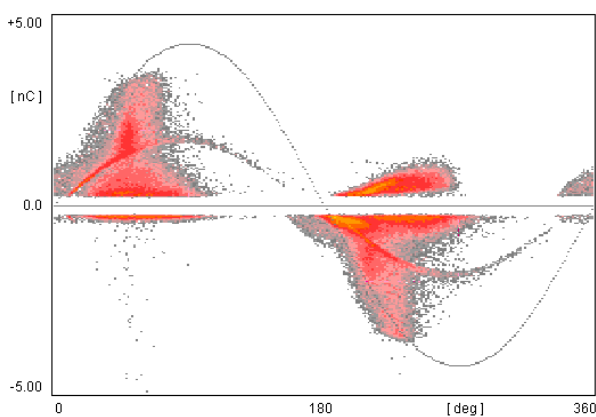


Fig. 10.39

Generator bar

Void discharge, surface discharge, delamination and surface discharge at the coupling capacitor
Fig. 7.17, p. 120

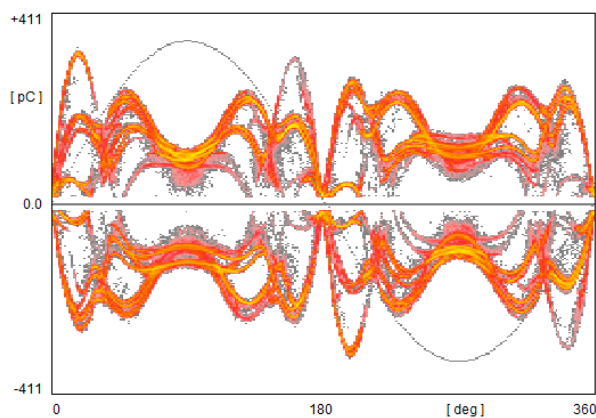
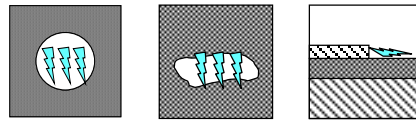


Fig. 10.40

Noise

Inverter switching noise
Fig. 7.7, p. 108

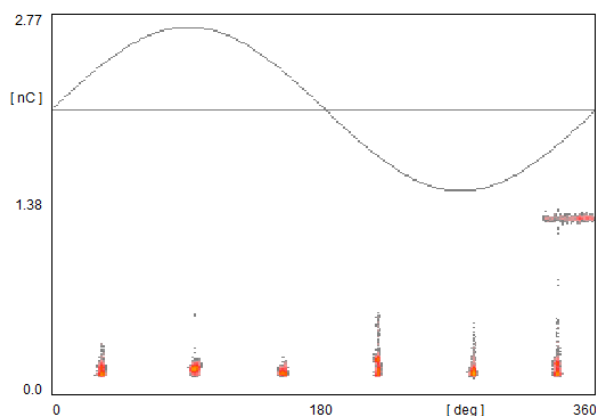


Fig. 10.41

Noise

Thyristor noise, six-pulse rectifier

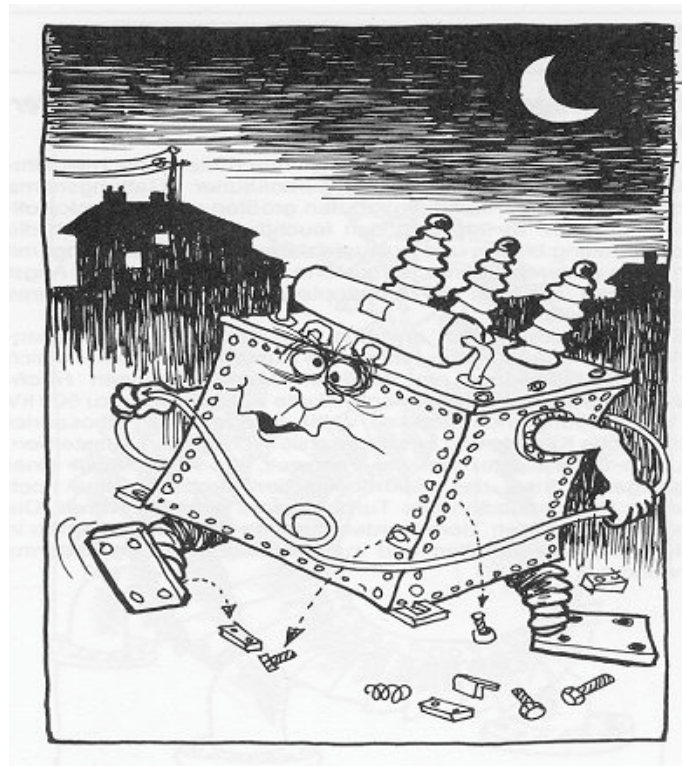


Fig. 10.42 What some transformers do at night...

Lutz Niemeyer

11 Literature

- [107₁] "Methods of measurement of radio noise", Edison Electric Institute, NEMA, Radio Manufacturers Association, 1940.
- [107₂] NEMA Publication No. 107, "Methods of measurement of radio influence voltage (RIV) of High-Voltage Apparatus", NEMA Pub. No. 107-1964.
- [107₃] NEMA 107 "Methods of measurement of radio influence voltage (RIV) of High-Voltage Apparatus", NEMA Pub. No. 107-1987.
- [16-1] CISPR 16-1, "Specification for radio disturbance and immunity measuring apparatus and methods – Part 1: Radio disturbance and immunity measuring apparatus", Edition 1, 1993.
- [17025] ISO/IEC 17025, General requirements for the competence of testing and calibration laboratories, ISO/IEC 17025:2005.
- [18-2] CISPR 18-2, "Radio interference characteristics of overhead power lines and high-voltage equipment - Part 2: Methods of measurement and procedure for determining limits", Edition 1, 1986.
- [23-01] Cigré WG 23-01, "Recognition of discharges," Electra, 1969, No. 11, p.61.
- [270] IEC Publication 270, Partial discharge measurements, 1968.
- [434] VDE 0434, "Richtlinien für Teilentladungsprüfungen an Betriebsmitteln mit Wechselspannung bis 500Hz", VDE Bestimmungen 0434, Teil I und II. Berlin: VDE Verlag 1966.
- [60270₁] IEC60270, High-voltage test techniques – Partial discharge measurements, CEI/IEC 60270:2000.
- [60270₂] IEC60270, High-voltage test techniques – Partial discharge measurements, CEI/IEC 60270:2015.
- [60076] IEC60076-3 Ed. 3, Power transformers – Part 3: Insulation levels, dielectric tests and external clearances in air, CEI/IEC 60076:2013.
- [57113] IEEE C57.113-2010 "IEEE Recommended Practice for Partial Discharge Measurement in Liquid-Filled Power Transformers and Shunt Reactors".
- [571200] IEEE C57.12.00-2015 "IEEE Standard for General Requirements for Liquid-Immersed Distribution, Power, and Regulating Transformers".
- [571290₁] IEEE C57.12.90-2006 "IEEE Standard Test Code for Liquid-Immersed Distribution, Power, and Regulating Transformers".
- [571290₂] IEEE C57.12.90-2015 "IEEE Standard Test Code for Liquid-Immersed Distribution, Power, and Regulating Transformers".

- [57127] IEEE C57.127-2007 "IEEE Guide for the Detection and Location of Acoustic Emission from Partial Discharges in Oil-Immersed Power Transformers and Reactors".
- [Aia15] Manual of the AIAcompact partial discharge detector, Power Diagnostix Systems GmbH, Version 2.44, March 27th, 2015.
- [Alt02] Altenburger, R., Heitz, C., Timmer, J., "Analysis of phase-resolved partial discharge patterns of voids based on a stochastic process approach," J. Phys. D: Appl. Phys. 35, 2002, pp. 1149-1163.
- [Akb16] Akbari, A., Werle, P., Akbari, M., Hasnan, R. M., "Challenges in Calibration of the Measurement of Partial Discharges at Ultrahigh Frequencies in Power Transformers," IEEE El. Insul. Magazine, Vol. 32, No. 2, March-April, pp. 27-34.
- [Boe99] Boek, W, et al., Joint TF 15/33/03.05, "Partial Discharge Detection System for GIS: Sensitivity Verification for the UHF Method and the acoustic Method," *Électra*, No. 183, pp. 75-87, Apr. 1999.
- [Bar19] Barkhausen, H. "Zwei mit Hilfe der neuen Verstärker entdeckte Erscheinungen." *Physische Zeitschrift*, 1919, year 20, no. 17., 401–403.
- [Ben97] Bengtsson, T, Kols, H., Jönsson, B., "Transformer PD diagnosis using acoustic emission technique," Conf. Proc. of ISH, August 25-29, 1997, Montréal, Canada, Vol 4, pp. 115-119.
- [Bin00] Binder, E. et. al., "Development and erification test of diagnosis methods for hydro-generators," in *CIGRE Session 2000, Paris, France, August, 28-31, 2000, Report 11-301*.
- [Bra00] Bräunlich, R., Hässig, M., Fuhr, J., and Aschwanden, T. "Assessment of insulation condition of large power transformers by on-site electrical diagnostic methods", ISEI International Symposium on Electrical Insulation, Anaheim, CA, U.S.A., April 2-5, 2000.
- [Cal16] Power Diagnostix Calibration Laboratory, Accreditation Certificate 2016, D-K-15068-01, www.dakks.de/as/d/D-K-15068-01-00.pdf.
- [Car03] Carlson, Å., Fuhr, J., Schemel, G., and Wegscheider, F. Testing Power Transformers. ABB Business Area Power Transformers, 2003, ISBN 3-00-010400-3.
- [Cla00] Clatterbuck, D.M., et al. "An extended model of the Barkhausen effect based on the ABBM model" J. of Applied Physics 87 (2000), 4771.
- [Cur80] Jacques and Pierre Curie "Développement par compression de l'électricité polaire dans les cristaux hémihédres à faces inclinées" (Development, via compression, of electric polarization in hemihedral crystals with inclined faces), *Bulletin de la Société minérologique de France*, vol. 3, 1880, pages 90-93.
- [Fru92] Fruth, B., Niemeyer, L. "The Importance of Statistical Characteristics of Partial Discharge Data", IEEE Trans DEI, Vol. 27, No. 1, February 1992, pp. 60-69.
- [Fru93] B. Fruth, M. Florkowski, D. Gross, "Partial Discharge Signal Generation, Transmission and Acquisition", Proc. of the Int. Conf. on Partial Discharge, University of Canterbury, 1993.
- [Fru94₁] Fruth, B., Gross, D. "Phase Resolving Partial Discharge Pattern Acquisition and Spectrum Analysis", Proc. of the ICPDAM, July 1994, Brisbane NSW, Australia, 94CH3311-8, pp. 578-581.

- [Fru95₁] Fruth, B. Gross, D., "Partial Discharge Signal Generation, Transmission, and Acquisition," IEE Proc., Science, Measurement and Technology, Vol. 142, No. 1, January 1995, pp. 22-28.
- [Fru95₂] B. A. Fruth, D. W. Gross, "Modelling of Streamer Discharges Between Insulating and Conducting Surfaces", Conference Proceedings of the 1995 5th Int. Conf. on Conduction and Breakdown in Solid Dielectrics, Leicester, England, 1995.
- [Fru96] B. A. Fruth, D. W. Gross, "Partial Discharge Signal Conditioning Techniques for On-Line Noise Rejection and Improvement of Calibration", Proc. of the 1996 IEEE Intl. Symposium of El. Insulation, Montreal, Quebec, Canada, June 16-19, 1996, pp. 397-400.
- [Fru97] B. Fruth and D. Gross, "Partial Discharge Data Acquisition System for Substation Monitoring", EPRI Substation Conference, 1997, New Orleans.
- [Fuh04] Fuhr, J., Aschwanden, T., "Experience with Diagnostic Tools for Condition Assessment of Large Power Transformers," ISEI 2004 Conference, Indianapolis, IN, September 19-22, 2004, 04CH37561C.
- [Gao13] Gao, W., et. al., "Propagation Attenuation Properties of Partial Discharge in Typical In-Field GIS Structures", IEEE Transactions on Power Delivery, Vol. 28, No. 4, Oct. 2013, pp. 2540-2549.
- [Gem32₁] Gemant, A., "Die Verlustkurve luftiger Isolierstoffe" (Losses of insulators with an air content), Zeitschrift für techn. Physik 13, 1932, 3, pp. 184-189.
- [Gem32₂] Gemant, A., Philippoff, W., "Die Funkenstrecke mit Vorkondensator" (Spark gap with pre-capacitor), Zeitschrift für techn. Physik 13, 1932, 9, pp. 425-430.
- [Gro95] Gross, D. and Comanns, R. "TE-Messung und Fehlerdiagnose an Kabeln und Garnituren", ETG Fachtagung, Esslingen, Germany, Mai 31st - June 1st, 1995, ISBN 3-8007-2089-2, pp. 213-217.
- [Gro98₁] Gross, D.W., Fruth, B.A, "Characteristics of phase resolved partial discharge pattern in spherical voids," CEIDP 1998, Atlanta, GA, USA, October 25-28, 1998, pp. 412-415.
- [Gro98₂] Gross, D.W., Fruth, B.A, "Distortion of phase resolved partial discharge pattern due to harmonics and saturation," CEIDP 1998, Atlanta, GA, USA, October 25-28, 1998, pp. 416-419.
- [Gro99] Gross, D. "On-site partial discharge diagnosis and monitoring on HV power cables," Conf. Proc. of Jicable, June, 1999, Versailles, France, pp. 509-514.
- [Gro02₁] Gross, D., Soeller, M., "Partial Discharge Acceptance Testing and Monitoring on Power Transformers," ETG Fachtagung, Diagnostik el. Betriebsmittel, Berlin, Germany, February 26-27, 2002, ISBN 3-8007-2671-8, pp. 213-216.
- [Gro02₂] Gross, D., "Partial Discharge Measurement and Monitoring on Rotating Machines," ISEI 2002 Conference, Boston, MA, April 7-10, 2002, 02CH37316, pp. 570-574.
- [Gro03₁] Gross, D., "Signal Transmission and Calibration of on-line Partial Discharge Measurements," ICPADM, Nagoya, Japan, June 1-5, 2003, 03CH37417, pp. 335-338.
- [Gro03₂] Gross, D., "Partial Discharge Diagnosis of Motor Defects," Nordic Insulation Symposium, Tampere, Finland, June 11-13, 2003, ISBN 952-15-1034-X, pp. 21-28.

- [Gro04₁] Gross, D., Soeller, M. "Partial Discharge Diagnosis on large Power Transformers," ISEI 2004 Conference, Indianapolis, IN, September 19-22, 2004, 04CH37561C, pp. 186-191.
- [Gro04₂] Gross, D., Soeller, M., "Commissioning and On-line Testing of GIS and GIL," in ISEI 2004 Conference, Indianapolis, IN, September 19-22, 2004, 04CH37561, pp. 265-268.
- [Gro06] Gross, D., Soeller, M., "Strategies to locate partial Discharge in large Power Transformers," INSUCON 2006, '10th International Insulation Conference', Birmingham, UK, May 24-26, 2006.
- [Gro07₁] Gross, D., Soeller, M., "On-Site Partial Discharge Testing of Distribution Class cables using VLF and Power Frequency Excitation," JiCable 2007 Conference, Versailles, France, June 24-28, 2007.
- [Gro07₂] Gross, D., Soeller, M., "Calibration of on-line partial discharge measurements of gas-insulated equipment," ISH 2007, Ljubljana, Slovenia, August 27-31, 2007.
- [Gro12] Gross, D., Soeller, M., "On-site Transformer Partial Discharge Diagnosis," ISEI 2012, IEEE Conference, San Juan, Puerto Rico, June 10-13, 2012.
- [Gro15₁] Gross, D., "Acoustic Location of Transformer PD under non-ideal Conditions", The 19th International Symposium on High Voltage Engineering, Pilsen, Czech Republic, August, 23 – 28, 2015.
- [Gro15₂] Gross, D., Soeller, M., "Commissioning and Operation of large GIS Partial Discharge Monitoring Systems," SCD1 Colloquium, Cigré Brasil, Rio de Janeiro, Brazil, Sept. 13-18, 2015.
- [Gut95] Gutfleisch, F., Niemeyer, L. "Measurement and Simulation of PD in Epoxy Voids", IEEE Trans DEI, Vol. 2, No. 5, October 1995, pp. 729-743.
- [Hae03] Hässig, M., Fuhr, J., Aschwanden, T., "Grundsteine der TE-Messung an Transformatoren vor Ort," HighVolt Kolloquium 2013, Dresden, Germany, May 22-23, 2003.
- [Hei99] Heitz, C. "A generalized model for partial discharge processes based on a stochastic process approach", J. Phys. D, Sept. 1999, pp. 1012-1023.
- [Hen96] C. Henningsen, K. Polster, B. Fruth, D. Gross, "Experience with an on-line Monitoring System for 400 kV XLPE Cables", Proc. IEEE Transmission and Distribution Conf., Los Angeles, September 15-20, 1996, 96HC35968, pp. 515-520.
- [Hol91] Holbøll, J. T., Braun, J. M., Fujimoto, N., Stone, G. C., "Temporal and spatial development of partial discharges in spherical voids in epoxy related to the detected electrical signal," Conference on Electrical Insulation and Dielectric Phenomena (CEIDP). 1991 pp. 581–588.
- [How78] Howells, E. and Norton, E. T., "Detection of partial discharges in transformers using acoustic emission techniques", *IEEE Trans. Power Appar. Syst.* 97, 1978, 1538–1549.
- [Hud93] Hudon, C., Bartnikas, R., Wertheimer, M. R., "Spark-to-glow discharge transition due to increased surface conductivity on epoxy resin specimens," *IEEE Transactions on Electrical Insulation*, 1993. 28(1):1–8.

- [Hud01] Hudon, C., Torres, W., Bélec, M., and Contreras, R., "Comparison of Discharges Measured from a Generator's Terminals and from Antenna in Front of the Slots," EIC/EMCW Conference, Cincinnati, Ohio, October 2001, 01CH37264C.
- [Jer28] Jernegan, M. W., "Benjamin Franklin's "Electrical Kite" and Lightning Rod", The New England Quarterly, 1928, 1 (2): 180–196.
- [Kaw00] Kawada, M., Tungkanawanich, A., Kawasaki, Z., "Detection of Wide-Band E-M Signals Emitted from Partial Discharge Occurring in GIS Using Wavelet Transform", IEEE Transactions on Power Delivery, Vol. 15, No. 2, April 2000, pp. 467-471.
- [Koe93] König, D., et. al., *Partial Discharges in Electrical Power Apparatus*, VDE Verlag GmbH, Berlin, 1993.
- [Kre64] Kreuger, F. H., *Discharge Detection in High Voltage Equipment*, London, Temple Press, 1964.
- [Kue13] Küpfmüller, K., Mathis, W., Reibiger, A., *Theoretische Elektrotechnik*, 19. Springer Verlag GmbH, 19. Auflage, 2013.
- [Lee27] Lee, E. S., Foust, C.M., "Measurement of Surge Voltages on Transmission Lines Due to Lightning," General Electric Review, Vol. 30, No. 3, March 1927, pp. 135-145.
- [Lun92₁] L.E. Lundgaard, "Partial discharge XIII. Acoustic partial discharge detection - fundamental considerations", IEEE El. Insul. Mag., Vol. 8, Issue 4, July-Aug. 1992, pp. 25-31.
- [Lun92₂] L.E. Lundgaard, "Partial discharge XIV. Acoustic partial discharge detection-practical application", IEEE El. Insul. Magazine, Vol. 8, Issue 5, Sept.-Oct. 1992, pp. 34-43.
- [Mar05] Markalous, S., Tenbohlen, S., Feser, K., "New robust non-iterative algorithms for acoustic PD-localization in oil/paper-insulated transformers", 14th Int. Symp. on High Voltage Engineering, August 25-29, 2005, Beijing, PR China, paper no. G-040.
- [Muh04] Muhr, H.M., Schwarz, R., Pack, S., Koerbler, B., "Unconventional partial discharge measurements", CEIDP 2004, Boulder, CO, USA, October 17-20, 2004, pp. 430-434.
- [Muh06] Muhr, H.M., Schwarz, R., "Partial Discharge Impulse Characteristics of Different Detection Systems", Proc. Intl. Conf. on Condition Monitoring and Diagnosis, Changwong, Rep. of Korea, April 2-4, 2006.
- [Nie89] Niemeyer, L., Ullrich, L., Wiegart, N., "The Mechanism of Leader Breakdown in Electronegative Gases", IEEE El. Insul. Magazine, Vol. 24, No. 2, April 1989, pp. 309-324.
- [Nie95] Niemeyer, L. "A generalized approach to partial discharge modeling", IEEE Trans DEI, Vol. 2, No. 4, August 1995, pp. 519-528.
- [Neu00] Neumann, C., et al. "PD measurements on GIS of different designs by non-conventional UHF sensors," in *CIGRE Session 2000, Paris, France, August, 28-31, 2000, Report 15-305*.
- [Pee15] Peek, F.W., *Dielectric Phenomena in High Voltage Engineering*. McGraw-Hill Book Company, 1915, pp. 216-217.
- [Riv13] Manual of the RIVmeter, Power Diagnostix Systems GmbH, Version 2.15, March 10th, 2013.

- [Riz14] Rizk, F.A.M., Trinh, G.N., *High Voltage Engineering*. CRC Press, Taylor & Francis Group, 2014.
- [Rob95] E. Robles, B. Fruth, D. Gross, "A High Sensitivity Technique to Detect Incipient Failures on In-Service High Voltage Bushings", Proc. 9th Int. Symp. on High Voltage Engineering, Graz, Austria, 1995, pp 5664-1.
- [Sch20] Schering, H., "Brücke für Verlustmessung," Z. Instrumentenkunde 40, 1920, 124.
- [Sch69] Schwab, A., *Hochspannungsmeßtechnik*. Springer-Verlag, 1st Edition, 1969.
- [Srz16] Schwarz, R., *Teilentladung in der elektrischen Energietechnik*. Scriptum zur Vorlesung 433.035, SS2016, TU Graz.
- [Sun98] Sundermann, U., Fruth, B., and Gross, D. "On-Line Partial Discharge Testing of Power Transformers". EPRI Substation Equipment Diagnostics Conference, New Orleans, USA, February 16-18, 1998.
- [Sys16] Manual of the ICMsystem partial discharge detector, Power Diagnostix Systems GmbH, Version 4.32, July 15th, 2016
- [Tan93] Tanaka, T., "PD pulse distribution pattern analysis", Proc. of the Int. Conf. on Partial Discharge, University of Canterbury, 1993.
- [Teh13] Tehlar, D., Riechert, U., Behrmann, G., Schraudoph, M., Herrmann, L.G., Pancheshnyi, S. "Pulsed X-ray Induced Partial Discharge Diagnostics for Routine Testing of Solid GIS Insulators", IEEE Trans DEI, Vol. 20, No. 6, December 2013, pp. 2173-2178.
- [Tow15] Townsend, J. S., *Electricity in Gases*. Oxford University Press, 1915.
- [Tro10] Troeger, A., Riechert, U., Burow, S., Tenbohlen, S., "Sensitivity Evaluation of Different Types of PD Sensors for UHF-PD-Measurements," International Conference on Condition Monitoring and Diagnostics 2010, Tokyo, Japan, September 6-11, 2010.
- [Vio14] Viola, F., Romano, P., "Building Partial Discharge Signal Wireless Probes", *Progress in Compact Antennas*, InTech Publisher, ISBN 978-953-51-1723-0, 2014.
- [Wer10] Werle, P., Kouzmine, O. "New methods for condition assessment and onsite testing," Transformer Life Management 2010, Schering Institut, Leibnitz Universität Hannover, Halle, Germany, June 21-22, 2010.
- [Zin00] Zinke, O., Brunswig, H., *Hochfrequenztechnik 1*. Springer-Verlag Berlin, 2000.